Imperial College London

Department of Chemical Engineering

DEVELOPMENT OF GRAPHENE OXIDE HOLLOW FIBRE MEMBRANES FOR SOLUTION-BASED APPLICATIONS

NORFARAH DIANA BINTI ABA

A Thesis Submitted for the Degree of Doctor of Philosophy and the Diploma of Imperial College London

December 2016

Untuk kesayanganku, Fadzil & Fiyya Elena
Untuk doa yang tak pernah putus, Atokmak & Atokabah
Untuk kasih sayang yang tak pernah lekang, Nenek & Atok

DECLARATION OF ORIGINALITY

I hereby declare that the work reported in this thesis was composed and originated entirely by me. Information derived from published and unpublished results of others has been acknowledged in the text and in the relevant references included within the thesis.

NorFarah Diana Aba

Imperial College London,

December 2016

ABSTRACT

Graphene oxide (GO) is a chemical derivative of graphene which possesses interesting characteristics, such as atomic thickness, a 2D structure and robust mechanical strength, as well as a complex chemical structure constituted by various oxygen functional groups. GO flakes can be easily stacked on top of each other in order to form large area thin-film membranes. Since 2012, when the membrane potential of the GO was demonstrated for the first time, GO membranes have continued to attract high levels of interest from research communities which sought to continuously develop high performance membranes within the framework of various disciplines of separation. Nevertheless, the transport mechanism of the GO membrane in the separation process is not entirely understood, thus significant efforts have been made in order to further explore the unique characteristics the GO has to offer as a new generation of membrane material.

The first part of this thesis explores the feasibility of GO membranes in the case of nanofiltration separation. GO membranes are unstable in dry air due to the shrinkage problems occurring under such conditions. When a membrane is exposed to air, a high tensile stress is imposed, which is far beyond what the membrane can withstand. In order to overcome the shrinkage problem, GO membranes were kept in water so as to preserve their intrinsic microstructures. Prior to depositing the GO membranes in water, controlled drying was required in order to avoid the redispersion of the membranes in water due to the hydrophilic nature of the GO. Depositing the GO membranes in water has successfully preserved their nanofiltration performance over a three-week interval, during which time the membranes that were exposed to dry air failed to achieve similar results. At the end of this first part, the transport mechanism in nanofiltration is discussed.

Although GO membranes have been found to be feasible in the case of nanofiltration separation, they have also been demonstrated to be incapable of removing smaller ionic species, such as magnesium chloride and sodium chloride, solely on the basis of their pristine nature. The second part of this thesis explores the feasibility of GO at the level of desalination applications. It is well known that the rejection of salts relies not only on the pore size of a membrane, but also on the charge of the membrane and the solute, thus creating electrostatic repulsion. Cross-linking GO membranes with Al^{3+} have successfully changed the negatively charge GO membranes to highly positive charge. On the basis of space charge model, the cross-linking has successfully increased the density of membrane charge, at the same time narrowing the effective channels for ion transport, simultaneously increasing the rejection towards salt solutions.

The third part of this thesis further explores the feasibility of GO in the pervaporation dehydration of ethanol. For the pervaporation dehydration of ethanol, the surface of a GO membrane was modified with hydrophilic silane in order to turn it into a highly hydrophilic membrane. The performance of the modified GO membrane improved significantly with moderate separation factors. The transport mechanism in pervaporation is discussed at the end of this part. Moreover, the techno-economic analysis indicates that this modified GO membrane is environmentally benign and economically robust as a result of its small membrane area and energy requirements.

ACKNOWLEDGEMENTS

Alhamdulillah..

All praises to Allah for the strengths and His blessings that gave me courage, strength, and persistence to successfully complete this PhD study. While my name may be alone on the cover of this front thesis, I am by no means its sole contributor. This doctoral thesis would have not been possible without the support and encouragement of numerous people around me. Therefore, I would like to offer my deepest appreciation and sincere thank you to all of them.

My greatest gratitude is especially to my Supervisor; Prof. Kang Li. It has been an honour to be one of his students. Thank you for believing in my capability and for assisting me to become a good researcher. Thank you for the valuable advice, constant support, encouragement and immense knowledge. His guidance helped me in all the time of research and writing of this thesis.

I would also like to express my sincere thank you to my second supervisor, Dr. Cecilia Mattevi. I can't thank her enough for all the insightful discussion and comments, encouragement and guidance throughout this journey. Thank you for always being so supportive of my work and the laughs we have shared.

My deepest appreciation also goes to Dr. Bo Wang. Thank you for the unrelenting support and insightful discussion we have shared. Thank you for encouraging me to think outside the box and to be a better researcher and most importantly, thank you for believing in me.

I appreciate the support of Patricia Carry, Dr. Ardakani, Dr. Ecaterina Ware, Dr. Victoria Bemmer for their excellent technical assistance and kind answers to all of my queries. I also owe my sincere gratitude to the postgraduate administrators, Jessica Baldock and Susi Underwood, and not to forget, Ben and Keith from Chemical Engineering Store, who have always been very nice to me.

A special thanks to my friends in Prof Li's group Dr. Xinlei Liu, Dr. Li Tao, Ji Jing, Fairus, Izwanne, Yaala, Lucy, Chris, Jeng Yi (my co-author, thank you for all the insightful discussion on GO) and also Melanie (thank you so much for your time to proofread my thesis). Not to forget, my officemates, Mahmood and Joao, thank you for the good moments we have shared. I am forever indebted to Dr. Santanu Karan and Muzammir Mahat for their help in the XPS analysis of this thesis. May you find success in everything you do and may all your treasured

dreams come true. To my special best friend, Nilay; thank you for being there to share all the laughs and tears throughout this journey. To Nurhidayati and Ana Gil; thank you so much for the encouragement and the warmth you extended to me during our times together. Not to forget, my high-school best-friend, Najwa. Thank you for your effort to proofread my thesis, despite your conditions. Not to forget, my crazy bestfriends: Ida, Alwani, Shahirah, Aliyah, Amira, Norasiah, Shikin and Adibah. Thanks for all the friendship.

I would like to acknowledge my scholarship sponsors from Public Service Department of Malaysia. Thank you for this opportunity and the indispensable generous scholarship.

My heartfelt thank you also goes out to my close friends and neighbours. My time in London would have been difficult without the warmth presence of Irina, Aliyyah, Ezzaty, Haida, Norle, Maziah, Liyana, Lin, Aishah, Amalina, and many others whom I have not mentioned here. With them I have shared many delightful moments and I learnt to be a better person. The simple phrase, “thank you” cannot present how much their friendship means to me.

My parents, my parents-in-law, my sisters and brothers and my whole family deserve a special mention here for their love, support and constant prayers throughout my PhD study. Thank you for forgiving me for the time we have lost in my pursuit of this Ph.D. They always let me know that they are proud of me, which motivated me to work harder and do my best.

Most importantly, special thanks and love to person who helped me to keep things in perspective; my husband, Muhammad Fadzil for his unconditional love, support, encouragement and great patience during my Ph.D study and above all, to sacrifice your career just to be with me and our daughter, Elena. To my darling Elena, I could cry imagining this life without you. Thank you for being so much joy and I promise I will make up for lost time. All of this is for the sake of our future. This Ph.D is for you.

Lastly, I offer my warm regards and blessings to all of those who supported me in any respects during the course of the project.

LIST OF PUBLICATIONS

Publications

1. Aba, N. F. D., Chong, J. Y., Wang, B., Mattevi, C., & Li, K. (2015). Graphene oxide membranes on ceramic hollow fibers – Microstructural stability and nanofiltration performance. *Journal of Membrane Science, 484*(0), 87-94.
2. Chong, J. Y., Aba, N. F. D., Wang, B., Mattevi, C., & Li, K. (2015). UV-Enhanced Sacrificial Layer Stabilised Graphene Oxide Hollow Fibre Membranes for Nanofiltration. *Scientific Reports, 5*, 15799.
3. Aba, N. F. D., Chong, J. Y., Wang, B., Mattevi, C., & Li, K. Graphene Oxide on Ceramic Hollow Fibres- Cationic Cross-linking and the Efficiency for Water Desalination. *Final stage of submission to Journal of Membrane Science (2016).*
4. Aba, N. F. D., Chong, J. Y., Wang, B., Mattevi, C., & Li, K. Ultrafast Water Removal from Ethanol by Pervaporation Using Surface-Modified Graphene Oxide Hollow Fibre Membranes. *Final stage of submission to Chemmical Communication (2016).*

Conference Presentations

1. Chemical Engineering Day, (25-26 March 2013), Chemical Engineering Department, Imperial College London. *Poster Presentation*: Graphene Oxide hollow Fibre Membrane for Fluid Separation.

2. 13th International Conference on Inorganic Membranes, (6-9) July 2014, Brisbane, Australia. *Oral Presentation*: Stability of Graphene Oxide Hollow Fibre Membrane for wet process separation application. (Presented by Dr. Bo Wang)

3. The 10th International Congress on Membrane and Membrane Processes, (20-25 July 2014), Suzhou, China. *Oral Presentation:* Graphene Oxide Hollow Fibre Membrane, stability and application in wet process separation application.

4. Euromembrane Conference 2015, (6-10th September 2015), RWTH Aachen University. *Oral Presentation*: Surface modification of Graphene oxide hollow fibre membrane for pervaporation application.

TABLE OF CONTENTS

LIST OF FIGURES

LIST OF TABLES

CHAPTER 1

Introduction

1.1 Background

The limited resource of clean water and environmental problems are enormous challenges faced by mankind nowadays, which have been successfully tackled by advancements in membrane separation technology. Membrane separation has been employed for more than four decades in water and wastewater treatments, while offering numerous advantages over conventional processes in terms of energy efficiency, as well as being environmentally benign technology that brings about economic benefits. Loeb and Sourirajan in the 1960s produced a remarkable invention as a result of developing commercial membranes via the phase inversion process [6]. Meanwhile, in more recent times, the emergence and development of synthetic membranes have been recognized, while several major membrane processes, including microfiltration (MF), ultrafiltration (UF), nanofiltration (NF), reverse osmosis (RO), pervaporation (PV) and gas separation, have been established and deployed in real industrial applications worldwide.

To date, polymeric membranes have conquered membrane area in terms of research and development as well as membranes market expansion. Polymeric membranes, such as polyamide, cellulose acetate, polysulfone and poly(vinylidene fluoride) (PVDF), have been successfully commercialized and have been used widely in various separation applications. However, as the industry grows, polymeric membranes have exposed to different degrees of challenges that include harsh and extreme conditions such as high temperature, high acidity and alkalinity as well as wider range of feed solutions. Due to demand from industry that required membrane with better chemical, thermal and mechanical stabilities, ceramic membranes became increasingly popular. The main advantages offer by ceramic membranes, which polymeric membranes were failed to offer, which include; robustness, sterilisability, and the ability to be cleaned in harsh conditions. Due to that, ceramic membranes have started to emerge in terms of research and development as well as commercialization, in order to fulfil the demand from industry.

Recently, owing to excellent separation performance, significant mechanical strength, harsh chemical endurance and well-defined nanostructures, carbon-based materials have resulted in new research and discoveries as membrane materials. Carbon nanotubes (CNTs) were regarded as promising candidates due to their unique one-dimensional (1D) channel for ultrafast molecular transport, as well as superb mechanical strength. However, the major drawback of CNTs is that the synthesis is complicated and the experimental works are complex, resulting in limitation of experimental works. This hinders their potential for larger scale production. Recently, a two-dimensional (2D) carbon-based material, known as graphene and its derivatives, such as graphene oxide, offers an exciting opportunity as a new membrane material.

Graphene oxide (GO), which was first discovered by Brodie in 1895, is a 2D material, which possesses excellent mechanical, optical and chemical properties [7]. Although it was first discovered almost 160 years ago, only during the past few years has this material been recognized as an interesting material by our research communities, simply because it is one of the precursors for graphene. Unlike pristine graphene, which is impermeable to any molecule, even as small as that of helium, GO is an excellent candidate as a membrane material due to the various interesting characteristics such as tuneable microstructure, different oxygen functional groups and ease of production.

The most accepted chemical structure of GO was proposed by Lerf-Klinowski et al., as shown in Figure 1.1 [8]. They proposed that GO sheets are decorated with different oxygen functional groups, such as epoxy, hydroxyl, carboxyl and carbonyl, at the basal plane as well as at the edge of the sheets. The first GO membrane as developed by Nair et al. [2] had a thickness of around 10μm, which only allowed for the unimpeded permeation of water, whereas it blocked everything else in vapour form. In the process, Nair and colleagues successfully initiated a fundamental understanding with regard to the molecular transport of GO membranes [2]. A few years later, by appropriately engineering GO sheets, sub-micrometre GO membranes were able to be produced with high permeability and selectivity of gases [5, 9].

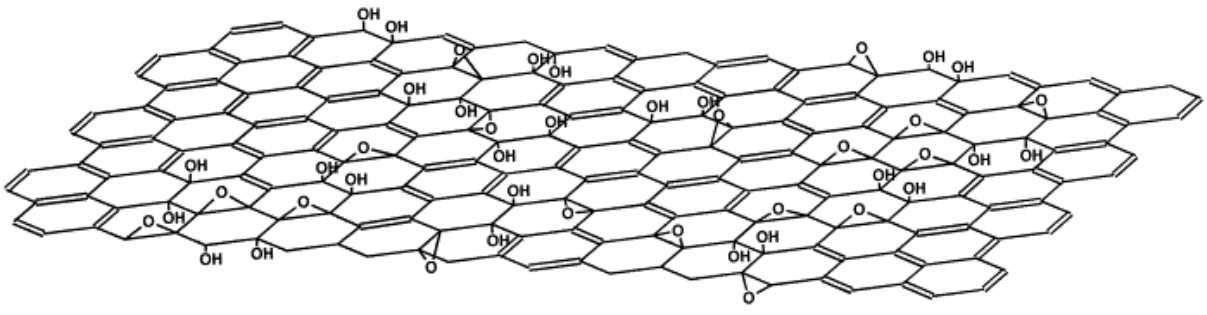

Figure 1. 1: Proposed chemical structure by Lerf-Klinowski [8].

Although there have been several research breakthroughs regarding GO membranes, they are still far from being employed in industrial applications. One of the major issues in this respect relates to GO membranes possessing ultra-thin characteristics. Thus, support is needed in order for them to withstand high pressure difference in industrial applications. In GO membrane studies, the supports used are usually in the flat plane shape. However, the main concern of the flat plane shape is its low surface area per volume ratio, thus requiring a large space when a huge volume of products is desired. On the other hand, hollow fibre membranes offer the highest packing density, which is around 10,000m^2/m^3, thereby providing better productivity with less space requirement.

In this work, GO has been synthesized using modified Hummer's method, which offers a safer reaction and ease in terms of large production. In addition, ceramic hollow fibres have been used as membrane support due to several advantages offered by this ceramic material, combined with hollow fibre configuration. The versatility of GO membranes has been explored with regard to different solution-based applications, involving a few modifications to GO to suit the application process. At the same time, the microstructure and stability of the membrane is properly understood, while the separation mechanism is discussed.

1.2 Research Objectives

Graphene oxide is considered as a new membrane material and has been proven to be feasible in different separation applications. However, due to the thin features of GO, a support is needed in order to obtain a good membrane that can withstand high pressure difference during separation process. In addition, in literature, the stability of the membrane in dry and wet environment has not been investigated. Furthermore, the performance of the membranes in

terms of permeance and selectivity is still considered low compared to commercialised membranes. Moreover, the proposed transport mechanism of separation with GO membranes has not been fully understood especially when GO membranes are applied in different separation application. Thus, the main objective of this study is to address the aforementioned research gap, which is to develop a highly stable and improve GO membranes performance using ceramic hollow fibre as a support, and provide an insightful discussion on the separation transport mechanism and finally employ it in different solution-based applications. In order to fulfil the main objective, the following specific objectives are to be completed:

i) To investigate the integrity of GO membranes in dry and wet environments

Before GO membranes can be employed in either gas separation or solution based application, it is crucial to understand the integrity of GO membranes in dry or wet environment. This can be achieved by systematically investigate the gas tightness of the GO membranes as it was identified previously that defect free GO membranes were impermeable to gas as small as helium [2] . Thus, gas-tightness of the membrane will be a good indication to resemble the integrity of the GO membranes in dry air. Moreover, the integrity of GO membranes in water has also been taken as precaution since GO is hydrophilic and will have a tendency to re-disperse when immersed in water. To this subject, proper pre-treatment such as control drying of as-prepared GO membranes or cross-linking with cation are important to be taken into consideration in order to ensure the integrity of the membrane in the water. Once the integrity of GO membranes in air and water is understood, the proper precaution, treatment and storage methods were proposed before GO membranes are employed for subsequent solution-based applications such as nanofiltration, desalination and pervaporation.

ii) To investigate the stability performance of GO membranes

The feasibility of GO membranes has been proven in various solution-based application such as nanofiltration [10, 11], but the stability performance remains unclear. Thus, it is crucial to address the gap by investigating the performance stability of GO membranes in dry air and in water for certain interval of time. This would be beneficial in future for a proper experimental procedure as well as storage of the GO membranes.

iii) To improve the performance of GO membranes.

The performance of GO membranes in solution-based applications is considered as still quite far away when compared with the state-of-the-art membranes, thus it is an important task to overcome this limitation. To achieve that, GO membranes with interesting characteristic such as various oxygen functional groups decorated on the surface as well as at the edge of the GO sheets were modified or crosslinked. The performances of modified and crosslinked GO membranes in terms of permeance and selectivity were investigate in desalination of divalent and monovalent ions as well as pervaporation dehydration of ethanol.

iv) To discuss a new perspective on proposed transport mechanism of separation with GO membranes

A few transport mechanisms that govern GO membranes when applied in separation application have been proposed in literatures and are is still debatable. It is understandable that it is quite difficult to reach a conclusion on the transport mechanisms as different factors have to be taken into consideration such as the nature of the separation process itself, differences in driving force, various solutions used as feed, the nature of GO membranes itself, etc., as they would affect the overall performance of the membranes and simultaneously the transport mechanisms. In this study, a new perspective with regards of the proposed transport mechanisms from literatures have been discussed for different solution-based applications.

1.3 Thesis Scope

The thesis consists of seven chapters and addresses different aspects regarding the development of GO hollow fibre membranes and their feasibility in different solution-based applications. Chapter 1 briefly introduces the background and main objectives, together with the structure of the thesis. Chapter 2 presents an understanding of the current findings and knowledge of GO for membrane separation, as well as an overview of the transport mechanism of GO membranes during molecular separation.

Chapter 3 describes the preparation method used in synthesizing GO suspensions and fundamental characterizations. In addition, the fabrication of GO membranes supported on ceramic hollow fibres are systematically elaborated for future reference.

Chapter 4 investigates the feasibility of GO membranes to be employed in nanofilration. In addition, the stability performances of GO membranes in dry air and wet environments are systematically carried out over a three-week interval period.

Chapter 5 explores the feasibility of GO membranes for smaller ionic species, such as sodium chloride. Cation cross-linking with GO membranes is carried out to investigate the effects on salt rejection performances.

Chapter 6 further explores the feasibility of GO membranes in pervaporation. In this chapter, the surface GO membranes are modified by hydrophilic silane, while the performance in relation to the dehydration of ethanol is investigated.

Finally, Chapter 7 is a summary of the main conclusions from this work, covering various important findings from Chapters 3 to 6, followed by some suggestions for future work concerning this subject.

CHAPTER 2

Literature Review

2.1 Introduction to molecular filtration and separation

Deteriorating water resources, alongside increases in water consumption, have forced people to opted for more advanced technologies in water treatment. Membrane technology has successfully implemented energy efficient and environmentally sustainable processes to deliver safe water supplies. Membrane is defined as a barrier with an ability to allow for the permeation of certain species, while blocking others, depending on the characteristic of the membrane and the species to be filtrated. Research in membrane technology has grown rapidly, with several types of membrane successfully implemented across various industries, such as in the purification of water, food industry processing and desalination. Research in the membrane area is still evolving, with scientists and engineers developing more cost-effective and precise membrane materials, which suit various industrial applications with different species to be treated. Indeed, there are already certain membranes that are well established in industry, but accuracy, ability and cost-effectiveness vary, depending on the membrane types, while improvement in these types of membrane are very much anticipated.

Membrane technologies can be divided based on the difference in the solute's particle size and the membrane pore structure. Table 2. 1 summarizes the types of membrane processes, which are reverse osmosis (RO), nanofiltration (NF), ultrafiltration (UF) and microfiltration (MF).

Table 2. 1: Characteristics of pressure driven membranes [12]

	Microfiltration (MF)	**Ultrafiltration (UF)**	**Nanofiltration (NF)**	**Reverse osmosis (RO)**
Permeability ($l/h.m^2.bar$)	>1000	10-1,000	1.5-30	0.005-1.5
Pressure (bar)	0.1 - 2	0.1-5	3-20	5-120
Pore size (nm)	100-10,000	2-100	0.5-2	<0.5

Current membranes, which have been established in terms of design, transport mechanism and industry, are classified as either polymeric [13-17] and inorganic membranes [18-23]. Polymeric membranes have been known for their high perm-selectivity and fast permeation, but low tolerance to harsh conditions, such as high acidity and alkaline environments, as well as limited resistance to high temperature conditions. On the other hand, inorganic membranes, mainly ceramics and metals, possess superior thermal properties and high mechanical and structural strength. The main disadvantages of inorganic membranes include the expensiveness of materials and the lower reproducibility of high-quality final products. Nevertheless, numerous efforts have been made to overcome these limitations.

Most recently, well-defined nanostructured materials, such as metal organic frameworks (MOFs), zeolites and carbon-based materials, have demonstrated a tremendous potential as membrane materials, due to the fact that this type of material possesses pore sizes that can be controlled precisely. Among them, carbon-based materials, mainly carbon

nanotubes (CNTs, have attracted considerable attention as possible membrane materials for molecular separation. CNTs represent unique nanochannel materials, which allow for the ultra-fast transport of molecules, as well as outstanding mechanical strength [24-29]. While research continues in discovering the interesting features of CNTs, graphene and the derivatives has gaining more attention by researchers.

The new carbon-based materials – namely, graphene consisting of 2D sheets composed of sp^2 hybridized carbon atoms, were first isolated in 2004 [30], where this material was exploited for various applications in electronics and optoelectronics, and, latterly, as a membrane material. When it was first discovered by Geim and Novoselov [31], they produced this graphene using the 'Scotch tape' method, whereby bulk graphite was exfoliated into single sheets of graphene.

Pure graphene, which contains no defects, is impermeable to any molecules, including those as small as helium, due to the closely packed arrangement of carbon atoms in the lattice [31]. On the other hand, GO, one of graphene's derivatives, is an exciting candidate as a membrane material, since it possesses a rich chemistry of different oxygen functional groups, resulting in different interactions between ions and GO. These functional groups, which are rich in oxygen, result from oxidation during the synthesis process, in which graphite is used as the raw material. Furthermore, its tuneable microstructures and physical properties allow for the effective design at the molecular level for the transport of selective fluid. All of these interesting characteristics offer exciting opportunities for exploring GO as an alternative material to produce high performance and economical membranes. In addition, GO nanosheets can be assembled into a laminar structure via filtration or coating methods, which provide fast and selective 2D nanochannels for enhanced molecular filtration [32]. The ground breaking work by Nair and colleagues was the first discovery of GO as a membrane material and achieved a fundamental understanding regarding molecular transport in GO membranes [2]. In their work, they found that GO membranes with a sub-micrometre thickness would allow

unimpeded water, while blocking everything else in vapour form. Although the molecular transport mechanism in GO membranes is still in debate and not fully understood, there is still copious opportunities for new studies and developments in respect of this outstanding material to be made.

Sp²and Sp³ structure of graphene and graphene oxide

It is understandable that the flexibility of graphene structure could be reflected by its electronic properties. It is well known that carbon can form different bonding through orbital hybridisation. In this case, the sp^2 hybridisation of graphene occurs when the carbon atom is bonded to three other carbon atoms. In details, the hybridisation occurs between one *s* orbital and two *p* orbitals resulting a trigonal planar structure with a formation of σ bond between carbon atoms that are separated by 1.42Å distance [33]. Similarly, from Figure 2.1 (a) Alzahrani has demonstrated from simulation calculation that the C-C bond length to be 1.41Å which is smaller than C-C bond length in diamond, which is 1.52Å. In addition, the C-C-C angle is measured to be 120° which is slightly larger than the diamond structure (109.5°)[1].

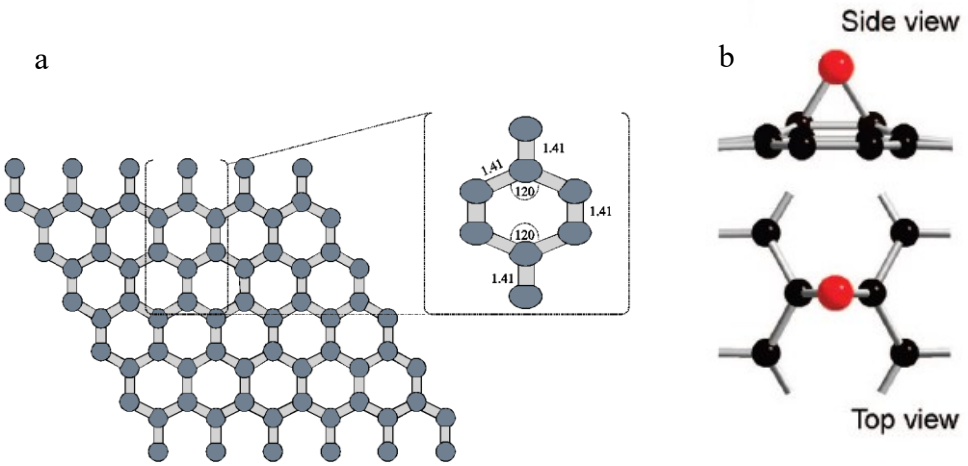

Figure 2. 1: (a)Schematic figure of pristine graphene. Inset shows structural parameters of the hexagon ring with bond length in Å and angles in (°) [1]. (b) Atomic structure of graphene sheet with single O atom bonded to two adjacent C atoms [4].

Graphene oxide, on the other hand is a combination of sp^2 and sp^3 hybridisation structure. Mkhoyan et al. [4] has revealed that the average surface roughness of GO is 0.6 nm and the structure was amorphous. The amorphous structure of GO was due to distortion from the high fraction of sp^3 C-O bonds which is around 40% for O/C ratio of 1:5. The change of the structure of graphene into amorphous graphene oxide can be explained by sp^2 bonds of carbon atoms have been modified into sp^3 bonds via oxygen bonding and the process of removing carbon atoms from their original sites in order to accommodate the off-plane sp^3 bonds. Figure 2.1 (b) shows the atomic structure of GO, and based on DFT calculation, it showed that the two carbon atoms bonded to oxygen atom are pulled above from the graphene planes. In addition, they revealed that the bond length between the two carbon was expand from 1.407Å for graphene to 1.514Å for graphene oxide.

2.2 Consideration of GO as a membrane material

History: Graphene oxide, previously named as graphite oxide, is essentially wrinkled 2D carbon sheets with several different oxygenated functional groups situated on the basal planes and peripheries. The thickness of GO is around 1nm, while its lateral dimension varies from a few nanometres to several microns [34]. The history of GO started with an unintended discovery by Brodie [7]. In 1859, Brodie, who was a professor at the University of Oxford, was attempting to find the molecular weight of graphite. Brodie noticed that graphite had very different properties to other carbon forms, such as diamond or charcoal. Believing that graphite was a unique element, he hypothesized that the best way to perform elemental analysis on graphite was to oxidize the graphite. While he already knew the molecular weight of hydrogen and oxygen, graphite was the only missing piece of puzzle.

The only major drawback to Brodie's finding was the use of dangerous chemicals. After the fundamental findings by Brodie, Staudenmaier introduced some changes in 1898 in response to Brodie's work in order to improve the oxidation process of graphite [35]. A century later, in 1957, Hummer and Offeman developed a safer oxidation method [36]. In present, GO has a potential to Today, GO has the potential to facilitate thousands of different applications. Although GO was discovered almost 160 years ago, it has only attracted the scientific community in this last decade, simply because it is regarded as a graphene pre-cursor. Despite its strong relevance as graphene's pre-cursor, GO itself possesses a strong scientific importance as a basic form of oxidized carbon, with various interesting properties able to be realised in different applications.

2.2.1 Ease of synthesis method

One of the main advantages of using GO in terms of membrane materials is the practical and simplified method involved. A simple method, such as the modified Hummer's method, enables GO to be produced on a large scale. Over the years, there has been commitment to evolve and simplify the methods in order to make them safer and practical, while simultaneously increasing the GO yield. Herein, GO synthesis methods will be briefly reviewed in chronological order, starting with the Brodie, Staudenmaier, Hummer's, modified Hummer's and Tour methods.

2.2.1.1 Brodie's and Staudenmaier methods

Brodie's method: In the 19th century, as was mentioned earlier, Brodie prepared the first batch of GO while investigating the chemistry of graphite. In his work, having known that graphite was unreactive in response to strong oxidants, he used potassium chlorate ($KClO_3$) and nitric acid (HNO_3) as the oxidising agents. The addition of $KClO_3$ into a slurry of graphite, along

with fuming HNO_3, produced a new batch of compound, which later on was found to contain carbon, oxygen and hydrogen. In the next step, the batch free from salts produced during the reaction was washed, dried at 100°C and again subjected them to an oxidation environment again. After three repeated treatments, the appearance of the substances was changed to a light yellow colour, which consequently did not change alongside any additional oxidation treatments. When he weighed the substances, there was a gain in weight with the original graphite, which indicated oxidization.

In the experiment, he highlighted that by one prolonged treatment, the product was difficult to produce. In order to maintain the original condition of the substance, the oxidation process had to introduce each time [7]. He proposed the molecular formula of the final product to be $C_{11}H_4O_5$, based on his elemental analysis, while naming it as graphitic acid. In addition, the substances were very small in size, as well as possessed limited thickness and an imperfect structure, which he deemed to be a crystal. Nevertheless, his observation and conclusion were limited not only on theories basis, also on the characterisation techniques available during the research conducted, thus leaving a considerable scope for further improvement.

Staudenmaier method: Nearly 40 years later, Staudenmaier improved the Brodie's method by making two major changes [35]:

1. By adding in multiple aliquots of potassium chlorate over the period of reaction.
2. By introducing concentrated sulphuric acid (H_2SO_4), to increase the acidity of the mixture.

These alterations have managed to produce a highly oxidized GO product, in which the composition remain unchanged as obtained by Brodie. The approach introduced by Staudenmaier made the reaction much simpler and more practical in terms of performing it in single-reaction vessels [35].

2.2.1.2 Hummer's method and modified Hummer's method

Only 60 years after Staudenmaier's accomplishment, Hummer and Offeman developed a different approach in synthesizing GO [36]. The two chemists from Mellon Institution of Industrial Research established an oxidation reaction of graphite with a mixture of concentrated sulphuric acid (H_2SO_4), sodium nitrate ($NaNO_3$) and potassium permanganate ($KMnO_4$) at 45°C [36]. They claimed that the overall oxidation process was complete within 2 hours, producing a higher degree of oxidation of the final product compared to Staudenmaier method. However, it was later found that the product of the Hummer's method was from an incomplete oxidation of graphite, such that the pre-expansion process is beneficial in terms of achieving a higher degree of oxidation. A pre-treatment of graphite with a mixture of H_2SO_4, $K_2S_2O_8$ and P_2O_5 at 80°C for several hours was comprehensively implemented after it was first introduced by Kovtyukhova in 1999 [37]. Prior to oxidation with the Hummer's method, the pre-treated mixture was diluted, filtered, washed and dried. Later on, it was found that, if the graphite flakes were expanded or the size of the flakes was smaller, those tedious pre-treatments could be skipped.

Several modifications to the Hummer's method have been made by increasing the amount of potassium permanganate, adding phosphoric acid in proper proportions, excluding sodium nitrate, increasing the reaction time etc. [38, 39]. These modifications should increase the degree of oxidation and improve the final production of GO. GO product made by the modified method comprises a typical thin flakes with 1 nm thickness and around 1 μm of lateral dimension on average. The degree of oxidation and GO yield have been comprehensively improved than the original results produced by Brodie's method. Nonetheless, the separation and purification process of GO using the modified Hummer's method is still rather complicated

and time consuming. More details on the reaction involved in the modified Hummer's method will be presented in Chapter 3.

2.2.1.3 Tour method

The improved modified Hummer's method, or the Tour method, was first introduced in 2010 by the Tour Group from Rice University. This group avoided using sodium nitrate, while increased the amount of potassium permanganate. In addition, they also introduced a new acid, namely, phosphoric acid, into the reaction vessel [39]. By performing the reaction in a 9:1 ratio of H_2SO_4/H_3PO_4 in six equivalents of $KMnO_4$, the group improved the efficiency of the overall reaction, as well as proved that adding extra $KMnO_4$ provided a greater amount of hydrophilic oxidized GO materials. The biggest advantage of implementing this method is the elimination of $NaNO_3$, which results in the avoidance of the generation of toxic gas, such as NO_2, thus making it more environmentally friendly

2.2.1.4 Summary of the GO synthesis method

In summary, at least four different methods have been developed for the GO synthesis throughout history. It is quite encouraging to see different synthesis approaches and improvements in terms of the oxidation degree, ease, safety, yield and the quality of the final product. Figure 2. 2 summarizes the general steps in producing GO, regardless of the type of oxidant mixture used. More importantly, the main aim of this GO synthesis procedure is to produce a purified GO suspension, which ought to suit many different applications.

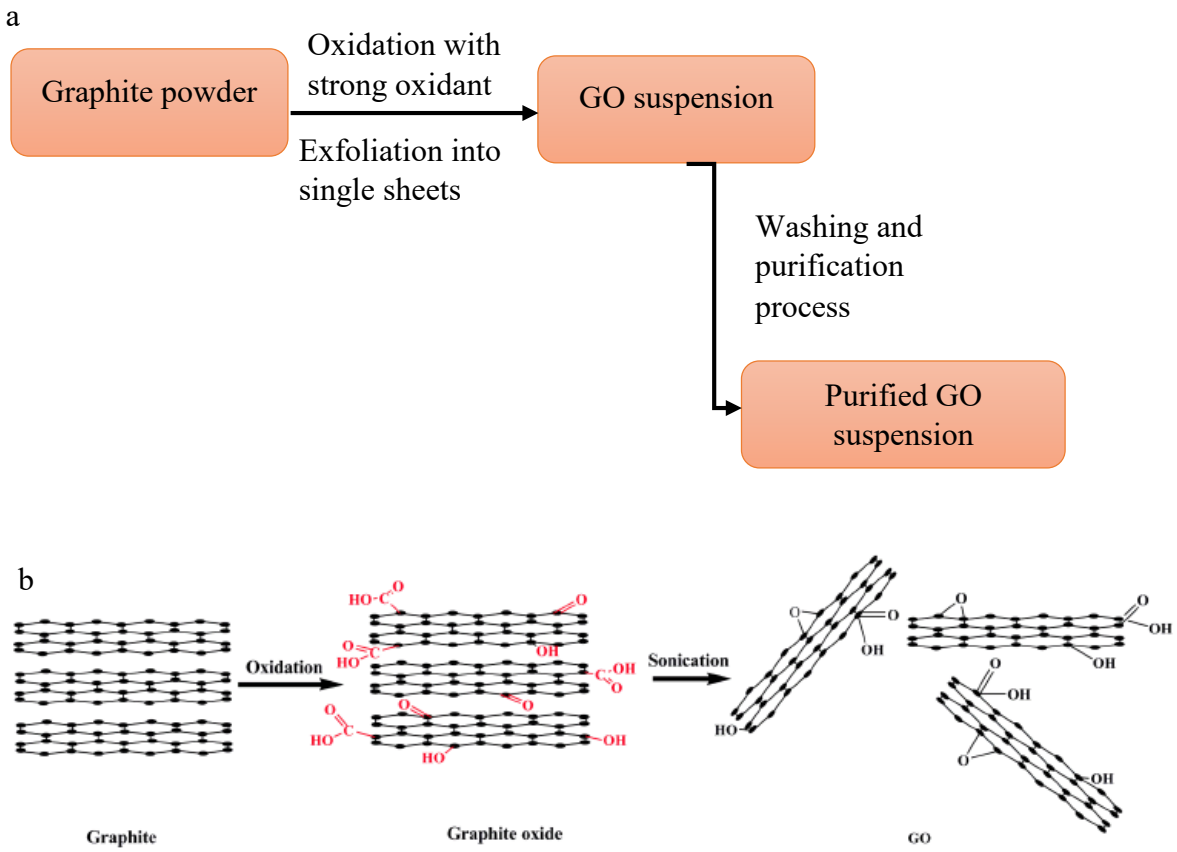

Figure 2. 2: (a) General procedure in GO synthesis; (b) schematic diagram illustrating the fabrication mechanism of GO from graphite [40].

2.2.2 Unique structure of GO

On a fundamental level, GOs are monolayer-thick and 2D nanomaterials. Although the exact chemical structure of GO has been debated for many years, Lerf-Klinowski proposed a generic model, which has been widely accepted by the scientific community [41, 42]. It was not an easy path to propose the structure, in which various techniques have been used: 1) solid-state nuclear magnetic resonance (NMR) spectroscopy, 2) elemental analysis, 3) X-ray diffraction analysis, 4) FT-IR spectroscopy and 5) material reactivity.

Since GO is a product of strong oxidation processes, its atomic structure is quite disordered from the original graphene, which is a perfect hexagonal lattice of a crystal structure. From the proposed structure, the single layer sheet of GO usually consists of oxygen-rich functional groups, namely hydroxyl and epoxide that are located on the basal plane and carboxyl, carbonyl and phenols on the edge of sheets [8, 41, 42]. These negatively charged functional groups will interact with molecules or ions with different strengths, depending on their atomic charge and polarization. Furthermore, the oxygen functional groups have successfully made GO a hydrophilic material. This, will decrease the interaction energy between the graphene layers (thus increasing the interlayer distance from ~0.35 nm in graphite to ~0.7-1.0 nm in oxidized form) [43], in turn forming a stable dispersion of GO in various solvents, such as DMSO, THF and NMP, and, most importantly, water [44].

In addition, experimental evidence suggests that GO also consists of defect-free graphene areas (graphitic area) in the sp^2 configuration [4, 45-49]. Thus, in general, GO has two types of areas: functionalized (oxidized) and pristine (non-oxidized/graphitic area). The former area acts as a spacer, which keeps the sheets at a distance and, at the same time, accommodates water to intercalate between the sheets, once it is in the hydrated state. On the other hand, the non-oxidized area provide a interlayer space, which allow for an almost frictionless water flow [2].

Various oxygen functional groups located on the basal and edge of GO sheets make them hydrophilic, as well as easily dispersed in water, hence providing a facile processing and stacking of those sheets. Using various methods, GO sheets dispersed in water can be easily arrange into a macroscopic laminar membrane such as filtration and coating [2, 3, 5, 11]. Figure 2.3 is an example of free-standing GO membranes in the form of flat sheets and (a) a cross-section of SEM images (b) showing a paper-like structure of micrometre GO membranes. The

resulting GO laminates possess exceptional mechanical strength due to the strong hydrogen bonds between adjacent GO layers, which hold all the sheets strongly together.

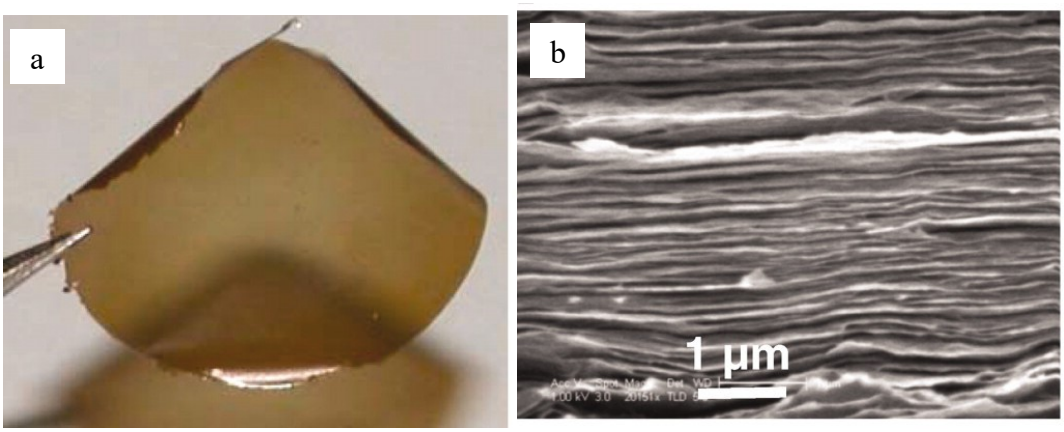

Figure 2.3: (a) Free-standing GO membrane after being peeled off from the substrate; (b) Cross-sectional SEM image of a GO membrane [2].

Furthermore, one of the most fascinating characteristics of GO is the fact that modification or functionalization of the structure can be carried out before or after the sheets are assembled into membranes to suit different application requirements. The modification can be done in relation to the objectives to tune the defects, nanopores they made, density and spatial distribution of functional groups, and the lateral size of sheets as well as the surface charge of GO [50-55]. The structure of GO membranes in liquid solvents is found to rely on the types of liquid molecules they interact with. For example, when GO membrane is immersed in ethanol, the membrane swallowed and change in XRD peak to 11.21Å which correspond to about one monolayer of ethanol at room temperature. In contrast, when GO membranes immersed in water, the XRD peak shift to around 12.27Å which can be attributed to insertion of two monolayer of water. Moreover, when GO membrane is immersed in mixture of ethanol and water, it can be observed that only one monolayer of ethanol is intercalated irrespective

what is the concentration of the mixture. In contrast, water will be hindered to enter the interlayer space of GO in high concentration alcohol mixture due to blockage from the ethanol itself and water will intercalated into the interlayer space only in high concentration water mixture condition [56]. Nair et al. also found that the interlayer distance changes, based on relative humidity, i.e., at a relative humidity of around 30-70%, with the interlayer distance changing from 0.7-1 nm, respectively [2].

2.2.3 Ease of functionalization; versatility

By exploiting the advantages of the rich oxygen functional groups on the basal plane, as well as on the edge of the GO sheets, these oxygen-reactive sites can be covalently functionalized in order to fulfil specific requirements for various applications. In addition, since GO is a mixture of sp^2 and sp^3 networks, the pristine sites (sp^2) on the GO sheets can also be non-covalently functionalized either through π-π stacking, cation-π or Van der Waals interaction.

2.2.3.1 Covalently functionalized GO

From the structural models proposed by Lerf-Klinowski [8], it is clearly shown that GO sheets have reactive oxygen functionality, such as epoxy and hydroxyl, at the basal plane, along with carboxyl and carbonyl-functional groups terminated at the edges. This reactive oxygen functional group provides a reactive site for covalent functionalization with a significant number of modifying reagents.

The modification of the epoxy group at the basal plane of GO could be as a result of nucleophilic substitution reaction. The study was conducted by Yang et al., using 3-amino-propyltriethoxysilane (APTS) grafted on graphene sheets. They suggested that silane moieties were grafted through nucleophilic, S_N2 displacement reaction between the epoxide group of

GO and the amine groups of APTS. The resulting silane-functionalized graphene was then incorporated into a silica monolith, which showed an improvement in mechanical strength and toughness performance [57]. In addition, Koushik and colleagues employed 3-glycidoxypropyltrimethoxysilane (GLYMO) to covalently functionalize the epoxy group of GO by using epoxy polymerization with aluminium acetylacetonate as a catalyst. The functionalized GO was subject to thermal reduction, while the final black products showed a better absorption of light and less reflectivity (≤ 1%), as well as electrical conductivity, thereby confirming a productive material for applications in light harvesting and electro-optical devices [58].

One of the modification examples for GO in relation to carboxylic functional groups was demonstrated by Park and colleagues. In their study, the aim was to enhance the mechanical strength of GO sheets via modification with divalent ions, that is, Mg^{2+} and Ca^{2+}. They found that the mode of interactions for the divalent ions with the GO sheets involved bridging the edges of the sheets through carboxylate chelates with the metal and intercalating between the basal plane and the hydroxyl groups or carbonyl. The former mode of binding was believed to be stronger, while the latter interaction was weak and could easily be removed by water rinsing. Thus, they concluded that the enhancement in the mechanical strength of the GO sheets resulted from the reaction with the carboxyl group of GO sheets [59].

2.2.3.2 Non-covalently functionalized GO

In addition, the non-covalent interaction of GO is also possible and primarily involves the Van der Waals interaction and π-π stacking, as well as cation-π stacking. These non-covalent bindings occur on the available sp^2 sites, which are not oxidized. Pyrene-functionalized poly(methyl methacrylate)-*block*-polydimethylsiloxane (Py-PMMA-*b*-PDMS) were used to

functionalize GO through π-π interactions between pyrene and the sp^2 sites. The modification resulted in an increase in the tensile strength, as well toughness [60]. On the other hand, Sun et al., systematically explored cation-π interactions of different types of cations (K^+, Mg^{2+}, Ca^{2+} and Ba^{2+}) and demonstrated that these interactions were responsible for the selectivity of GO membranes with regard to the penetration of different ions [55].

2.3 Fabrication of GO membranes

2.3.1 Fabrication methods for assembling laminar GO membranes

There were various different methods used in producing GO membranes in order to enable them to be used for different applications. GO membranes can be produced as free-standing or as a coat on the membrane support. The fabrication methods include vacuum filtration, pressurization, evaporation and different types of coating approaches, such as dip coating, spin coating, spray coating and drop casting [5, 9, 61-65]. Different fabrication methods were said to affect the microstructure of GO membranes, which impacted on the final formation of the stacking of, as well as the defects within the membranes. GO membranes, which were fabricated by pressure-assisted filtration, vacuum-assisted filtration and the evaporation method, produced three very different microstructures (Figure 2.4 (a)). The microstructures produced by the three different methods were highly ordered, loose and significantly random. The different stacking formations resulting from the different fabrication method also affected the performance of the membrane, with the pressure-assisted filtration showing the best performance in butanol dehydration due to a more ordered laminar structure [3]. It is believed that the water flow in the interlayer space, alongside with the electrostatic and Van der Waals forces, was mainly responsible for the sequential deposition of GO membranes into the laminar structure [32].

Besides the filtration method, another method to produce GO membranes is through various coating approaches, such as spray coating[2], spin casting [5] and drop casting [11]. Kim et al., compared the microstructure of GO membranes created with two different methods (Figure 2.4 (b)). The microstructure of the GO membrane produced by method 1 (contacting the support membrane surface to the air-liquid interface of the GO suspension, followed by spin coating) created GO membranes with a less interlocked structure. On the other hand, method 2 (spin casting of GO suspension onto the surface substrate) produced a highly interlocked GO membrane structure, which resulted in a higher selectivity of CO_2 [5].

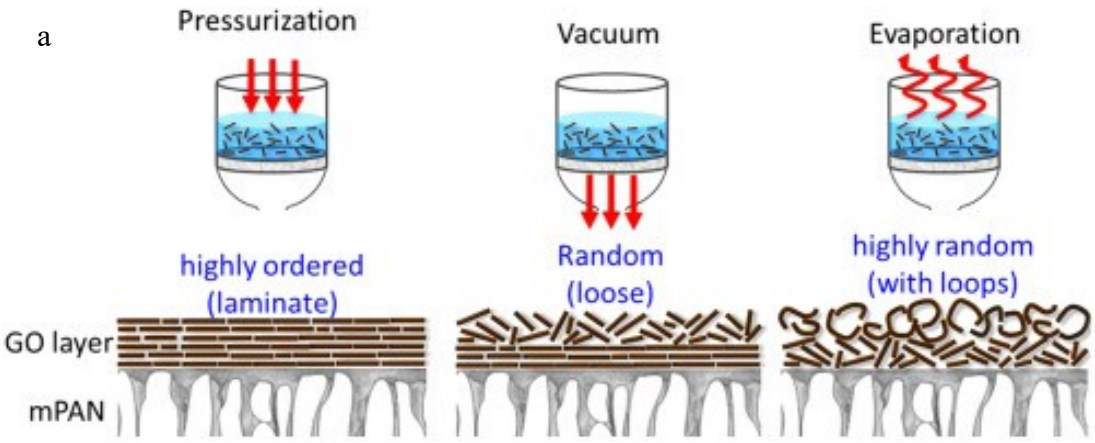

Figure 2.4: (a) Schematic GO membrane fabrication using three different methods (pressurization, vacuum and evaporation) [3]; (b) schematic GO membrane fabrication using the spin casting method; method 1: dip spin casting; method 2: drop spin casting [5].

2.3.2 Fabrication of ceramic hollow fibre as membrane support

Generally, it is important to produce thin GO membranes as a separation layer for filtration applications, which ought to be beneficial due to the reduced membrane resistance, such that high permeation fluxes may be obtained. The thin separation layer must be accompanied with a porous support layer in order for it to withstand high pressure differences across the membrane. Ceramic hollow fibre is an excellent candidate in terms of the material and geometry as a support material. It exhibits numerous advantages, such as high packing density, cost-effectiveness and higher tolerance at high temperature and under harsh conditions when compared to polymeric membranes and disk membranes.

In terms of ceramic hollow fibre membranes fabrication, there are three main steps when using combined phase inversion and sintering techniques: spinning suspension preparation, hollow fibre pre-cursor spinning, hollow fibre membrane sintering. The fabrication process is briefly discussed below.

2.3.2.1 Ceramic hollow fibre spinning suspension preparation

In order to prepare for a spinning suspension, there are four main components required: ceramic powders, polymer binder, additive and solvent. The main steps in the preparation of a spinning suspension are [66]:

1. Mixing solvent with dispersant
2. Adding ceramic particles to the solvent and dispersion suspension
3. Adding the required additives and binders

In the preparation of the spinning suspension, ceramic powder is the most important component, as well as being the final material for the hollow fibre, while others will be removed during the sintering process. The selection of ceramic powders with regards to their particle size and distribution is crucial since it will affect the final product of the membrane. The function of the other three main components is to predesign the morphology of the membrane, including the porosity, cross-section of the membrane and pore size. In addition, the other components facilitate the spinning and sintering process. A polymer binder is required in order to connect the ceramic particles for the ease of extrusion during the spinning process. The polymer binder used in the suspension preparation must be fully removed without leaving any residue during the sintering process of the membrane. One of the polymers that is commonly used in the fabrication of ceramic hollow fibre is polyethersufone.

On the other hand, additives used for the fabrication of hollow fibre membrane can be dispersant, anti-foaming, pore formers and chelating, depending on spinning suspension requirements. When ceramic powders are dispersed in the solvent, this tends to form agglomerates, such that adding dispersant can be beneficial. The dispersant will break down the soft agglomerates and disperse the primary particles, while keeping them in a homogenous suspension. In order to ensure the stability of the suspension, the amount of the dispersant needs to be maintained.

During the preparation of the spinning suspension, the solvent used must be capable of dissolving the additive and polymer binder. The exchange rate of the solvent with non-solvent/coagulant must be high, since it has important effect on the final membrane structure [23]. It is crucial to make sure that the spinning suspension is homogeneous, since it will determine the mechanical strength of the membrane by removing structural defects. Ideally, different particles sizes of spinning suspensions are preferred, such that the voids between the particles can be fill in by the smaller particles, thus increasing the packing density. In addition,

the spinning suspension components ratio should be properly controlled to avoid any unwanted residues, which will affect the final membrane products.

2.3.2.2 Ceramic hollow fibre pre-cursor spinning process

The phase inversion mechanism for ceramic hollow fibre membranes is usually different and more complicated than for polymeric membranes. Several parameters involved in the spinning process are important as they are directly associated with the structure and, in turn, the performance. The internal coagulant or bore fluid and external coagulant selection is critical as it affects the phase exchange and membrane voids formation. By varying the air gap, internal coagulant, flow rate and the polymer precipitation rate during the spinning, the membrane structure can be tailored [66].

2.3.2.3 Sintering process of hollow fibre pre-cursor

The final stage in ceramic hollow fibre fabrication is the sintering process, where the pre-cursor undergoes treatment at a high temperature. The main objectives of the sintering are to gain strength and to connect the ceramic powder without melting. The temperature during the sintering process is usually 50% to 80% of the melting temperature of the ceramic particles. During the high-temperature treatment process, all other spinning suspension components are burned out, except for the ceramic particles. A sintering profile, which includes temperature of the sintering process, dwelling time, heating and cooling rates, must be in an optimal condition. This is to make sure that the membrane pre-cursor withstand the entire sintering process without any defects. There are three main steps in the high-temperature treatment process [66].

1. Pre-sintering: The main purpose of pre-sintering is to remove any unwanted components from the membrane pre-cursor, including water, which might chemically combine with the ceramic particles. The heating rate was suggested to be as low as

possible, such as 1°C/min, in order to prevent any fractures due to the pressure produced from evolving vapour or different thermal expansion phases.

2. Thermolysis: In this stage, the purpose is to remove organic components, such as the polymer binder, dispersant and additives. All these organic components will be burnt out. Once again, a proper selection of the heating rate is vital to avoid any defects, such as cracks, deformations and distortions during this process.
3. Final sintering: During the final sintering process, major changes to the porosity and pore size will occur. In addition, the final shape of the hollow fibre membrane will be consolidated, while the membranes mechanical strength is improved.

2.4 Recent progress of GO membrane in solution based filtration

Pressure-driven separation using membranes is an important separation process, in which GO can be employed, based on their interesting characteristics. In the past two to three years, several breakthroughs have been made by researchers in the graphene-based membrane community, especially in nanofiltration, desalination and pervaporation [3, 10, 11, 51, 55, 61, 65, 67-69]. The distinctive mass-transport properties of GO membranes, such as ultra-fast permeation of water and outstanding selectivity for different types of solutes, result in benefits involving pressure-driven separations [2, 69]. Furthermore, increasing the pressure during separation will accelerate the permeation. In the following section, pressure-driven membrane processes related to GO membranes are reviewed.

Table 2.2 presents a summary of the separation performance of GO membranes for pressure-driven separation.

Table 2.2: GO membranes for pressure-driven separation

Membrane	**Membrane process**	**Fabrication method**	**Feed solution**	**GO Membrane thickness**	**Water flux (L $m^{-2}h^{-1}bar^{-1}$)**	**Rejection (%)**	Reference
Nanostrand-channelled GO/PC	Ultrafiltration	Vacuum filtration	Evans blue	2µm	695	83	[51]
Base-refluxing reduced GO/PVDF	Nanofiltration	Vacuum filtration	Methylene blue	22nm	21.8	99.2	[10]
				33nm	5	99.7	
				44nm	4.37	99.6	
				53nm	3.26	99.8	
Base-refluxing reduced GO/PVDF	Nanofiltration	Vacuum filtration	Na_2SO_4	53nm	3.26	60	[10]
			NaCl	53nm	3.26	40	
GO/PC	Ultrafiltration	Vacuum filtration	Evans blue	1µm	71	85	[52]
TMC-cross-linked GO/PSF	Nanofiltration	Layer by layer	Rhodamine-WT	5-50 layers	8-27.6	93-95	[70]
			Methylene blue			46-66	
			Na_2SO_4			24-46	
			NaCl			6-19	
GO-HPEI-EDA/Torlon	Nanofiltration	Layer by layer	$MgCl_2$	1-20 cycles	3.8-8	84-97	[67]
UV-enhanced GO/YSZ	Nanofiltration	Vacuum filtration	Methyl red	150nm	2.8	>90	[64]

***PC: polycarbonate; PVDF: polyvinylidene difluoride; TMC: 1,3,5-benzenetricarbonyl trichloride; HPEI: polyethylenimine; EDA: ethylenediamine*

From Table 2.2, Huang et al. produced novel nanostrand-channelled GO membranes by intercalation of positively charged copper nanohydroxide into negatively charged GO sheets. Subsequently, the GO membranes were partially reduced and the copper nanohydroxide nanostrands dissolved. This strategy successfully produced enlarged nanochannels with a narrow size distribution, which resulted in a 10-times higher permeance without sacrificing the rejection[51]. In addition, by tuning the filtration properties such as pH, salt concentration and pressure, Huang et al. observed that GO membranes could have obtained high rejection of Evans Blue at 85% with water flux of 71 L m^2 h^{-1} bar^{-1}. They explained that this performance could be due to molecular sieving effect as we all as charge effects of the membranes. By examined different types of solutes with different charges, they have shown that the nanochannels were selective towards one type of charges (negative charge), thus the rejection was highly dependent on type of the charge solutes where electrostatic repulsion could occur. Thus, they concluded that GO membrane rejection performance depend on the type and concentration of charge near the membrane surface. This was confirmed by showing the pH dependence of the membranes, in which at lower pH, the electrostatic repulsion between GO membranes was weaken due to the protonation of carboxylic acid. As a result, the flux rate was decrease and the rejection rate increased [52]. Moreover, Han et al. produced ultrathin GO membranes with the thickness from 22- 53nm and the prepared membranes were tested under dead end filtration. GO underwent a thermal reduce by refluxing GO in 0.01M NaOH aqueous solution for 1 hour. The base refluxing GO membranes has successfully rejected organic dyes with 99% rejection but lower rejection for salts (20-60%). The water flux high, which is the highest with the thinnest membranes as shown in Table 2.2. They concluded that the physical sieving and electrostatic repulsion governed the rejection mechanism [10].

Hu and Mi [70] produced GO membranes using layer by layer deposition method and crosslink them with 1,3,5 benzenetricarbonyltrichloride. The water flux varied with the number

of layer deposition and they have observed that the water flux did not show dependence on the thickness of the membrane. The membranes showed rejection over 90% for rhodamine WT dye and 46-66% for MB dye and again showed a poor rejection towards salt solution. Moreover, they noticed that rejection when salt concentration increased, which can be explained by the basis of varies debye length at different concentration of salts, thus affected the electrostatic repulsion between the salt ions and the charged membrane. Recently, Jeng et al. [64] has shown that GO membrane was not stable in dry air due to drying shringkage related problem. In order to stabilise the membranes, sacrificial layer using poly(methyl methacrylate) (PMMA) has been utilised to create space between the support membrane and the GO membrane thus allowing stress-free shrinkage. The defect free membrane was shown to be impermeable to gas and exhibit a very low water flux. UV-treatment has been done to induce control microstructural defects on the GO membranes, thus enhanced water permeability to 2.8 L m^2 h^{-1} bar^{-1} with molecular weight cut-off of 250 Da.

Thus, it can be summarized that the purification of water performance using GO membranes is evaluated by means of organic dye retention and salt rejection. In short, GO membranes present an outstanding performance in nanofiltration in terms of organic dyes rejection, such as evans and methylene blue with rejection rates of higher than 85%. In addition, most recently, GO membranes with reasonable water flux have shown a molecular cut-off of up to 230Da (methyl red). The efficient separation might be attributed to the molecular sieving effect of laminar GO membranes, as well as charge effects. Unfortunately, the rejection performance of GO membranes for divalent or monovalent salts is still poor (less than 50%), which could be due to the large interlayer distance that allows the passage of salts.

Furthermore, although the membrane's performance is important, the stability of the GO membrane, when employed in solution-based applications, should also be carefully considered. This is due to the fact that GO is known for its hydrophilic nature and can be readily

dispersed in water, which could cause it to either re-disperse or peel off from the support directly. So far, no studies have been conducted to investigate the structural stability of GO membranes in solution-based applications, which ought to be crucial before GO membranes are employed in real industrial applications.

Besides, GO membranes could be one of the potential membrane candidates for pervaporation applications. The transport of water between GO nanosheets and the intrinsic hydrophilicity of GO membranes could be beneficial in dehydration of solvents through pervaporation. To date, GO membranes have been explored in terms of the selective water removal from concentrated alcohol solutions, such as ethanol, n-butanol and isopropyl alcohol. Table 2.3 summarizes the GO membranes, which have been employed in pervaporation dehydration of solvents.

Hung et al. [68] has crosslinked GO membranes with different size of diamine monomers which resulted in varying interlayer space of the membranes. The crosslinked GO membranes produced interaction between C-N bonds that successfully suppressed the stretching of interlayer space when immersed in water as opposed to GO membrane with crosslinked that tended to swell when immersed in water. Crosslinked GO membrane with the shortest diamine monomers delivered the best performance of dehydration of ethanol with separation factor of 4,491 and total flux of 2.297 kg m^{-2} h^{-1}. Moreover, Tang et al. produced GO membrane using pressurized method and it was found that different pressure applied produced different packing density of GO membrane simultaneously affect the pervaporation performance. In addition, it was also found that concentration of water in the feed solution would affect the performance of GO membranes. At higher water concentration, the permeability of the membrane increased, but the selectivity was decreased because of the interlayer space of GO membrane swelled, thus increasing the interlayer space and allowed more ethanol to pass through.

Tsou et al. [3] fabricate GO membranes using three different methods; evaporation, vacuum filtration and pressure filtration. All these three different methods produce different microstructure of GO membranes and simultaneously affect the pervaporation dehydration of butanol performance. Between the three methods, GO membranes fabricate using pressure assisted method produce GO membrane with exceptional performance of 99.6% separation factor and 2.54 kg m^{-2} h^{-1} of total flux. They believed that this is due to more highly ordered GO membranes that effectively block permeation of butanol, hence better separation factor of the membranes.

In terms of transport mechanism in pervaporation, Huang et al. claimed that the transport mechanism in pervaporation dehydration of solvent was primarily decided by the membrane surface sorption ability, together with the diffusivity through the membrane. In addition, the preferential sorption of water on the membrane surface will cause water molecules to gather at the surface, thus impeding other molecules, hence better separation factor [71]. However, the transport mechanism of GO membranes in pervaporation remains unclear, with considerable work is still required.

Table 2.3: GO membrane performance for pervaporation

Membrane	**Fabrication method**	**GO membrane thickness**	**Feed condition**	**Total flux (kg m^{-2} h^{-1})**	**Separation factor**	**Reference**
EDA cross-linked GO/CA	Pressure-assisted self-assembly	412 nm	80°C, 90/10 wt% (ethanol/water)	2.297	4,491	[68]
Free-standing GO laminate	Pressurized	2 μm	24°C, 75/25 wt% (ethanol/water)	1.3	211	[63]
GO/Al_2O_3 tube	Pressure-driven filtration	260 nm	70°C, 90/10 wt% (ethanol/water)	1.1	250	[65]
			70°C, 90/10 wt% (n-propanol/water)	1.3	1,293	
			70°C,90/10 wt% (Isopropanol/water)	1.7	2,942	
GO/mPAN	Pressure-assisted self-assembly	231 nm	70°C, 90/10 wt% (1-buthanol/water)	4.34	1,791	[3]
GO/ceramic hollow fibre	Vacuum filtration	1 μm	25°C, 97.4/2.6 wt% (dimethyl carbonate/water)	1.702	743	[71]
GO-chitin/ceramic hollow fibre	Vacuum filtration	-	30°C, 90/10 wt% (1-buthanol/water)	>10	2,580	[72]

** *CA: cellulose acetate; mPAN: modified polyacrylonitrile*

2.5 Transport mechanism in GO membranes

2.5.1 Water transport through GO membranes

A study on the pure water transport across GO laminates was first investigated by Nair and colleagues [2]. In their study, they fabricated GO membranes via vacuum filtration. The prepared membranes were used for a leakage test. The sub-micrometre-thick GO membranes were completely impermeable to liquids, vapours and gases as small as helium, but allowed for the unimpeded permeation of water vapour. Figure 2.5 (a) shows the schematic transport path for possible water vapour transport through GO membranes. Nair et al., explained that, in GO laminates, hydroxyl and epoxy groups act as a spacer while pristine sites form 2D network capillaries. These 2D network capillaries provide the ultra-low friction of water molecules, which results in the ultra-fast flow of water. According to their model and explanation, as illustrated in Figure 2.5 (b), water can form a 2D network in pristine area, in which its expected to have faster mobility, similar with the CNTs case [26, 73]. On the other hand, on the oxidized region, water is expected to have slower mobility due to the interaction between the oxygen functional groups. However, in the case where humidity is low, the nanocapillaries will become narrow, in both oxidized and pristine area, which results in blocking of transportation of water [2].

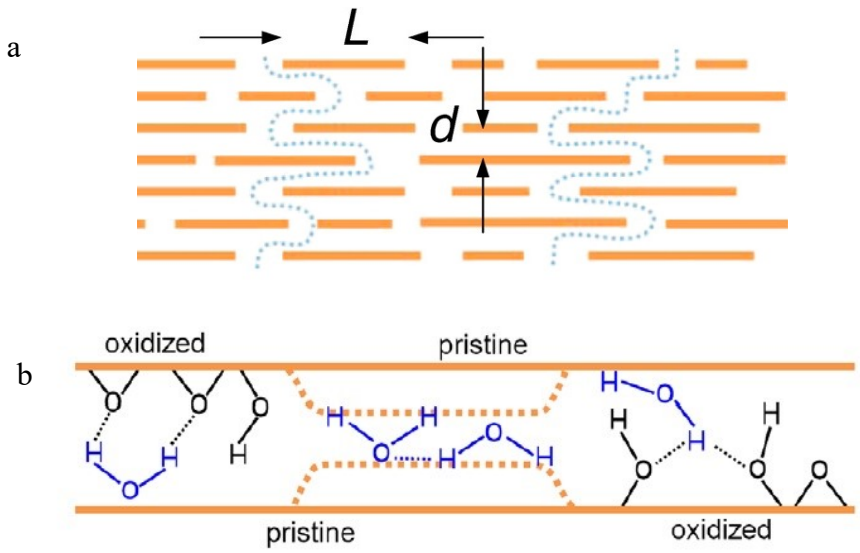

Figure 2.5: (a) Schematic transport of water vapour through GO membranes; (b) schematic model of nanocapillaries in GO films comprising pristine and oxidized regions [2].

Nair et al., described the permeation of water vapour through nanochannels of GO by assuming that the water inside these nanochannels behaves as a classical liquid, meaning that Poiseuille's law can be used to describe the flow between laminar GO membranes:

$$J = \frac{d^4 . \Delta P}{12 L^2 . \eta . h}$$

Where J is the flux, d is the size of the channels, L is the average lateral length of GO sheets, η is viscosity of water, and h is the thickness of the membrane. According to the outcome of this calculation, there was an enhancement in the flow by a factor of a few hundred for the nanoconfined water inside the GO laminates compared to the classical laminar regime. In addition, knowing that the basic assumptions of the Hagen-Poiseuille equation are laminar, with no slip (or liquid flow with zero velocity at the walls) at the boundary layer, the experimental flux was shown to deviate from the classical equation. This suggests that the velocity of the liquid flow at the pristine wall is not zero. Nair and his colleagues suggested

that an interfacial slip length of 10-100 nm was estimated in order to describe the flow enhancement of water in GO laminates.

The fast transport of water in GO was further observed by Han et al., in their ultra-thin GO membrane. They attributed the remarkably fast water transport to slip flow theory. The pristine region without functional groups provides fast water transport due to frictionless carbon walls. In order to verify the slip flow theory, they conducted tests with non-polar liquids, such as isopropanol, ethanol, hexane, cyclohexane and toluene. From the results, the flux for the non-polar liquids was much lower than water due to greater interaction between the more non-polar liquids and the hydrophobic pristine wall, which is consistent with the slip flow theory. Nevertheless, this should be treated with caution since slip flow theory itself is still a controversial topic [10].

Most recently, Wei and colleagues demonstrated that, by using atomistic simulation and theoretical analysis technique, the flow enhancement of water in GO membranes ought to be broken down due to a side-pinning effect by water confined between oxidized regions. In addition, they suggested that the flow enhancement might be majorly attributed to GO membranes porous microstructure, such as the expanded interlayer distance and the wide channel formed at the wrinkles, holes and at the inter-edge (Figure 2.6). Meanwhile, the boundary slip factor for the flow enhancement was less significant [68]. In addition, the recent experimental study by Wei et al., showed that GO membranes have a serious flux attenuation and obvious changes in surface morphology due to hydraulic pressure. They found that the structure of GO laminates and its support membrane change when compaction occurred. Wrinkles, as part of water channels in GO laminates, became narrower when pressure was applied, leading to higher permeation resistance. Thus, the flux of the GO membranes was reduced [74].

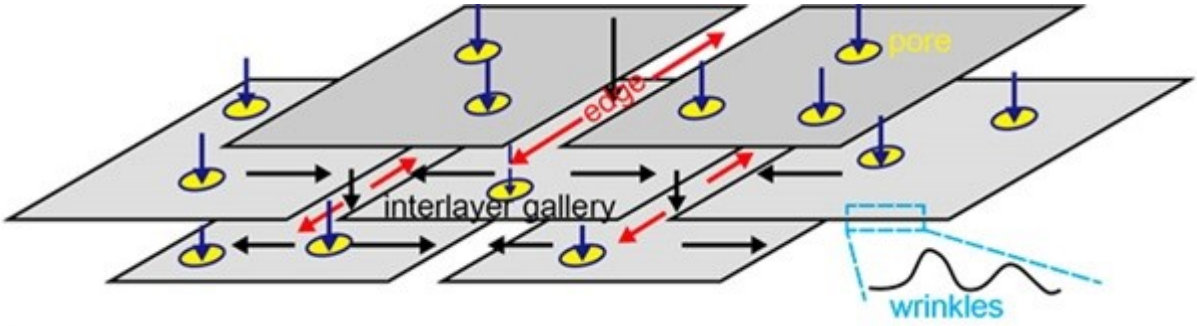

Figure 2.6: Proposed water transport through a GO membrane by Wei et al., [68].

In terms of the diffusion of water through the nanochannels, Sun et al., investigated the diffusion of water through nanochannels within GO membranes using isotope labelling techniques. The diffusion of water in GO membranes was investigated by dissolving a certain amount of deuterium oxide (D_2O) as a tracer to label the trace water. Subsequently, the transmembrane diffusion of D_2O was investigated in order to extrapolate it for water. It is noteworthy that, from the isotope labelling technique, they found that liquid water transport without external hydrostatic pressure through laminar GO membranes can result in an ultra-fast permeation with a diffusion coefficient of four to five orders of magnitude higher than that for the bulk case [75].

Nevertheless, water transport in nanochannels of GO membranes is not yet fully understood and is quite challenging to make any conclusions about the overall mechanism. Several factors have to be considered, especially the effect of the oxidized and non-oxidized (pristine) regions of GO membranes in either the enhanced or hindered flow of water. In addition, the porous microstructure of GO membranes is also important and must be taken into account when determining the transport mechanism of GO membranes.

2.5.2 Solute permeation through GO membranes

The selective transport of solutes through GO membranes was systematically investigated by Sun and colleagues [11]. In their study, the GO membranes were prepared by simple drop casting methods, while the penetration properties of sodium salts, heavy metal salts, organic contaminants and the mixture of their aqueous solutions were investigated. From the permeation studies, the sodium salts permeated through the GO membrane rapidly, as opposed to heavy metal salts, which permeated at a much slower rate. Furthermore, copper sulphate and rhodamine B (RhB) were almost completely blocked because of the strong interaction with the GO membrane. They believed that nanocapillaries, formed within the lamellar structure of the GO membrane, together with the chemical interaction of metal ions with the oxygen functional groups of the GO membrane, were responsible for the selective permeation.

Recently, Sun et al., further studied the mechanism related to selective ion permeation through GO membranes [11, 55]. The proposed mechanism is represented by Figure 2.7. Alkali and alkaline earth prefer to interact through cation-π interaction with the sp^2 cluster of GO membranes. On the other hand, transition-metallic cations prefer to interact with the sp^3 C-O matrix via coordination interaction. In addition, from their simulation results, the binding energies between metal atoms and graphene follow the order of K > Ba > Na > Ca > Cu > Cd, which further reveals that cation-π interaction is much stronger for main groups of metal ions, as well as further proves that transition metal cations would preferentially coordinate with the sp^3 matrix.

Moreover, electrostatic repulsion can be one of the factors that contributes to the selectivity of ions through GO membranes. The negative charge originating from the ionization of the attached oxygen functionalities might give rise to the electrostatic repulsion of anions and the electrostatic attraction towards cations in solutions. According to the exclusion theory, the potential at the interface of the solution and membrane tends to exclude co-ions. In order to keep the electroneutrality of the solution for each side of the membrane, the counter ions will be rejected as well [10, 70].

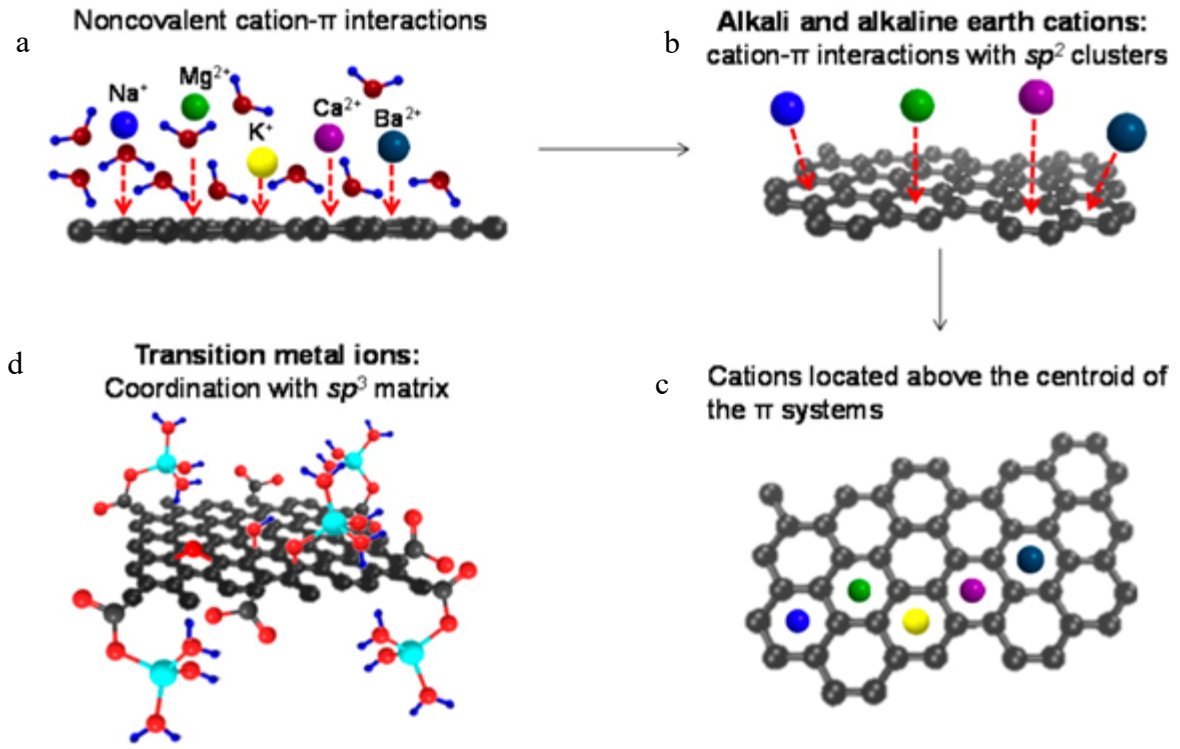

Figure 2.7: The proposed mechanism for the selectivity of cations through a GO membrane; (a)-(c) cation-π interaction of alkali and alkaline earth with the sp^2 cluster of GO; (d) coordination interaction of transition-metal with sp^3 C-O matrix of GO [11, 55].

Furthermore, Joshi and colleagues comprehensively investigated the selective mass transport through GO membranes with a larger range of solutes [69]. Using U-shaped tube which was divided into feed and permeation side for permeation test, and 5 μm thick GO membrane was in the middle, they found that, when the GO membrane was immersed in water, it was able to act as a molecular sieve. It will block all the solutes with hydrated radii greater than 0.45 nm which showing a clear cut-off of the GO membrane. They explained this behaviour by the effect of the physical size of the nanocapillaries within the GO membranes, in which only species that could be fitted into the nanocapillaries could permeate, and larger species would completely block.

Recently, several feasibility studies on GO membranes in pervaporation dehydration of solvents were carried out [3, 63, 65, 71]. From their findings, the performance of the GO membrane was attributed to GO's hydrophilicity, which means that water is preferentially adsorbed onto the oxygen functional groups, and subsequently penetrates into the interlayer channels and diffuses rapidly. In addition, water molecules, which are able to permeate through the GO membrane, should at least impede or block solvents from permeating through.

Nevertheless, selective permeation of solutes through GO membranes can be achieved by various effects. For larger-size solutes with hydrated radii greater than 0.45 nm, the rejection can be made on account of the sieving properties of the GO membranes. On the other hand, for small ions, the selective permeation can be achieved by diverse interaction between different ions and the different regions in GO, which is sp^2 (pristine/non-oxidized region) and sp^3 (oxidized region). In addition, the charge effects should also be taken into consideration for the selective permeation of ions through GO membranes.

2.5.3 Summary of molecular transport through GO membranes

In summary, the molecular transport of water and solutes through GO membranes may be governed by three main factors:

1. Interlayer distance between GO sheets in a laminar structure
2. Defects or pores of the GO membrane
3. Reaction between functional groups of GO with water or solutes

Generally, molecular transport through GO membranes may be the combination of two or three of the aforementioned factors. The laminar structure of GO decorated by pristine (non-oxidized) and oxidized regions provides not only fast and selective nanochannels, but also preferential interaction sites for transporting molecules or ions. Moreover, the interlayer distance, which can be enlarged in a hydrated state, may provide molecular sieve separation mechanisms for transporting solutes. In addition, defects or pores in GO sheets may also serve as a shortcut for the transport of molecules. Furthermore, the interaction between different solutes with the functional groups and the pristine sites of GO could also contribute towards the selective transport of solutes through GO membranes. The charge of GO nanosheets, combined with the interlayer distance of GO, might become two dominant factors to be considered for determining the transport mechanism of molecules through GO membranes. Nevertheless, the transport mechanism for GO membranes could be more complicated, such that an advanced characterization technique, combined with simulation and further experiments, is needed to properly understand the mechanism.

2.6 Review conclusions: Challenges and perspectives of GO as a membrane material

Over the past year, there has been substantial progress in the research and development of graphene and its derivatives, especially GO, for the purposes of being employed as membrane material. Numerous interesting characteristics possessed by GO make it an excellent candidate in this respect. ***Below is the summary of the advantages offered by GO as a membrane material.***

1. *Fabrication method*: The synthesis process of GO is relatively easy and low-cost, meaning that it has a higher potential for achieving large-scale production.
2. *Physical and chemical properties*: GO exhibits a high mechanical strength and is chemically inert, which are important characteristics for membrane materials.
3. *One-atom thickness*: Since GO is only one-atom thick, it is expected to form a membrane with minimum transport resistance and maximum permeate flux.
4. *Microstructure*: GO can be assembled into a laminar structure via filtration or coating approaches, providing unique 2D nanochannels for transporting small molecules. The channels can be engineered to provide various opportunities for the selective transport of water, ions and gases.
5. *Physiochemical properties*: GO offers much richer oxygen functional groups, not only resulting in a difference in the interaction between molecules, but also offering stability in various solvents, especially water (due to the hydrogen bonding in GO). In addition, the reactive sites of the oxygen functional groups enable it to be modified or functionalized to suit various applications, thus making it a greatly versatile membrane material.

Despite the advantages and exciting characteristics that GO offers as a membrane material, there are still numerous challenges to be tackled before GO membranes can be employed on a larger scale. ***Below are some of the challenges that need to be addressed:***

1. *Stability*: To date, there are very few reports concerning the stability of the membrane in a solution or gas environment. In addition, the long-term stability of GO membranes in filtration should be carefully investigated. The stability of GO membranes in relation to their structure and physiochemical properties remains unclear, such that more effort should be devoted to fabricate structurally and chemically stable GO membranes.
2. *Support layer:* Since GO membranes were produced as very thin selective layers, it is important to have a support layer, which provides mechanical support to withstand high-pressure differences across the membrane for pressure-driven applications. Thus, it is crucial to choose proper support without introducing additional transport resistance, which, at the same time, is strong, rigid and inert.
3. *Separation mechanism*: The separation mechanism in GO membranes is not fully understood, although several mechanisms have been proposed. Advanced simulations and characterization techniques are needed to develop a better understanding of the transport mechanism, which could be through the interlayer distance, selective defects or functional groups behaviour.

Thus far, significant progress has been made to improve the understanding of the mass transport mechanism of novel GO membranes, as well as explore their different spectra of potential applications. Indeed, there are some agreements and disagreements on the observed results and the proposed transport mechanism. However, it should be borne in mind that GO is a new material, with more research on this interesting material need to be undertaken before the transport mechanism of GO in membrane separation is clearly understood.

CHAPTER 3

Synthesis of Graphene Oxide, Characterisations and Graphene Oxide Hollow Fibre Membranes Fabrication

Abstract

This chapter briefly elaborates the methods used in graphene oxide suspension synthesis via the Modified Hummer's method. In addition, fundamental characterisations were made for an essential fundamental understanding of graphene oxide. Furthermore, the ceramic hollow fibre fabrication method was also briefly explained in this chapter. Finally, the preparation of graphene oxide on hollow fibre support was systematically elaborated.

3.1 Introduction

Despite different methods in synthesizing this 2D materials, the most commonly used method in the production of GO is the modified Hummer's method. As explained in the literature review earlier, Hummer's method offers more advantages compared to earlier methods such as Brodie's and Staudenmaier's methods in terms of yield, simplicity and safety [38, 39].

As a membrane material, GO offers tuneable microstructures and interesting physiochemical properties, which allow efficient design of selective transport of fluid at the molecular level. Thus, interesting opportunities in producing high performance and cheaper clean water technologies could be offered. In addition, fabrication of laminated GO-based membranes using micrometer-sized GO sheets possess eminent characteristics, such as hydrophilic, robust mechanical strength, as well as excellent flexibility, which make it a perfect applicant for filtration applications at nanoscale level [52]. Furthermore, the strongly oxygenated and highly hydrophilic nature of GO makes it stable when dispersed in water and thus, can be easily stacked on each other.

Since GO sheets are very thin, it is important for them to be supported in order for this material to withstand high pressure differences in industrial applications. In terms of the support membrane selection, although polymeric membranes are commercially available, the tolerance towards high temperatures and harsh conditions are very low, limiting their application range. Ceramic materials on the other hand, offer stronger tolerance towards these harsh conditions. In addition, in terms of the support membrane configuration, when compared to the planar support, ceramic hollow fibres offer numerous advantages, such as high packing density,and chemical and structural stabilities [23].

In this chapter, the procedures and steps involved in the synthesis of GO and fundamental characterisation of the materials were briefly elaborated. In addition, the procedures for the fabrication of GO membranes on ceramic hollow were systematically given.

3.2 Chemicals and Materials

For graphene oxide synthesis, graphite powder with the size of <200μm and sodium nitrate ($NaNO_3$) were purchased from Sigma Aldrich, UK. Sulphuric acid (H_2SO_4) supplied by VWR, UK with 95% purity. Potassium permanganate, KMnO, ≥99% was purchased from Sigma Aldrich, UK. YSZ (3 mol% yttrium stabilised zirconia (3-YSZ) powder, 30–60 nm, Inframat Advanced Materials, LLC) was used as membrane material for fabrication of ceramic hollow fibres. Dimethyl sulfoxide (DMSO, VWR International) was used as sovent, Polyethersulfone (PESf, Radal A300, Ameco Performance, USA) as polymer binder, and Arlacel P135 (polyethyleneglycol 30–dipolyhydroxystearate, Uniqema) as dispersant, respectively.

3.3 Graphene oxide synthesis via modified Hummer's method

Hummer and Offeman from Mellon Institution of Industrial research established a different approach in producing GO compared to the method developed by Brodie [7] and Staudenmaier [35]. The synthesis method proposed by them used sulphuric acid, sodium nitrate and potassium permanganate at 45°C and based on their description, the whole oxidation process can be finished in 2 hours and the degree of oxidation was higher than Staudenmaier's method [36]. Although the structure is difficult to be determined, as briefly discussed in the previous chapter, it is understandable that GO consists of interrupted epoxide, alcohols, ketone carbonyls and carboxylic acids [8, 41, 42].

In this study, modified Hummer's method proposed by Hirata et al., has been used to synthesize the GO [38]. Figure 3. 1 summarizes the procedure in GO synthesis used in this study. Briefly, 1 g of graphite powder (Sigma Aldrich, UK) and 0.75 g of $NaNO_3$ (Sigma Aldrich, UK) were placed in a flask with a stirring chip. Then, 34 mL of (VWR UK, 95% purity) H_2SO_4 was added into the mixture.

The mixture was stirred while being cooled in an ice water bath. 4.5 g of $KMnO_4$ was then added progressively over 1 hour and the cooling process was completed in 5 hours and the ice water bath was removed. The mixture was allowed to stand for 5 days with slow stirring to obtain a highly viscous liquid. After 5 days, 500 mL of water was added and the resultant mixture was further stirred for 2 hours. Then, 20 ml of H_2O_2 was slowly added to remove any excess of manganese ions and stirring was continued for 2 hours. The resultant GO dispersion obtained was washed with deionized water and centrifuged to grade the size of GO flakes.

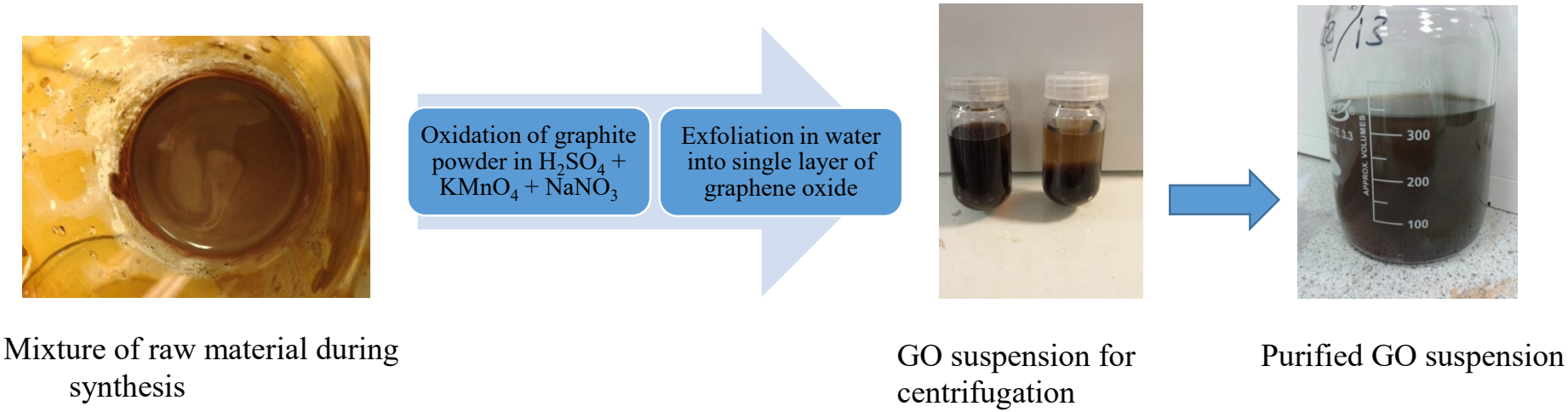

Mixture of raw material during synthesis

GO suspension for centrifugation

Purified GO suspension

Figure 3. 1: GO synthesis steps using modified Hummer's method

The most important source of graphite used for the chemical reaction is flake graphite, which is a natural occurring mineral. This type of graphite is purified to remove hetero-atomic contamination [76]. Due to this reason, it contains abundant localized defects in its π-structure. This defect may assist during the oxidation process. In the oxidation procedure of GO, the oxidation of raw graphite was undertaken by $KMnO_4$ in H_2SO_4 and $NaNO_3$ and later this compound becomes the intercalation compound of positively charged carbon layers and negative hydrogen sulphate ions. The intercalated compound tends to separate more during the oxidation stage when the oxidation period is longer, but unfortunately the separation is insufficient. Therefore, by hydrolysing the intercalation compound, both sides of each single layer of carbon were attached with acidic hydroxyl and ether groups [77-79]. During the high purification process, the small ions derived from the oxidants were thoroughly removed and many layers tend to dispersed from each other automatically. This separation was caused by electrostatic repulsion between the interlayer flakes, that produced thin film particles in aqueous dispersions [38].

Besides the source of graphite, the oxidation reagents are also an important factor in determining the oxidation degree of the flakes. The most common used oxidation agents in the synthesis of GO are $KMnO_4$, combined with H_2SO_4. The permanganate ion is known as a typical oxidation reagent. The reactivity of MnO_4^- can only be activated in acidic media, mostly defined by the formation of dimanganese heptoxide from $KMnO_4$ in the presence of strong acid as given in scheme 3.1[80].

$$KMnO_4 + 3H_2SO_4 \rightarrow K^+ + MnO_3^+ + H_3O^+ + 3HSO_4^-$$

$$MnO_3^+ + MnO_4^- \rightarrow Mn_2O_7$$

Scheme 3.1: Dimanganese heptoxide formation from $KMnO_4$ with the existence of H_2SO_4 [80]

3.4 Characterisation of graphene oxide

All samples for characterisations were prepared by coating GO on flat sheet PES membranes to ensure accurate measurement, unless otherwise stated.

3.4.1 Fourier transform infrared spectroscopy (FTIR)

FTIR (Perkin Elmer, Spectrum 100 spectrometer) from 500-4000 cm^{-1} wavenumber was used to study the structure and functional groups of graphene oxide. Since GO is hygroscopic, and approximately 25% of water molecules can be adsorbed in its structure, it has become the biggest challenge in FTIR analysis. Nevertheless, spectrum obtained from FTIR analysis can be used to represent the functional groups in GO. In this study, in order to get more accurate functional group characterisations from FTIR, free standing GO membranes have been employed.

Figure 3. 2 demonstrates typical FTIR spectra of a GO membrane prepared in this study. The characteristic peaks show apparent adsorption bands for the hydroxyl C–OH (3379 cm^{-1}), carbonyl and carboxyl C=O (1727 cm^{-1}), aromatic C=C (1614 cm^{-1}), epoxy C–O (1254 cm^{-1}), and alkoxy C–O (1064 cm^{-1}) groups. The existence of oxygen-containing functional groups, such as C=O and C–O, further confirmed that the graphite certainly was oxidized into GO and was consistent with the data found in literatures [81-84].

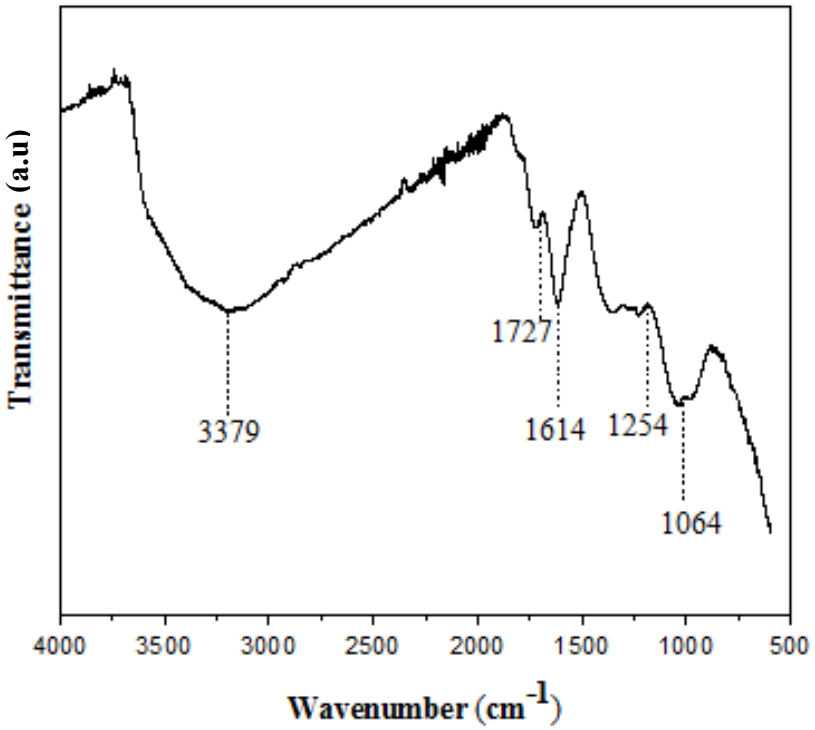

Figure 3. 2: FTIR spectra of free-standing GO membrane

3.4.2 UV-Visible spectrometer analysis

Figure 3. 3 shows an UV-Vis spectra of GO dispersion prepared in this study. The formation of stable graphene oxide dispersions allows the dispersion to be analyse using UV-vis spectroscopy (UV-2101PC, Shimadzu, UK). UV-Vis spectrum of GO in water typically features a peak at around 233 nm, which could be assigned to the π-π^* transition of C-C bond. In addition, there is an appearance of shoulder at around 300 nm, which corresponds to the n-π^* transition of C=O. [85-87]

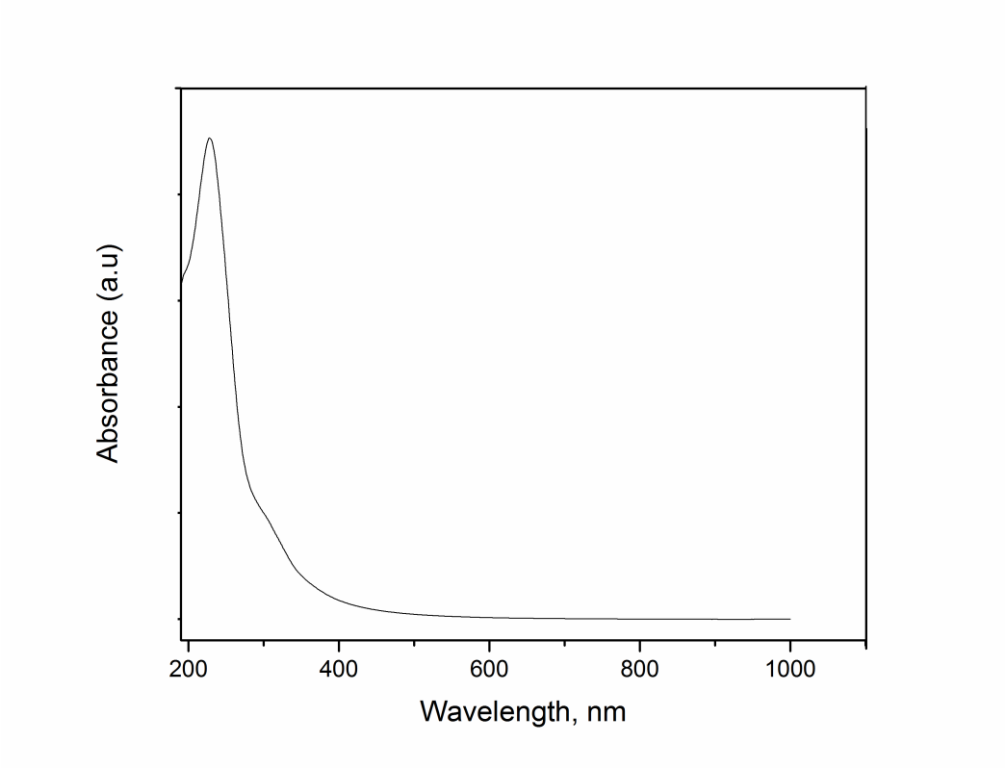

Figure 3. 3:UV-Vis spectrum of GO suspension

3.4.3 Raman spectroscopy

Raman Spectroscopy was used to further investigate the structural properties of GO, especially the structural defects. During the synthesis of GO, defects were introduced during the oxidation with the strong acid and oxidant. For GO, there are two characteristic bands; that is D band which appears at around 1350 $cm^{-1}$and the latter is G band, which appears at around 1570 cm^{-1} (Figure 3. 4). The D band corresponds to the existence of structural defects which including vacancies, grain boundaries, and amorphous carbon species [88].

In addition, the D band also represents the out of plane vibration attributed to the structural defects. On the other hand, G band is a result of in-plane vibration related to the sp^2 graphitic domains (non-oxidized regions). In our study, the GO synthesized possessed an intensity ratio of D band to G band (I_D/I_G) of 1.16. GO would have a higher D band compared to pure

graphene. This is because, GO has oxidative functional groups attached on the basal plane as well as the edge that leads to the disruption of carbon's sp^2. Thus, when the D band is higher, it is an indication that sp^2 bonds are broken, which, in turn, means more sp^3 carbon are present.

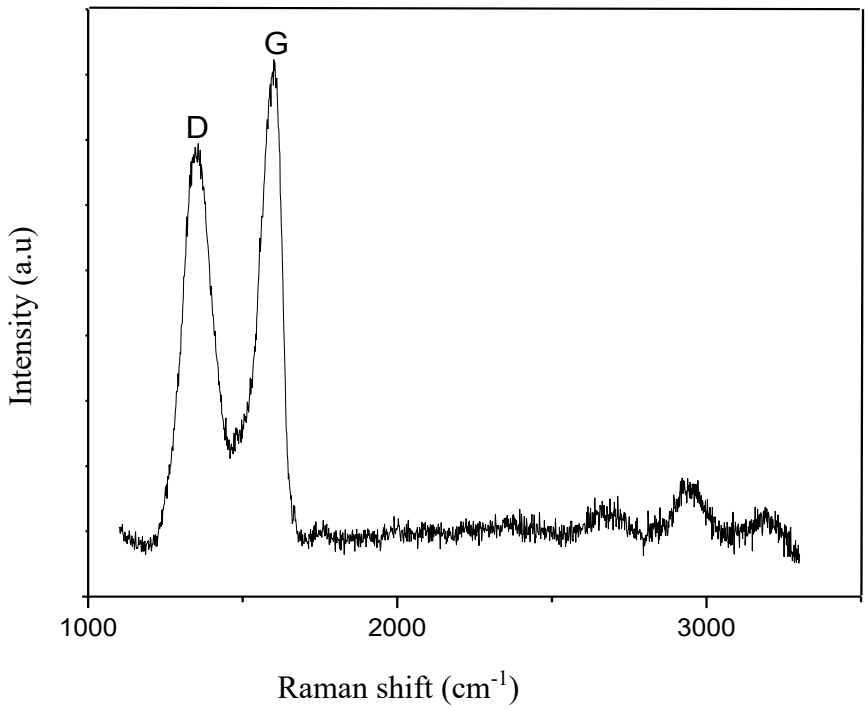

Figure 3. 4: Raman spectra of GO membrane

3.4.4 X-Ray diffraction spectrometer (XRD)

Oxygen-containing functional groups in GO can be further probed by XRD (XRD, X'pert Pro PANalytical) analysis. The XRD analysis used Cu-Kα as the radiation source and the scans were carried out in 2θ range from 5° to 40°. The equipment voltage and current were set at 40 kv and 40 mA respectively. Figure 3. 5 shows a typical XRD spectra of a GO prepared in this study. It is apparent that graphite powder exhibits a sharp diffraction peak at 2θ=26.7°, corresponding to interlayer space of 0.333 nm. In contrast to GO, the peak appears at around 10.59°, which represents interlayer space of 0.834 nm. The increase in the spacing was due to

the introduction of oxygen functional groups from the oxidation of graphite during GO synthesis. In addition, the absence of a peak at 2θ=25~30° further indicates that the graphite has been fully converted to graphene oxide. It should be noted that the interlayer spacing between the GO sheets tend to change depending on the relative humidity [2].

The interlayer space (*d)* of graphite and graphene oxide can be calculated from Bragg law equation:

$$n\lambda = 2d\sin\theta$$

where *n* is the diffraction series and λ is the X-ray wavelength in this case 0.154 nm.

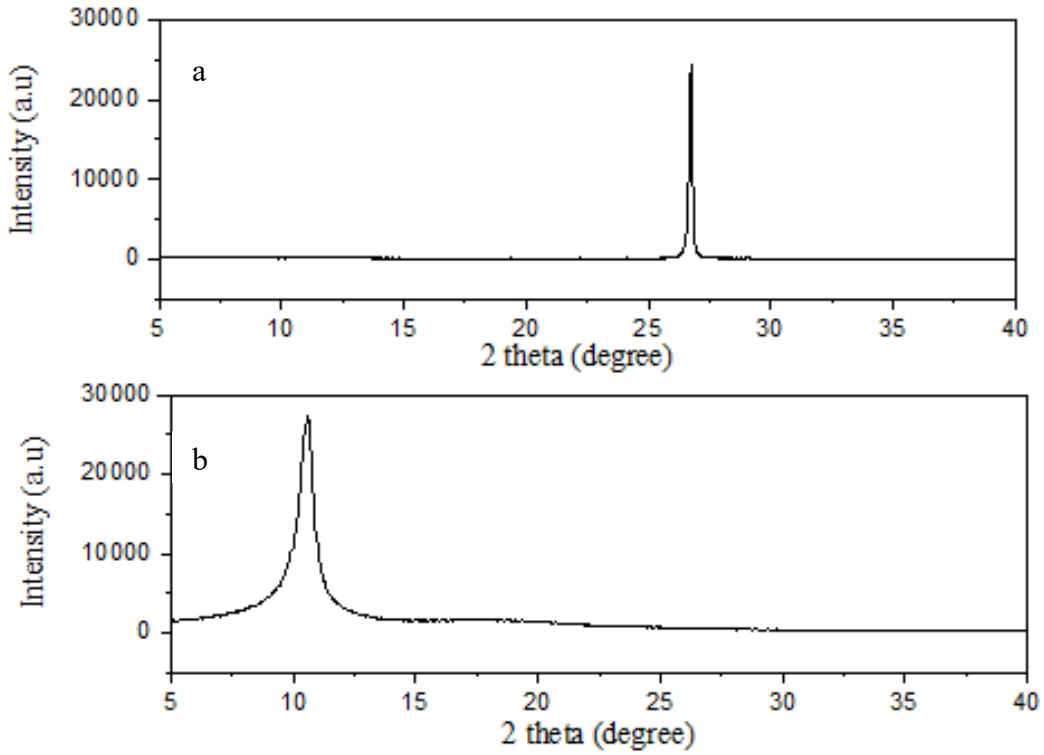

Figure 3. 5:XRD analysis of (a) pure graphite; (b) GO membrane on flat sheet

3.4.5 X-ray photoelectron spectroscopy (XPS)

Further analysis on oxygen functional group of GO can be analysed using X-ray photoelectron spectroscopy (ThermoFisher, K-Alpha spectrophotometer). The XPS scans utilised monochromatic Al-Kα X-ray source with energy of 1486.71 eV. Figure 3. 6 shows C1s spectrum of GO. Typical GO membrane comprises of four typical peaks approximately located at 284.4 eV for C-C (graphitic) group, 286.9 eV for C-O (ether, alcohol and epoxy) group,288.4 eV for C=O (carbonyl) group, and 290.2 eV for O=C-OH (carboxyl) group, respectively.

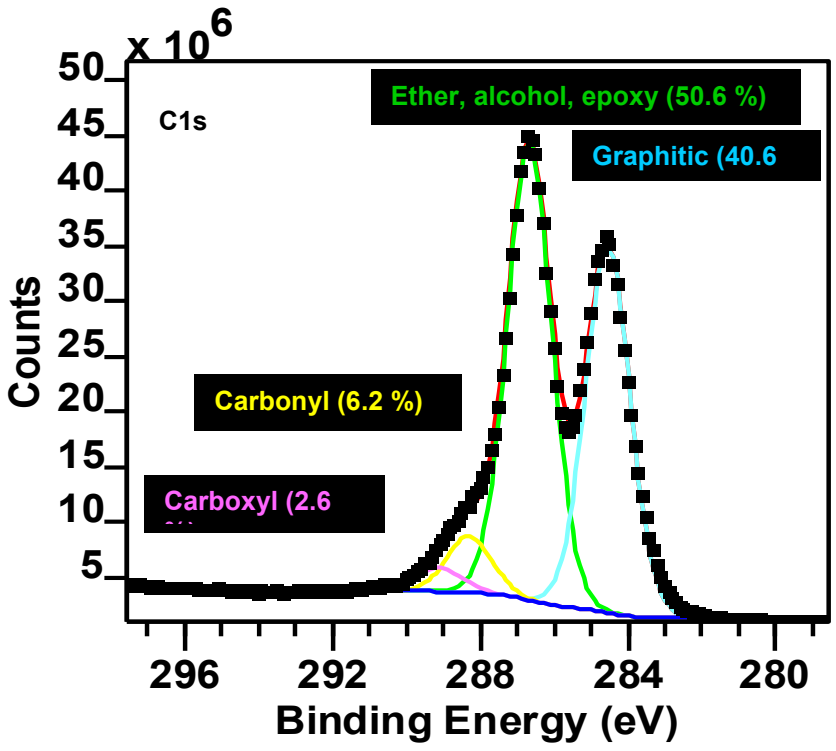

Figure 3. 6: XPS analysis of GO membrane

3.4.6 Scanning electron micrograph (SEM)

Figure 3. 7 show images carried out using high resolution SEM (Zeiss Auriga Cross Beam). The GO sample was prepared by drop cast GO solution on silicon wafer and dried in air for at least overnight. From the images shown below, it clearly revealed that GO produced from the modified Hummer's method consists of single sheets of GO flakes with crumples at the edge of the sheets. It is also evident that GO has successfully exfoliated into individual and ultrathin nanosheets. In addition, we can clearly see that the flakes' size is not uniform, but the average size of the flakes is around 5-10 µm.

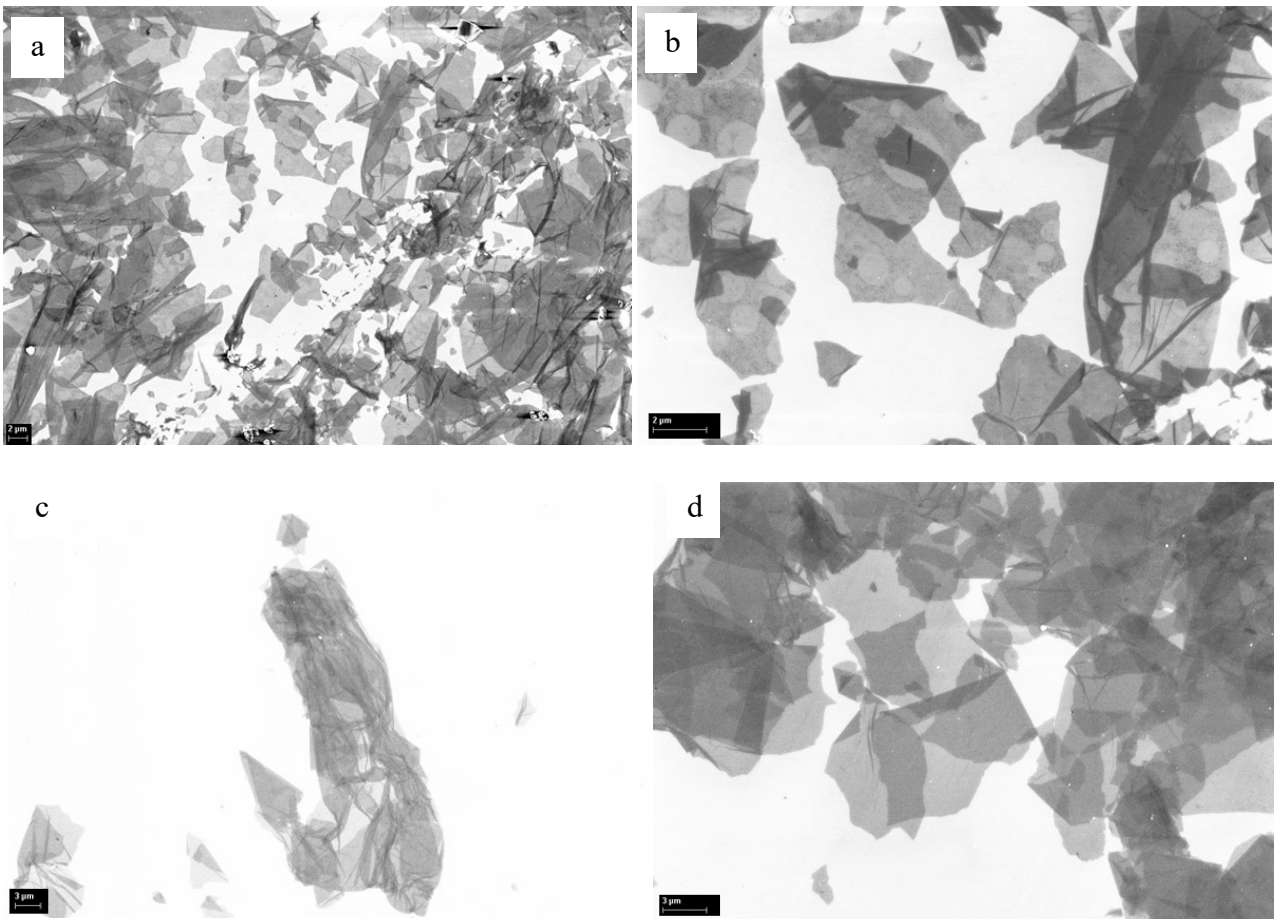

Figure 3. 7:(a-d) High resolution SEM images of GO sheets

3.4.7 Thermal gravimetric analysis (TGA)

TGA was used to provide information about the thermal stability of materials. Unfortunately, in this case, GO is thermally unstable due to the fact that it will start to decompose when heated in Argon or Nitrogen. In this study, TGA (Q500, TA Instrument) was used to analyse GO films under dry flowing Nitrogen. Free standing GO membrane, cut into small pieces, was used as the sample. The temperature was ramped from 25 °C – 800 °C with the lowest ramping rate of 1°C/min. As we can see from the TGA graph (Figure 3. 8), approximately 8% weight loss was observed due to the evaporation of physically adsorbed water at around 100°C, indicating that GO is hygroscopic. The major weight loss happened just below 200°C, corresponding to sample decomposition as a result of the evolution of oxygen-containing groups in the form of CO, CO_2, and/or H_2O. This finding on major weight loss was consistent with others in literatures [44, 84, 89].

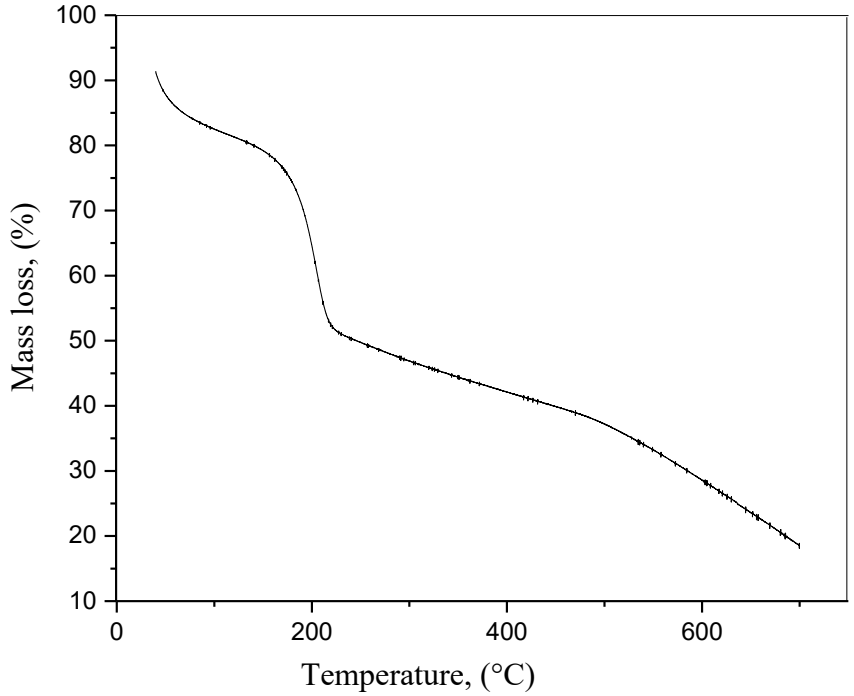

Figure 3. 8: TGA analysis of GO sheets.

3.4.8 Contact angle measurement

Contact angle measurement of GO membranes was carried out using a drop shape analyzer (DSA 10 MK2, Krüss GmbH, Hamburg, Germany). For contact angle measurement, YSZ disk was used as a membrane support. This to ensure that the surface of the membrane is completely flat and the contact angle measurement is accurate.

3.4.9 Atomic force microscopy (AFM)

AFM analysis was carried out to analyse the surface roughness of GO membranes specifically in Chapter 6 of this thesis. It was carried out under tapping mode using atomic force microscopy (Bruker Innova Atomic Force Microscope) with a scan size of 5 μm × 5μm. GO hollow fibre was cut to about 50mm and taped on microscope glass for the sample analysis.

3.5 Fabrication of graphene oxide membrane supported on ceramic hollow fibre

3.5.1 Fabrication of ceramic hollow fibre support

Ceramic membranes become continuously attractive in terms of research and development for separation applications at elevated temperatures, high or low pH levels, and various critical chemical species such as strong solvents. In particular, ceramic hollow fibre membranes show the advantage of high surface area per volume ratio compared with other membrane geometries. Due to their specific surface properties, ceramic hollow fibre membranes are applied to advanced filtration and separation applications with fluids containing high organic loads, which lead to strong fouling when other membrane materials are used.

In this study, two different ceramic hollow fibres were used, Al_2O_3 and YSZ. Both ceramic hollow fibre supports were fabricated through a combined phase-inversion/sintering process [90], and the pre-cursors were sintered at 1350 °C and 1150 °C to gain strength, respectively. The phase inversion and sintering method is a much simpler method compared to conventional multi-step methods. Brief fabrication steps were mentioned in Chapter 2. Firstly, the inorganic suspension, which consists of ceramic powder, the solvent, and additives, was prepared. Next, the membrane shape was formed via the spinning process, during which the asymmetric structure could be established in a single step via polymer phase inversion induced by solvent and non-solvent exchange. Then, the membrane underwent heat treatment to remove organics, any solvent and non-solvent, dispersant, etc to consolidate its final shape and structure. Figure 3. 9 shows ceramic hollow fibres used in this study.

Although in this study used two different types of ceramic hollow fibre, YSZ was mainly used throughout this study. Al_2O_3 was only used in Chapter 4, in which the objective is to investigate the effect of surface roughness on the performance of GO membranes. Unless otherwise stated, YSZ ceramic hollow fibre supports were used throughout this study. Therefore, the spinning suspension composition and spinning parameters for the fabrication of YSZ hollow fibre support are listed below.

Table 3. 1: Suspension composition and spinning parameters for YSZ ceramic hollow fibre

Dope recipe		**Spinning conditions:**	
DMSO	:80g	Air gap	:2 cm
YSZ	:120g	Dope rate	:5 ml/min
PES	:20g	Water rate	:10 ml/min
Dispersant	:1g	Spinneret	:2mm OD 1mm ID

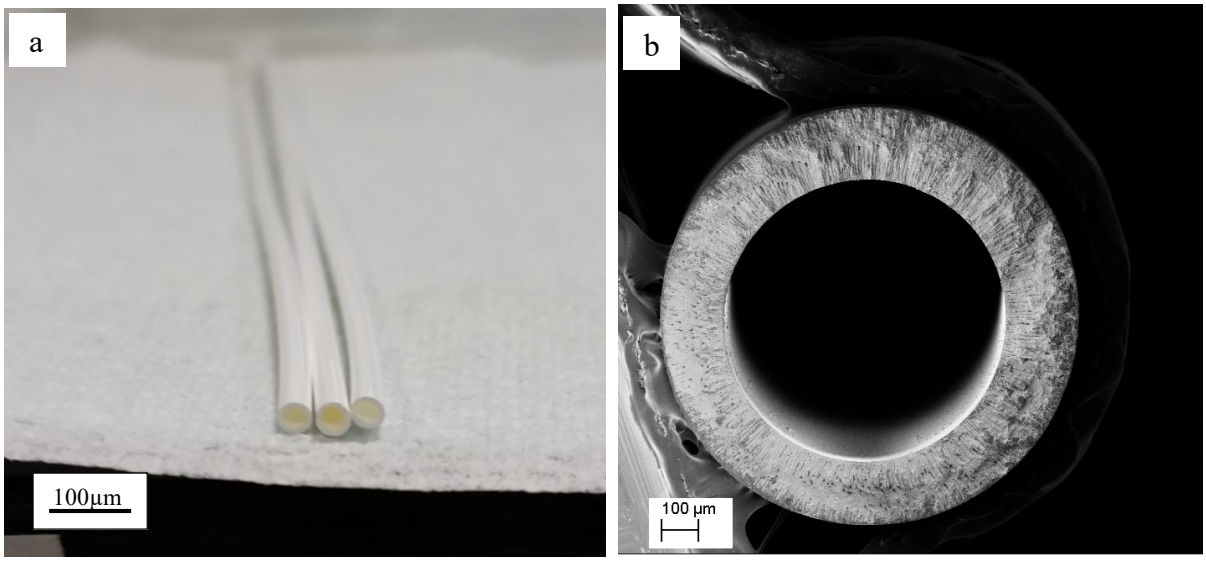

Figure 3. 9:a) Photograph of cross-section picture of ceramic hollow fibre pre-cursor; (b) SEM image of cross-section YSZ ceramic hollow fibre membrane showed asymmetric structure with sandwich-like structure.

Figure 3. 9 (b) shows the cross-section of ceramic hollow fibre used as a support for our GO membrane. The structure shows a sandwich-like structure, in which the sponge-like structure gives more strength. On the other hand, the finger like microchannels structure which is highly porous could contribute to negligible permeation resistance which benefits in the mass transfer process.

3.5.2 Fabrication of graphene oxide membrane

Different methods are available for producing GO membranes, such as dip coating, drop casting and filtration method. In this study, vacuum filtration method was employed, simply because the geometric configuration of hollow fibres support. GO nanosheets were believed could be easily stacked on them with a pressure driving force, due to the curvature of hollow fibre support.

Figure 3. 10 summarise the whole process of GO membrane coating on ceramic hollow fibre support. Prior to the coating process, ceramic hollow fibre supports were glued onto stainless steel holders. To deposit the GO membrane onto the surface of ceramic hollow fibres, it was immersed into a GO dispersion with one-end sealed and the other end connected to a vacuum pump. When a vacuum was applied to the lumen of the fibre, water was sucked into the fibre and the water flow directed GO flakes onto the hollow fibre substrate. GO membrane was formed by stacking the flakes layer by layer, with the aid of a pressure difference and water permeation. Thickness of the GO membrane was controlled by changing the initial concentration of the GO dispersion and the duration of filtration.

Similarly, flat-sheet GO membrane was also made through the vacuum-facilitated filtration method using a polyethersulfone (PES) microfiltration flat sheet membrane. The flat sheet GO membrane was about 10 μm thick, and they could be peeled off carefully from the PES support to form free-standing GO membranes for other measurements. All the GO membranes used throughout this study were dried in vacuum oven at 40°C for four hours except GO membranes used in Chapter 5.

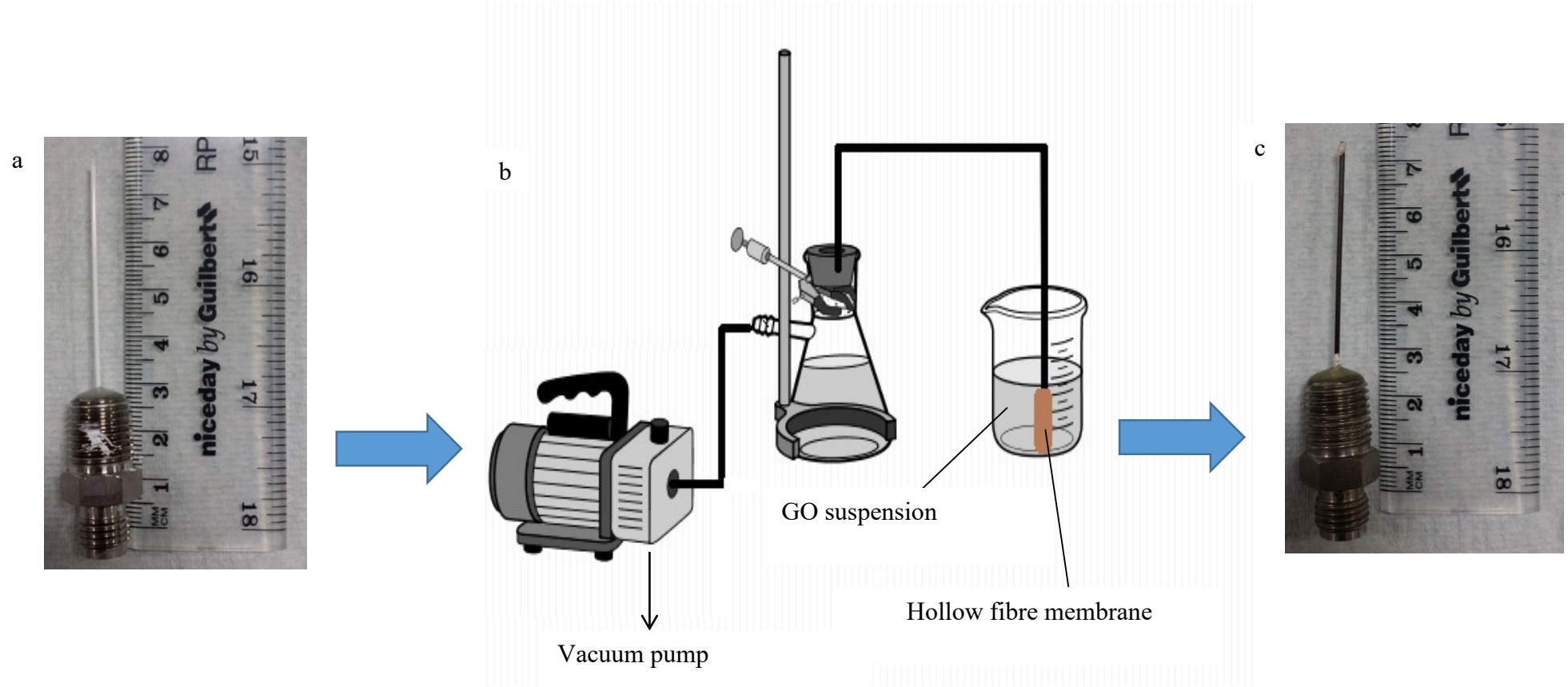

Figure 3. 10: The summary of the overall process of GO hollow fibre membrane fabrication; (a) Ceramic hollow fibre support; (b) Schematic diagram of vacuum filtration setup used in this study; (c) GO membrane on ceramic hollow fibre support

CHAPTER 4

Graphene Oxide Membranes on Ceramic Hollow Fibres – Microstructural Stability and Nanofiltration Performance

This chapter has been published in Journal of Membrane Science, DOI: 10.1016/j.memsci.2015.03.001

Abstract

Graphene oxide (GO) membranes have demonstrated great potential in liquid filtration. With the aim of real applications, GO membranes in a hollow fibre shape are of particular interest because of the high-efficiency and easy-assembly features at the module level. We report here that GO membranes on ceramic hollow fibre substrates are unstable at the dry state, mainly due to the drying-related shrinkage. And we also demonstrate that these GO hollow fibre membranes can be stabilized by keeping them wet after initial controlled formation of the membranes. The GO hollow fibre membranes show higher permeation fluxes of acetone and methanol than most commercial membranes, and reject molecules larger than 300 Dalton, showing a great potential in the use of value-added organic solvent nanofiltration processes.

4.1 Introduction

Due to the extremely thin feature, GO membranes have to be supported by a substrate in real separation processes to withstand high pressure difference across the membrane. So far GO membranes have been made on planar supports but they are difficult for mass production and their membrane area per volume ratio is limited. Hollow fibre membranes, often with a diameter of 1 mm or even less, are, in this context, more favorable for membrane module assembly in industry because they give the highest membrane area to module volume ratios (up to 9000 m^2/m^3), thus greatly reduce the size of separation plants and operating cost.

Polymeric hollow fibre nanofiltration membranes coated with a thin GO layer have been recently reported to improve the permeance and selectivity very effectively [91]. Compared to their polymeric counterparts, ceramic hollow fibres would be a better substrate for GO membranes, as they are strong and rigid, giving a good support to the GO membrane. The successful use of GO/ceramic hollow fibre composite membrane has been recently reported for dehydration of dimethyl carbonate, and high water flux and separation factors were obtained [92]. We report in this work, however, that GO membranes on ceramic hollow fibre substrates are unstable in the air, mainly due to the drying-related shrinkage. We also demonstrate that GO hollow fibre membranes can be stabilized by keeping them wet after initial linking of GO flakes. The stability requirements imply such GO hollow fibre membranes are not suitable for gas separation, but have great potential in wet separation processes such as nanofiltration.

4.2 Experimental

4.2.1 Pure solvent permeation, nanofiltration and gas permeation tests

The pure solvent permeation and nanofiltration tests were conducted using a dead-end mode. The scheme of the testing setup is available in Figure 4. 1. The GO hollow fibre membrane was mounted into the sample cylinder of the setup, in which the pure solvent was filled and pressurized to 10 bars. The permeate through the membrane was collected with a bottle, which was sealed with parafilm to prevent evaporation during the collection. The permeance of the solvent was determined by the weight gain and the duration of the permeation test; the dye concentration of the feed and the permeate were determined by a UV-spectrometer (UV-2101PC, Shimadzu, UK), and the rejection is calculated through the below definition:

$$R_{dye} = \left(1 - \frac{c_p}{c_f}\right) \times 100\%$$

Where R_{dye} is the rejection of the GO membrane to the dye, c_p and c_f are the concentration of the permeate and the feed, respectively.

Epoxy resin was used to seal the hollow fibre membrane. In the cases of methanol and acetone, a solvent-resist epoxy resin was used to ensure there was no leak through the sealant. Gas permeation was conducted on a setup similar to Figure 4.1, except gas instead of liquid was pressurized in the sample cylinder, and a bubble meter was used to measure the flow rate of the downstream permeated gas.

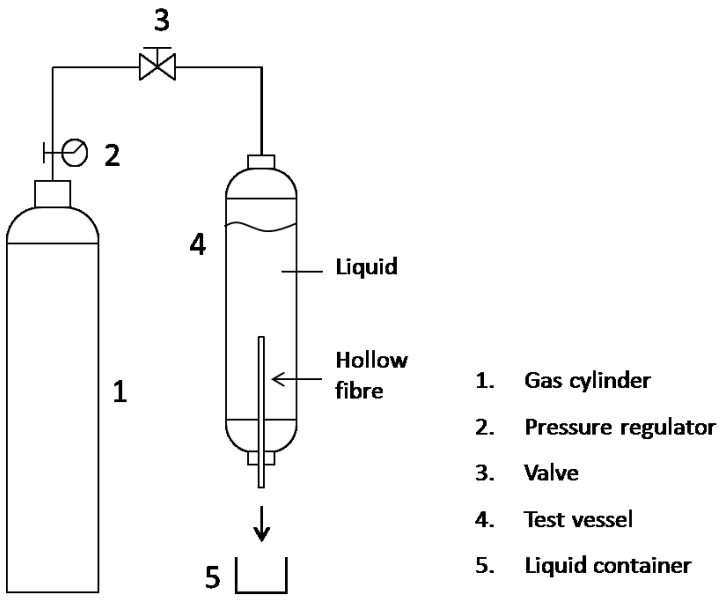

Figure 4. 1: Scheme of the setup used in this research for pure solvent permeation and nanofiltration tests.

4.3. Results and discussion

4.3.1 Morphological features and microstructures

In this study, GO suspension synthesized using modified Hummer's method produce GO flakes with size approximately 5-10 μm based on estimation from SEM image, (Figure 4. 2).

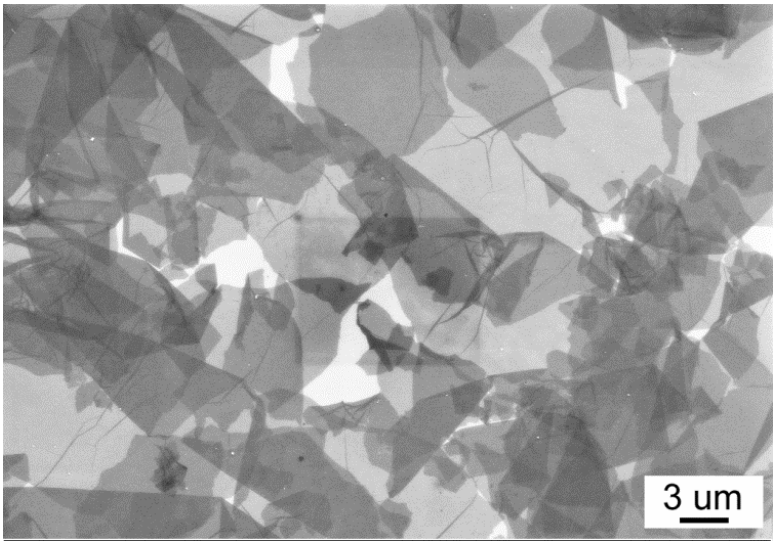

Figure 4. 2: SEM image of the GO flakes used in this research

Two types of porous ceramic hollow fibres made of alumina and yttrium stabilized zirconia (YSZ), respectively, were used in this research to realize GO hollow fibre membranes. Figure 4. 3 (a) shows an example of the obtained GO/Al_2O_3 hollow fibre membranes, and Figure 4. 3(b-d) show scanning electron microscope (SEM) images of the cross section and the outer surface of the GO hollow fibre. The GO/Al_2O_3 hollow fibre presents a visually shining brown surface, which is distinct from the original white alumina hollow fibre substrates. The alumina hollow fibre substrate has an asymmetric wall structure (Figure 4. 3(b)) where the finger-like micro-channels were developed from the lumen due to the hydrodynamic interfacial instability during the phase-inversion fabrication process [93, 94].

The inserted image in Figure 4. 3(b) gives more details of the wall structure. The outer part consists of closely packed alumina particles and interconnected inter-granule pores, whose average size is about 650 nm and 450 nm, respectively (estimated from SEM images), which is ideal for GO coating; and the highly porous inner part of finger-like micro-channels has an ignorable permeation resistance, which benefits the mass transfer in separation processes. Figure 4. 3(c) shows simultaneously both the surface of the alumina substrate (the lower part)

and the GO membrane (the upper part). The specimen was obtained when fracturing the GO hollow fibre, during which process the GO membrane covering the lower part was peeled off. The image indicates the well known weak adhesion between the GO membrane and the ceramic substrate. Figure 4. 3(d) gives a cross-section image of the GO layer, which shows clearly the laminar structure of the GO membrane, and the thickness of the GO layer is about 400 nm.

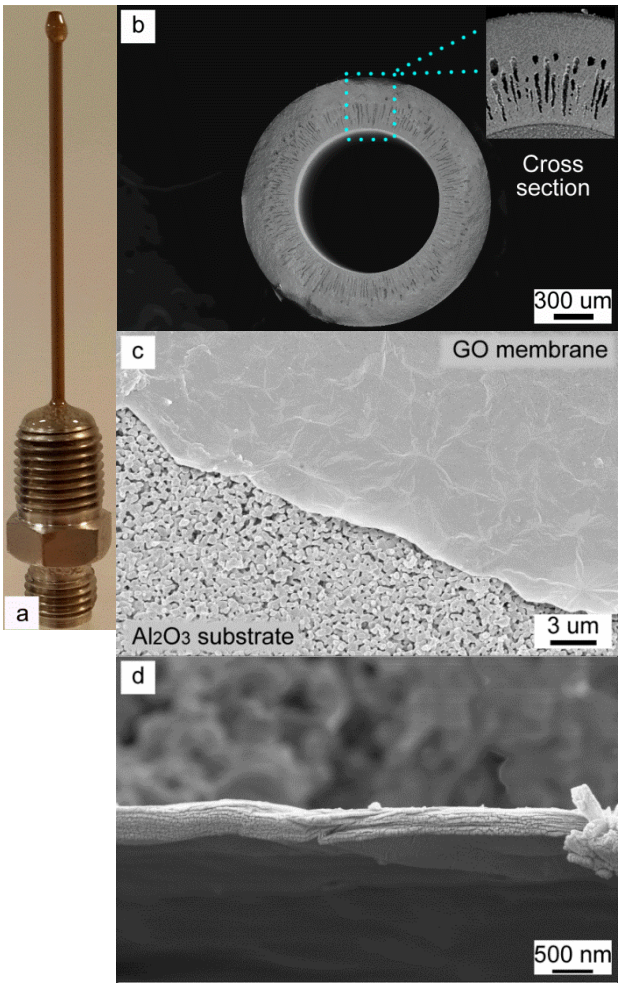

Figure 4. 3: (a) A picture of a GO/ Al_2O_3 hollow fibre membrane glued on stainless steel holder (b) SEM image of cross section of the alumina substrate, the inserted image shows details of the asymmetric wall structure; (c) SEM image of GO membrane on ceramic support; (d) SEM image of details of the GO layer

Figure 4. 4 shows the YSZ hollow fibre substrate and the GO layer. Compared with the alumina hollow fibre, the YSZ hollow fibre substrate shows a sandwich-like structure (Figure 4. 4(a)). The surface of the substrate is composed of fine YSZ particles and inter-granule pores, whose size is about 170 nm and 80nm, respectively (Figure 4. 4(b)), both substantially smaller than the alumina substrate. Figure 4. 4(c) shows the GO layer on the YSZ substrate, which also exhibits a laminar structure, and the thickness is about 400 nm, similar to the GO/ Al_2O_3 hollow fibre membrane shown in Figure 4. 3.

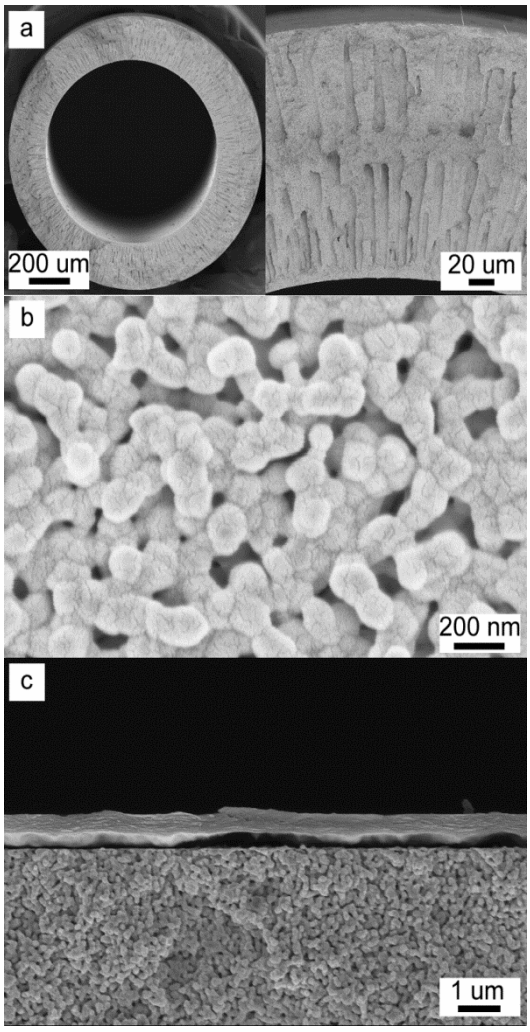

Figure 4. 4:(a) SEM image of the cross section of the YSZ hollow fibre substrate; (b) outer surface of the YSZ hollow fibre substrate showing fine porous surface structure; (c) An SEM image of the GO layer that sits on the YSZ hollow fibre substrate.

The laminar structure of the GO membranes prepared through the vacuum-facilitated filtration method can be further confirmed by XRD results. Figure 4. 5 shows the XRD pattern of a flat-sheet GO membrane, which presents a sharp peak at 2θ = 11°, corresponding to an interlayer space of 0.8 nm between GO flakes in the membrane. The result is concurrent with a typical interlayer space value of air-dried GO membranes that is reported in the literature [32, 69].

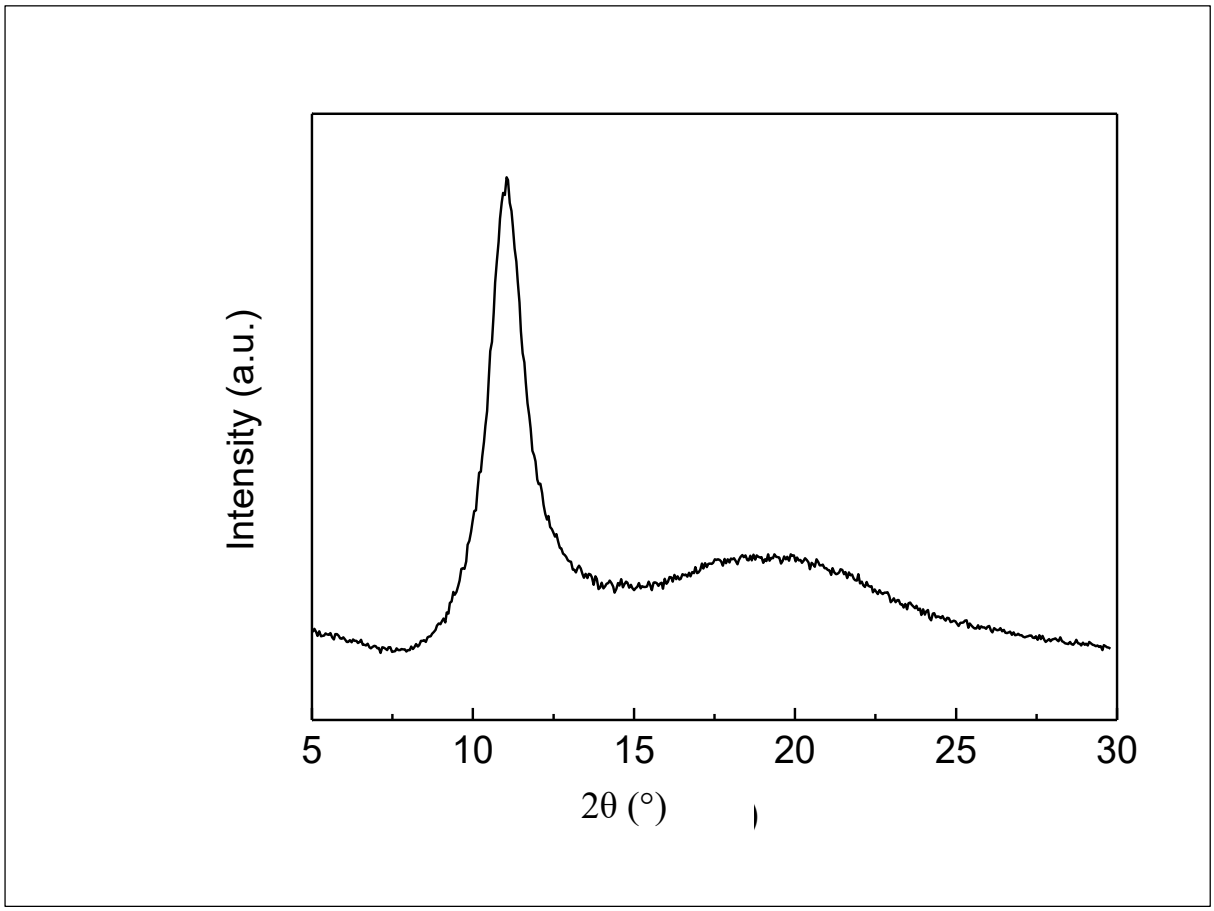

Figure 4. 5: XRD pattern of a flat-sheet GO membrane made through the vacuum-facilitated filtration method

4.3.2 Stability of GO/ceramic hollow fibre membranes

Firstly, we have evaluated the integrity of the GO/Al_2O_3 hollow fibres with gas permeation tests. It has been reported that free-standing GO membranes with a submicron thickness are impermeable to gases [95], and hence gas-tightness test will give us a good indication of the quality of the membrane. We tested the GO/Al_2O_3 hollow fibres with N_2 for several cycles, and the gas-tightness was found to be degraded with time. Figure 4. 6(a) shows a typical test result of a GO/Al_2O_3 hollow fibre. In the first test cycle, it can be seen the permeance was quite low and did not change with the pressure difference across the membrane, showing a Knudsen-diffusion behavior and indicating the aperture size for permeation was in the range of nanometers. The tests afterwards showed that N_2 permeation kept increasing over time, and in each testing cycle, the permeance increased along with increasing pressure and followed a viscous-flow pattern, indicating a big aperture size, larger than hundreds of nanometers. The N_2 permeation test indicates that the GO/Al_2O_3 membrane was unstable, and it is reasonable to speculate that defects were developed during the tests or during the storage period, which resulted the increasing permeation flux. A similar unstable permeation result was also observed when the membrane was tested with O_2 (Figure 4. 6(b)), which indicates the instability of the GO membrane was not due to possible reduction of the GO flakes during the N_2 permeation test.

(Note that the error bar is too small to be visible)

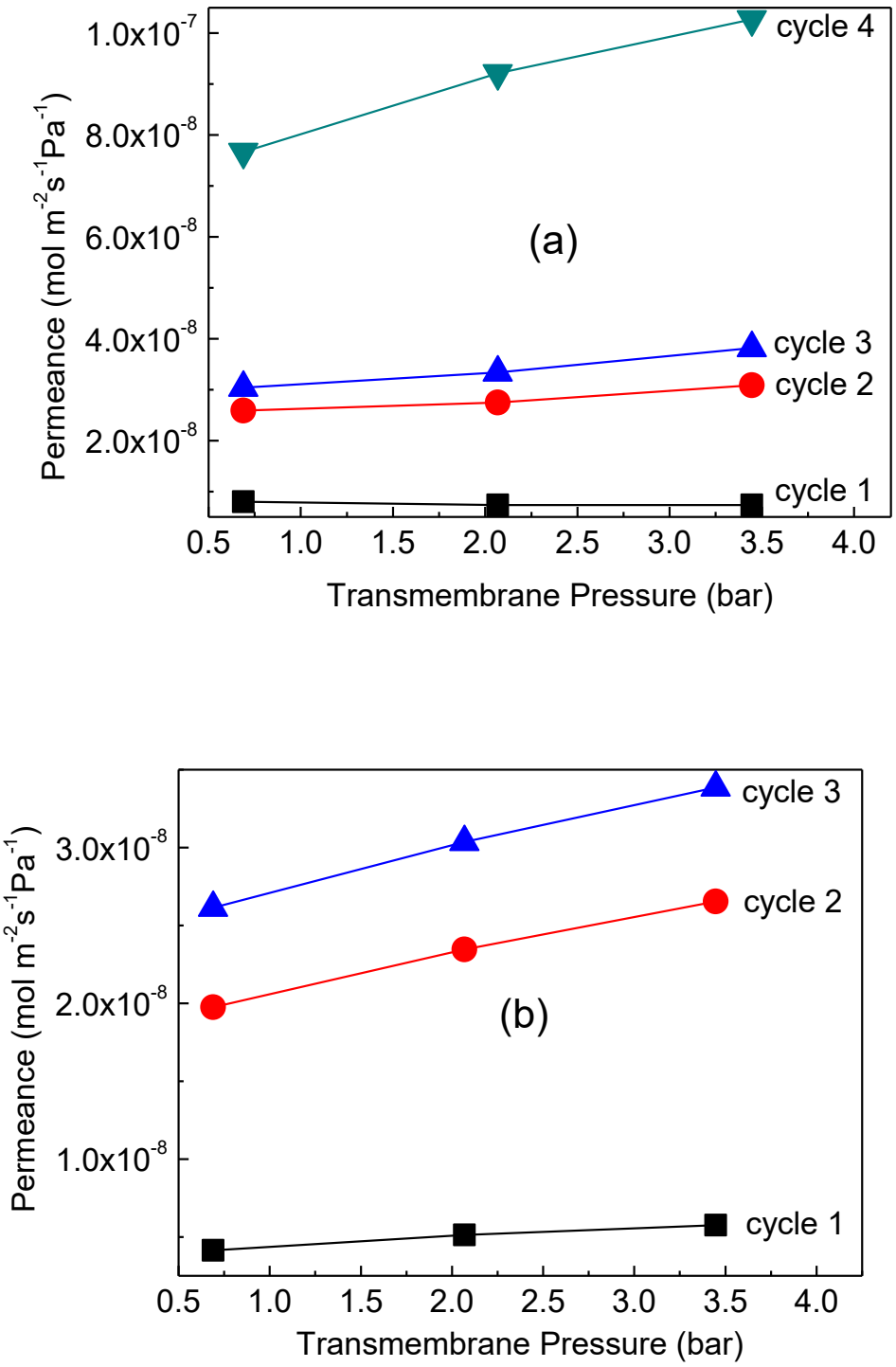

Figure 4. 6: The result of sequential N_2 (a) and O_2 (b) gas-permeation tests of a dry GO/Al_2O_3 hollow fibre membrane. The timeline of each test cycle was 1 day, 2 days, 4 days and 7 days after the GO membrane was dried for cycle 1, cycle 2, cycle 3 and cycle 4, respectively.

We understand that surface characteristics might affect the quality of the GO hollow fibre membrane. The alumina hollow fibre substrates used above have an average surface pore size of 450 nm, which is relatively larger than the supports used for GO membranes in the literatures. Hence we have also used YSZ hollow fibre substrates to prepare GO hollow fibre membranes. The YSZ hollow fibre substrates have an average surface pore size of 80 nm, which is comparable to the anodic aluminum oxide (AAO) substrates used in the literatures [10, 96]. However, the stability of the GO hollow fibre membranes was not improved by the finer surface microstructure of the YSZ hollow fibre, and the N_2 permeation test gave results similar to the alumina hollow fibre substrate (Figure 4. 7). Thus we conclude the surface morphology of the substrate is not the major reason that led to the stability problem. It is not surprising to us, since we used GO flakes with a size of 5-10 μm, which is much bigger than the pore size of the substrates, and a high tolerance to any small imperfection of the substrate surface is expected.

(Note that the error bar is too small to be visible)

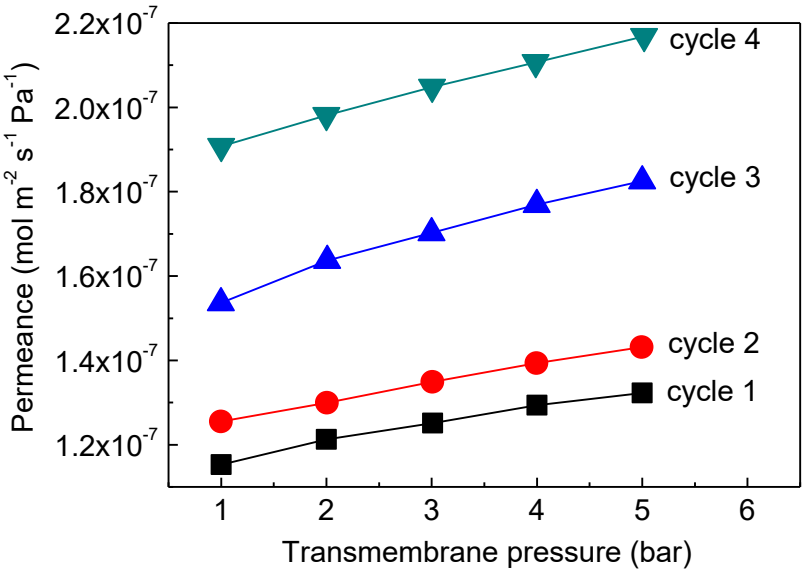

Figure 4. 7:The result of sequential N_2 gas permeation tests of the GO/YSZ hollow fibre membrane. The timeline of each test cycle was 1 day, 1.5 days, 2 days and 4 days after the GO membrane was dried for cycle 1, cycle 2, cycle 3 and cycle 4, respectively.

It is well-known that stress is often introduced into multi-layer composite materials because of the asynchronous change of different layers [97]. In the case of the GO/ceramic hollow fibre, it can be expected that the GO layer will undergo a shrinkage during the drying process, whereas the rigid ceramic substrate is kept unchanged. Hence the GO layer will be imposed a tensile stress which might lead to cracks in the GO layer. To understand whether the shrinkage of GO layer has led to the stability problem, we have cut some GO strips longer than 40 mm from a free-standing GO membrane and measured the change of their length during the drying process.

After initial drying for overnight, the GO strips were placed in a sealed bottle that was filled with silica gels, and we found that the GO strips had a linear shrinkage of 1% after drying (Table 4. 1). Taking the elastic modulus of GO membranes as 32 GPa [98], at such a shrinking ratio, the GO hollow fibre membrane will be imposed a maximum tensile stress of 320 MPa, which is far beyond the maximum fracture stress (120 MPa) of GO membranes as reported in the literature [98]. It has also been reported that the maximum strain at the fracturing point of GO membranes is smaller than 0.6% [98], which is well less than the 1% shrinkage found in our cases. Therefore it is reasonable to believe that the stress induced by the shrinkage during the drying process is sufficiently big to produce micro-cracks or even macro-cracks in GO hollow fibre membranes.

Table 4. 1:Shrinkage of a free-standing GO membrane in the dried air at room temperature, and shrinkage of the dried GO membrane after annealing under vacuum at 150 °C for 24 hours

After 3 days	**After 1 week**	**After 3 months**	**After annealing**
1.0 ± 0.2 % shrinkage	No change	No change	2.0 ± 0.2 % shrinkage

Micro-cracks in GO membranes are difficult to observe even with SEM as the cracks are tortuous beneath the surface, but we did observe macro-cracks in some cases (Figure 4. 8), giving an evidence of the stress in the GO hollow fibre membranes. To further strengthen our argument, we annealed the free-standing GO strips in vacuum at 150 °C for 24 hours. Under such treatment, water and part of the oxygen-containing groups were removed from the GO membrane [99], and another 2% shrinkage was observed after the annealing. The effect of the intensified shrinkage is obvious when the GO membrane is supported, as shown in Figure 4. 9: for GO/PES flat sheet membranes annealed at 150 °C for 16 hours, the membrane bent drastically due to the shrinkage of the GO layer; on the other hand, for GO/ceramic hollow fibres, where the substrate is rigid, the GO layer broke and then peeled off completely after annealing.

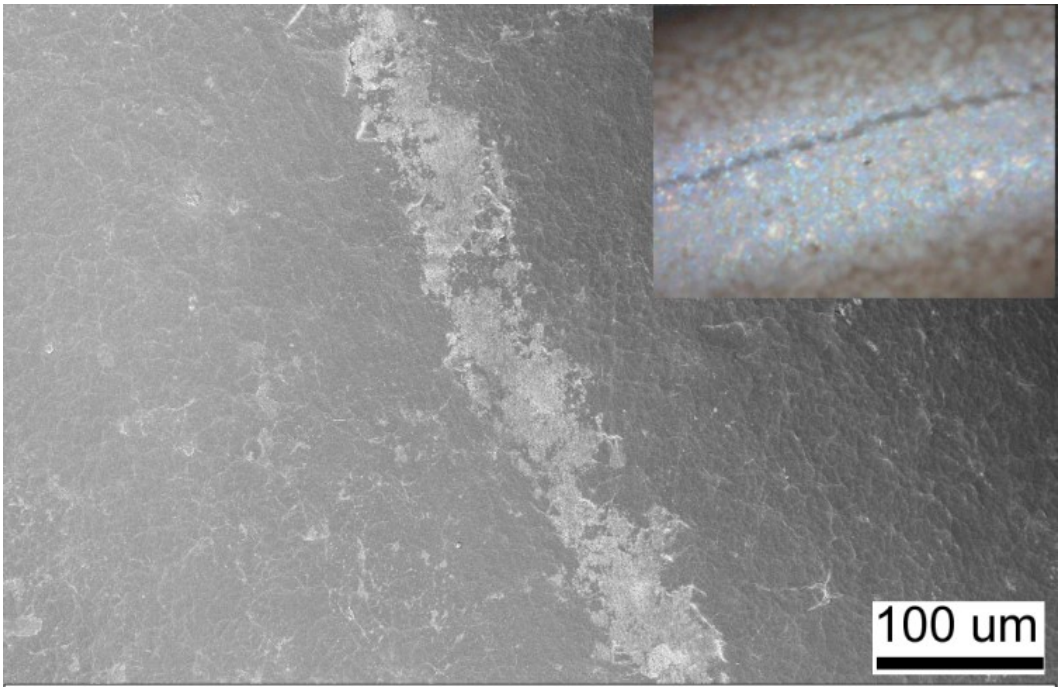

Figure 4. 8:SEM image showing a crack found on a GO/Al_2O_3 hollow fibre membrane. The inserted picture was taken by a digital microscope, which shows a macro-crack in the GO layer.

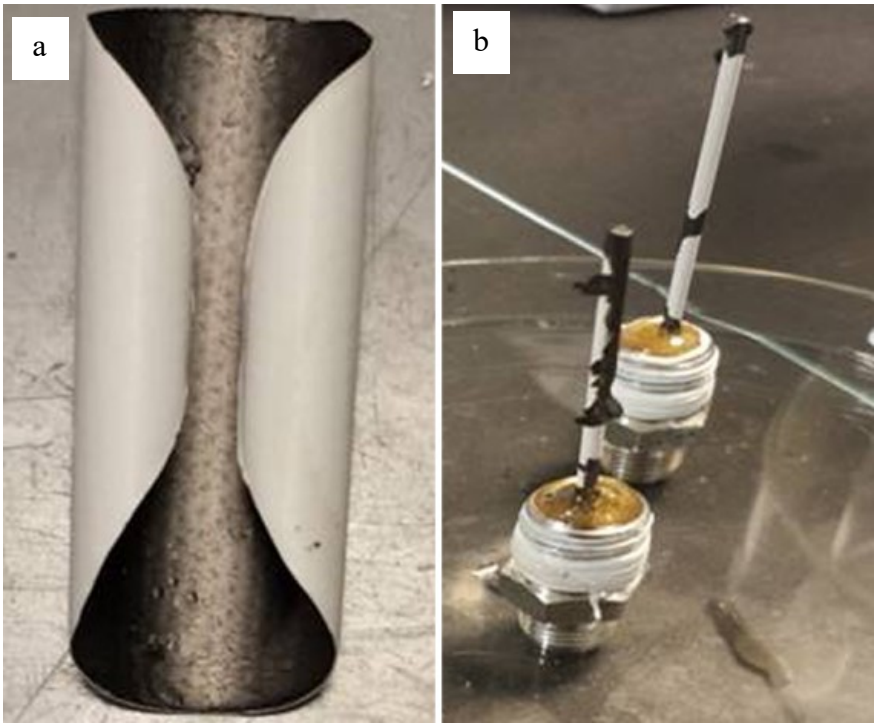

Figure 4. 9: Pictures of supported GO membranes after annealing under vacuum at 150°C for 16 hours. (a) GO membrane supported by a PES polymeric filter, (b) GO membrane supported by an alumina hollow fibre.

4.3.3 Nanofiltration performance

After understanding the instability problem and the reason causing it, GO hollow fibre membranes have been tested in applications whilst drying-related shrinkages can be avoided, and the strategy of storing such membranes was explored. In the membrane industry, it has been found that some polymeric membranes for water treatments such as polyvinylidene fluoride (PVDF) membranes are unstable in dry state. A simple and effective way of storing these polymeric membranes is to keep them wet all the time, either in water or in a water-miscible liquid with a high boiling point, e.g., glycerol. Inspired by the polymeric membranes, we adopt the same strategy for the GO hollow fibre membranes to keep them stable in water

and only use them in wet separation processes. Nanofiltration performance of the GO hollow fibre membranes in aqueous and organic solvent is verified following this strategy.

The feasibility of GO membranes in aqueous phase nanofiltration has been explored by other researchers, but no structural or performance stability was reported [10, 100]. We have tested the performance stability of GO/YSZ hollow fibre membranes in the aqueous nanofiltration process in a three weeks interval. The membranes were performed in two ways: one was to store the membranes in water during the interval between tests (wet membranes), and the other way was to store the membranes in the air after each test (dry membranes). The nanofiltration tests were conducted with five dye molecules of different molecular weights ranged from 327.3 to 973.7 Dalton. GO hollow fibre membranes with a thickness of 1.5 and 3.2 μm were used and the pure water flux of the membranes was 1.04 and 0.58 L m^{-2} h^{-1} bar^{-1}, respectively, showing a dependence on the membrane thickness.

As depicted in Figure 4. 10 , all fresh membranes showed a good rejection performance to the dyes with a rejection rate higher than 99%. The rejection rate increased when the molecular weight was higher and reached 100% for molecules larger than 534.3 Dalton. For the membranes kept in the air (dry membranes), the dye rejection rate dropped remarkably after three weeks. The dye rejection rate of the thicker dry membrane dropped slower than the thinner dry membrane, indicating the thicker membrane is more tolerant to the defects developed in the air. In contrast, for the membranes kept in water (wet membranes), the dye rejection rate was essentially unchanged after three weeks, as we have expected based on the failure mechanism discussed above.

(Note that the error bar is too small to be visible)

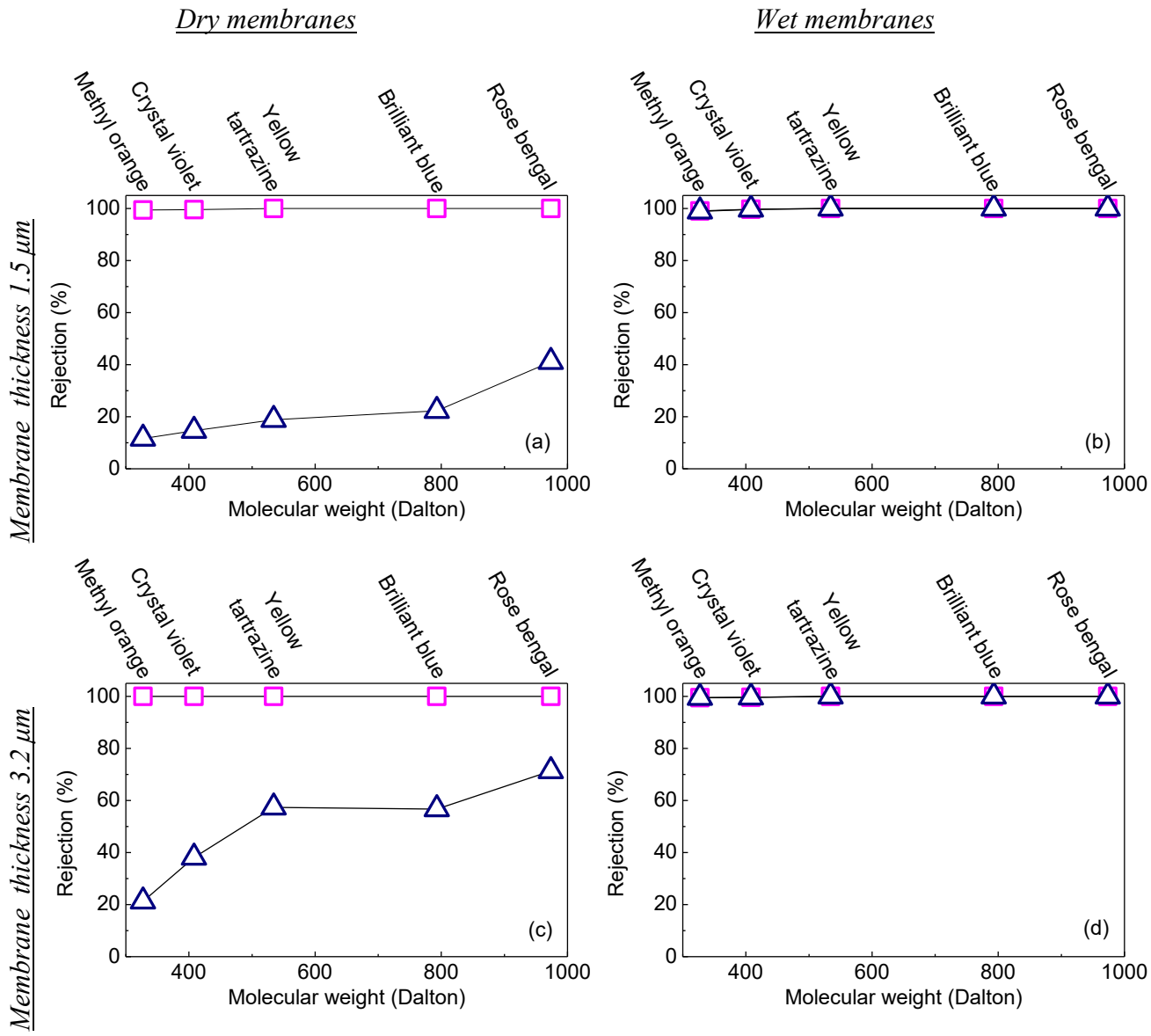

Figure 4. 10:The stability of dye rejection rate of GO/YSZ hollow fibre membranes. The data points marked with square (□) were obtained with freshly produced membranes, and the data points marked with triangle (Δ) were obtained after three weeks from the same membrane

Correspondingly, the pure water flux of the membranes also reflected the micro-structural changes, in which the water flux of the wet membranes basically didn't change after three weeks, but the dry membranes showed a considerably higher water flux than the fresh membranes (Table 4. 2).

Table 4. 2 : Pure water fluxes of the dry and wet GO hollow fibre membranes

Sample	**Water flux (L m^{-2} h^{-1} bar^{-1})**	
	1.5 μm thick	3.2 μm thick
Fresh membrane	1.04	0.58
Std. deviation	*0.12*	*0.19*
Wet membrane (after 3 weeks)	1.06	0.60
Std. deviation	*0.08*	*0.12*
Dry membrane (after 3 weeks)	2.54	1.51
Std. deviation	*0.13*	*0.19*

The GO membranes in overall showed a good performance in the aqueous nanofiltration process. The dye rejection results imply a low molecular weight cut off less than 300 Dalton; the water flux is not exceptional, but still comparable with many commercial membranes [101]. However, the dependence of the flux on the membrane thickness indicates a good potential of improving the water flux, and thus the GO hollow fibre membranes could be very promising in the field of aqueous phase nanofiltration.

On the other hand, compared with their polymeric counterparts, GO is a relatively inert material that is very stable in organic solvents [44], which makes it an excellent candidate for organic solvent nanofiltration. To explore the feasibility of GO hollow fibre membranes in organic solvent nanofiltration, we have tested the permeation flux of pure methanol and acetone, which are very commonly used in organic synthesis. Both solvents exhibited a higher permeation flux than water, where methanol reached 3.97 and acetone reached 6.35 L m^{-2} h^{-1} bar^{-1} for a 1.5-μm thick GO hollow fibre membrane.

We further tested the rejection rate of methyl orange (molecular weight 327.3 Dalton) in both solvents and the rejection rates were higher than 97% in both cases, similar to the results with an aqueous solution. The permeation flux of methanol and acetone are also higher than most commercial membranes with a molecular weight cut-off lower than 300 Dalton [102], which implies that GO membranes are very promising for organic solvent nanofiltration.

The permeation flux of the solvents was higher than water, and similar results have been observed in hydrophobic polymeric nanofiltration membranes [103, 104]. In models interpreting the transport of solvents in nanofiltration membranes, some studies suggested that the viscosity and the molecular size of the solvent, and the surface properties of the solvent and the membrane are the factors affecting the transport in nanofiltration membranes [103, 105, 106].

For the liquids tested in this study, the molecular size increase as per the sequence of water < methanol < acetone, but the order of permeation fluxes is in the opposite direction, which indicates that steric hindrance is not as important as the other factors. The viscosity (at 25 °C) of methanol (0.54 mPa·s) and acetone (0.31 mPa·s) are lower than water (0.89 mPa·s), however it does not account for all the improvement in the permeation flux since the flux is not proportional to the viscosity. Therefore, the surface properties of the solvent and the membrane may account for the rest of the improvement in the solvent fluxes. We measured the contact angle of water, methanol and acetone on GO membranes, it showed a contact angle of 43° for water, but 0° for methanol and acetone, implying the wettability of methanol and acetone is much better than water on GO membranes, and which might significant reduce the transport resistance on the membrane surface and hence facilitate solvent permeation.

The transport path of the liquids in GO membranes seems to be at least partially via the narrow inter-layer space between parallel GO flakes where the distance is 0.7-1.4 nm depending on the water content [69, 95], and it is supported by the high-precision molecular-sieving feature of the membrane. However, considering the very high aspect ratio of the GO flakes (meaning a very high tortuosity of the transport route) and the thickness of the GO membrane, the transport path would be very long (more than 5 mm for the 1.5 μm-thick membranes in this research), and thus a very low permeation rate is expected. It was proposed that water can pass through GO membranes very fast through the hydrophobic pristine graphene channels due to the low friction between the water and the wall [69]. However, recent results have shown that it may not be the case because of the side-pinning effect of the hydrophilic areas, and it was suggested that the fast water transport in GO membranes could be due to the porous microstructure [107], and such a porous microstructure could be attributed to the defects formed during dying. In fact, we have found that the shrinkage-related development of defects can be minimized by replacing water in the membranes before drying with a low surface tension solvent such as methanol and acetone.

For GO/YSZ hollow fibre membranes with a 350-400 nm thick GO layer treated with solvent displacement, dye rejection tests showed the dry membranes could completely reject Brilliant Blue and Yellow Tartrazine (molecular weight of 792.85 and 534.36 Dalton, respectively), which implies that the membranes are intact and no significant defects were developed during the drying process thanks to the low surface tensions of methanol and acetone. As a comparison, the dry membranes of similar thickness without solvent displacement showed no rejection to the dyes. However, the GO/YSZ hollow fibre membranes treated with solvent displacement showed an extremely low average pure water flux of 0.05 L m^{-2} h^{-1} bar^{-1}, whose permeability is almost two magnitudes lower than the 1.5 and 3.2 μm thick membranes used in this research.

Thus it is reasonable to believe that there are short-cuts in the thick nanofiltration GO membranes for the transport of the liquids. It has been shown that the drying process leads to time-evolving development of defects in the GO membranes. In this case, the defects developed in the membrane can act as the short-cuts which drastically reduced the effective membrane thickness, thus the liquids are able to pass the membrane with a considerable flow rate.

Figure 4. 11 schematically shows the discussion on two different transport routes in GO membranes, where the route A represents the transport in an ideally packed GO membrane, and the route B represents the transport in a GO membrane with defects. By properly controlling the initial drying conditions (temperature, time, and humidity), the defects can be controlled not to cross through the membranes, thus maintain the molecular-sieving feature. It is reasonable to believe that in the time-evolving development of defects, the time needed for the defects to cross through the membrane is affected by the membrane thickness, which explains why the dye-rejection rate of the thicker dry membranes drops slower than the thinner one as depicted in Figure 4. 10.

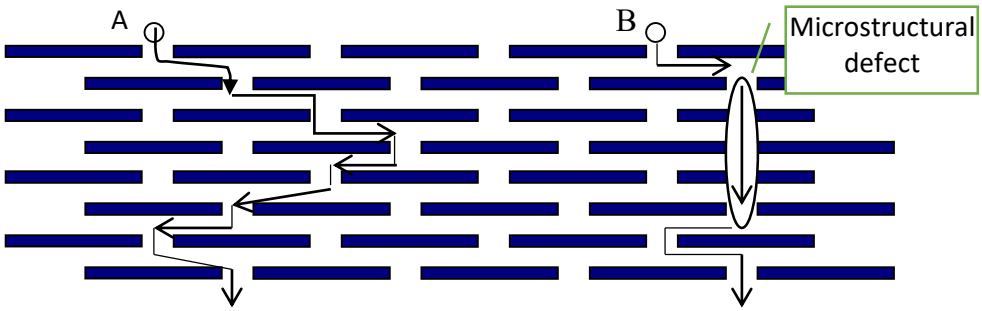

Figure 4. 11: Discussion on transport mechanism in nanofiltrationm

4.4 Conclusions

In conclusion, we have prepared GO membranes on ceramic hollow fiber substrates, but these GO membranes are not stable in the air, mainly due to the shrinkage-induced stress in the GO membrane. By avoiding further shrinkage after initial drying, in this case, through storing the membranes in water, GO hollow fiber membranes can be stabilized and are suitable for wet separation processes. The performance of these membranes in the application of nanofiltration shows a molecular weight cut off lower than 300 Dalton and organic solvent permeation fluxes higher than most commercial nanofiltration membranes, which indicates a great potential of the GO hollow fiber membranes in value-added separation processes.

CHAPTER 5

Graphene Oxide Membranes on Ceramic Hollow Fibres – Cationic Cross-linking and the Efficiency for Water Desalination

Abstract

Graphene oxide membranes have shown potential in the process of nanofiltration, where small molecules of several hundred Daltons can be effectively filtered. But for even smaller ionic species, such as sodium chloride, GO membranes are incapable of removing them due to the pristine nature thereof, and as a result pristine GO membranes are difficult to use in the desalination process.

Based on the space charge model, it is well acknowledged that the rejection of salts relies on the pore size of a membrane and charge density of the pore wall [108]. In this study, pristine GO membranes are cross-linked with Al^{3+} *and this provides a more stable membranes structure. More importantly, without affecting the inter layer space between GO, the* Al^{3+} *can narrow down the effective channels size for ion transport and turned the GO membranes from being negatively charged to highly positively charged, resulting in a high rejection rate of the sodium chloride solution. The test results demonstrate that GO membranes can be tuned by modification to suit the requirements of the desalination process, expanding its potential application to one of the most important water treatment processes.*

5.1 Introduction

Several studies, including simulation and experimental works, have shown that graphene and graphene oxide membranes have a considerable potential for desalination applications [11, 51, 52, 70, 109-112]. Unfortunately, the rejection towards monovalent ions, especially sodium salt, is still too low to be useful in desalination applications. The main limitation and challenge in terms of applying graphene or graphene oxide membranes in desalination is to control the pore sizes of the membrane. The pore size of graphene and the interlayer space between the GO sheets should not be too large, in order to prevent small ions, such as sodium salt, from passing through. Additionally, these values should not to be too small, as this could potentially hinder the passage of water. As suggested by Cohen and Tanugi based on their simulation study, the effective pore size of graphene membranes must be around 5.5Å in order to hinder the passage of salt ions [109]. In the case of the graphene oxide membranes, as suggested by Mi, the interlayer space of the GO membranes should be reduced to be less than 7Å in order for it to effectively remove sodium salt (Na^+) from water [113]. This could be achieved by reducing the GO membranes to a reduced graphene oxide (rGO) membrane. However, reducing the GO membranes may entail a more hydrophobic behaviour which is not favourable in water filtration applications. In addition, previous experiment showed that if the interlayer space is reduced to less than 6Å [114], the nanocapillaries within the membranes completely hinder water from permeating through. Such a limited tunable range, (<1Å) continues to pose a challenge. Nevertheless, Mi et al., shed some light by suggesting that Na^+ can be sieved from water when the interlayer space of the GO membranes is larger than 7Å, provided that the charge distribution along the GO membranes can be controlled [113].

When GO membranes have an interlayer space larger than 7Å, it is important to consider the interaction between the solutes and the functional groups existing at basal plane as well as the edge of the GO membranes, together with the cation-π interaction. This interaction may facilitate the rejection of charged solutes [11, 55]. Therefore, further fine tuning or cross-linking may be necessary for the GO membranes to achieve a high rejection rate (of at least 90%), especially for the rejection of monovalent salts, in order for it to be feasible in desalination applications.

GO membranes are well known for being easily re-dispersed in water if there is no cation to facilitate the cross-linking of the GO flakes, for example on a polymeric support [115]. Therefore, stabilising the GO membranes before applying the membrane in water treatments is crucial in order for the latter to remain stable in water. Recently, Yeh et al., have discovered that unintentional Al^{3+} cross-linked in the GO membranes coated on an AAO disk has resulted in a stable GO membrane in water. This unintentional cross-linking not only rendered the GO membranes to be water-stable, but also enhanced its stiffness up to 340% as opposed to an increase of only 10% achieved by the original works of divalent metal cross-linking [59].

Inspired by these two findings, Al^{3+} was intentionally added to the GO membranes in order to introduce excess cations that would not only cross-link the GO flakes, but also narrow the effective channels for ion transport, and therefore facilitate the rejection of salts, thus rendering the GO membranes more suitable for the purpose of water desalination.

5.2. Experimental

5.2.2 Cross-linking procedure

The cross-linking of the GO membranes using the pressure-driven filtration method has been published by Park et al., [59]. However, instead of using pressure filtration, vacuum filtration is used in this instance in order to suit the fabrication of the GO hollow fibre membranes. In this method, the cross-linking of the GO hollow fibre membranes were prepared by immersing the as-prepared GO hollow fibre membranes in solutions containing $AlNO_3$ and by vacuum filtering the solution for the required time. Figure 5. 1 summarises the cross-linking procedure.

5.2.2 Desalination experiment

The salt rejection experiment was carried out using a dead end system. The salt rejection experiment was carried out at room temperature (20 ± 2 °C) under a pressure of 10 bar with a saline solution concentration of 0.2 wt%. The stainless steel membrane cell was filled with saline water feed solutions (approximately 350 ml). The GO hollow fibre membrane was glued onto a stainless steel holder prior to coming into contact with the saline feed solution. Nitrogen was supplied into the vessels at a constant 10 bar pressure during the test. The pressure of the permeate side was maintained at ambient pressure. The permeate was collected after 3 hours and the ion concentration was analysed using the conductivity meter (Hanna Instrument, HI-8733N).

The rejection (Ri) of the ions was calculated on the basis of the following equation:

$$R_i = \frac{C_f - C_p}{C_f} x\ 100\%$$

Where C_f and C_p represent the ion concentrations in the feed and permeate solutions, respectively.

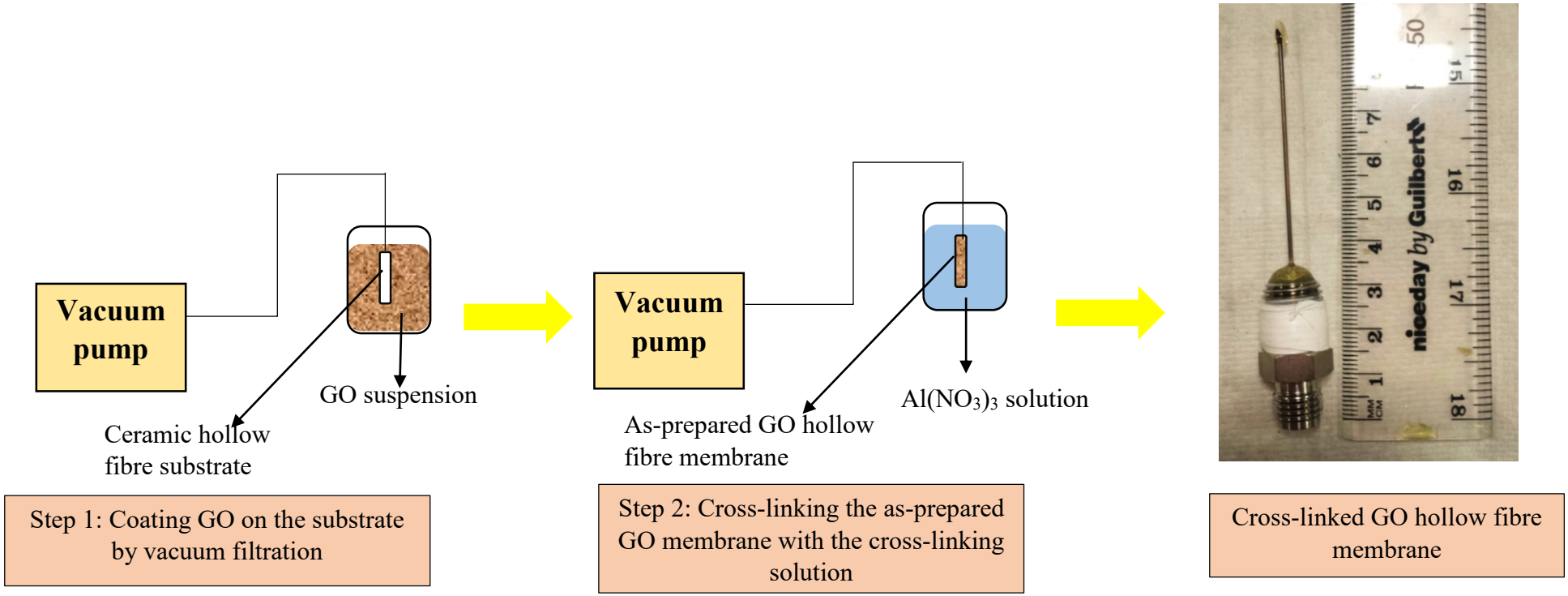

Figure 5. 1: Step-by-step fabrication procedure for cross-linking the GO hollow fibre membranes.

5.3. Results and Discussion

5.3.1 Morphological and chemical characterisation of the membranes

Figure 5.2 (a) and (b) show the typical morphology of the GO membrane used in this study and the thickness of the membrane, which is measured to be approximately 300 nm. The thickness of the membrane was controlled by the initial concentration of the GO suspension used during the vacuum facilitated coating process. Figure 5.2 (c) and (d) show the surface of the GO membrane before and after cross-linking. The surface of the GO membrane before cross-linking shows a typical morphology of the GO film in which the wrinkles can be clearly seen. On the other hand, the surface of the GO membrane after cross-linking shows no GO film grain boundary, which is indicative of a possible cross-linking between the metals and the GO membrane.

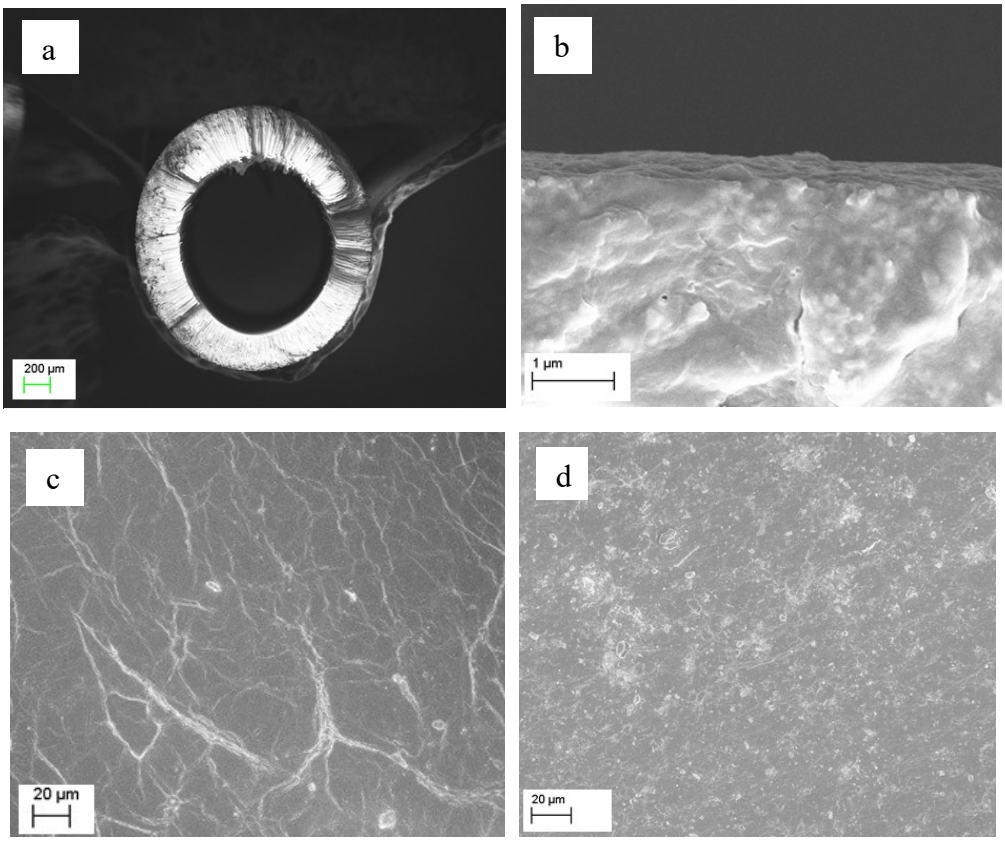

Figure 5. 2: SEM images of the GO membrane; (a) Cross sectional view; (b) Thickness of the GO membrane ;(c) Surface of the GO membrane before cross-linking; (d) Surface of the GO membrane after cross-linking

The XPS analysis of the GO membrane before and after cross-linking with 1.0 M $Al(NO_3)_3$ is shown in Figure 5. 3 (a) and (b). The XPS analysis of the GO membrane before and after cross-linking is important in order to determine the interaction between the GO flakes and the cross-linker. As can be seen from Figure 5. 3 (a), the pristine GO membrane exhibits typical GO peaks, which represent carboxyl, carbonyl, ethyl, alcohol and epoxy as well as graphitic which is consistent with other findings [116, 117]. On the other hand, the GO membrane after cross-linking (Figure 5. 3 (b)) shows a distinct pattern, especially in relation to the peak corresponding to the graphitic functional groups. From these results, it may be inferred that the cation was successfully cross-linked with the ethyl/alcohol/epoxy functional groups rather than with the carboxylic functional groups of the GO. Furthermore, the XPS survey scan (Figure 5. 3 (d)) showed an apparent peak of Al after cross-linking with the cation. In contrast, the XPS survey scan of the pristine GO membrane (Figure 5. 3 (c)) showed no other apparent peaks other than C and O, which further proves that the cation has successfully cross-linked with the pristine GO membrane.

The intensity of the alcohol/ether group after cross-linking with the cation largely decreased due to the fact that after cross-linking, the net electronegativity of the oxygen connected to carbon is reduced. On the other hand, carboxyl functional groups remain similar after cross-linking. It may thus be recalled that based on the proposed GO structure, the ethyl/alcohol groups are decorated at the basal plane, whereas the carboxyl groups are decorated at the edge of the sheets. Thus, it is more likely for the alcohol/ether groups to donate free electrons to the Al^{3+} cation as opposed to the carboxyl groups that exist at the defective sites in which the cross-linking with the Al^{3+} cation will be more difficult.

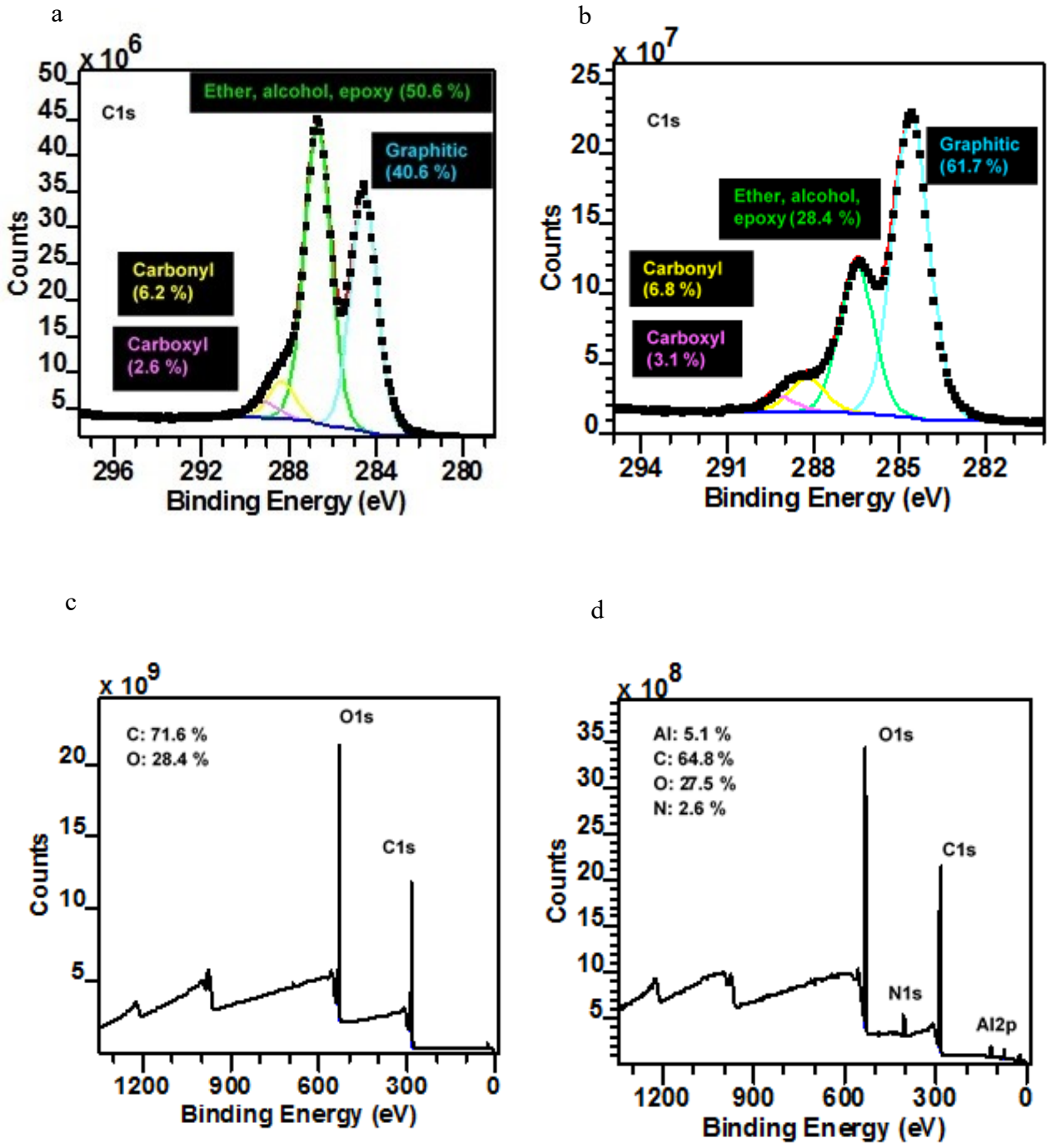

Figure 5. 3:XPS analysis of the GO membrane(a) before cross-linking, (b) after cross-linking; XPS survey scan of (c) the GO membrane before cross-linking, (d) the GO membrane after cross-linking

5.3.2 Desalination Performance of Cross-linked GO membranes

Park et al., first modified the GO membranes with alkaline earth metals ions, namely Mg^{2+} and Ca^{2+}, in order to enhance the mechanical strength of the GO via chemical cross-linking. Based on their work, cross-linking GO with a small amount of metal ions (less than 1 wt% cations) would yield a total amount of 2 mmol of Mg^{2+} and Ca^{2+} which is more than enough to link the oxygen-containing functional groups in the GO sheets. Thus, on the basis of their calculation, it was believed that excessive metal ions existed and that it was possible to unbind or weakly bind metal ions present in the gallery regions between the GO sheets [59]. Furthermore, Yeh et al., recently cross-linked the GO membrane with Al^{3+} in order to render it water-stable and prevent it from degrading in water [115]. Several studies have proven that the electrostatic repulsion between salts and charged GO sheets may contribute to the rejection of salts [51, 70, 110]. From their findings, it is obvious that the charge in the GO membranes is important especially when the interlayer space between the GO sheets is larger than 0.7nm. However, so far none of the studies could successfully reject salts, especially in the case of monovalent ions with a rejection rate of more than 80%. Thus, the GO membranes are still under development in order to be used in reverse osmosis based water desalination applications at a later stage. Taking into account all the advantages of cross-linking cations with GO sheets, GO has been purposely cross-linked with $Al(NO_3)_3$ in order to change the overall charge of the GO sheets to higher positive charging, and thus provide higher surface charge density and narrowed down the effective channel size for ion transport, allowing an efficient salt removal.

The separation performance of the cross-linked GO membrane was tested using the suggested concentration of the cross-linker at 0.1M [115]. In addition, the rejection rate of the pristine GO membrane to salts (without cross-linking) has also been examined in order to compare it with the cation-cross-linked GO membrane. $MgCl_2$ and NaCl were used as representatives of divalent and monovalent salts. The cross-linking time varies from 4 hours to 24 hours.

From the results shown in Table 5. 1, it is clear that the rejection performance of the membrane increased for both monovalent and divalent salts after cross-linking, particularly for the GO membrane which was cross-linked after 24 hours. The GO membrane without cross-linking clearly showed a very poor rejection rate to sodium and magnesium cations, which was also found in other studies using unmodified GO membrane [11, 52, 70, 110, 112]. It may be possible that the Al^{3+} attached on the GO surface has narrowed down the effective channel size for the transport of the ion, which would in turn enhance salt rejection on the basis of the space charge model [108]. In addition, the obtained results suggest that the increase in the cross-linking time can increase the amount of cation cross-linked with GO sheets, and hence increased the surface charge density, which would then facilitate the improvement of salt rejection according to the space charge model [108].

Table 5. 1: Permeance and salt rejection of the GO membrane at different cross-linking times

Membrane	**Permeance ($lm^{-2}h^{-1}bar^{-1}$)**	**$MgCl_2$ rejection (%)**	**NaCl rejection (%)**
Pristine GO membrane	1.28	78.21	7.98
Std. deviation	*0.10*	*0.31*	*0.32*
4h cross-linked	1.42	85.80	10.06
Std. deviation	*0.07*	*0.55*	*0.33*
24h cross-linked	1.51	95.20	15.97
Std. deviation	*0.08*	*0.31*	*0.23*

Nevertheless, increasing the cross-linking time to a greater extent will not be beneficial since it will subsequently take longer time to produce the cross-linked GO membrane. Therefore, it was sought to increase the concentration of $Al(NO_3)_3$. In this study, concentrations of 0.1M, 0.3M, 0.5M, 0.7M and 1.0M of $Al(NO_3)_3$ were used.

Figure 5.4 shows the performance of the GO membrane cross-linked with different concentrations of the $Al(NO_3)_3$ solution. As can be seen from the results, there is a clear increasing trend in the NaCl rejection rate along with an increased concentration of $Al(NO_3)_3$. At the same time, the total permeance of the membrane was slightly increased. The permeance of the membrane increased from 1.51 $lm^{-2}h^{-1}bar^{-1}$ to 1.86 $lm^{-2}h^{-1}bar^{-1}$ at a concentration value of 0.1M and 1.0M, respectively. On the other hand, the rejection rate increased significantly from 17% to 89% when the concentration of $Al(NO_3)_3$ increased from 0.1M to 1.0M, respectively.

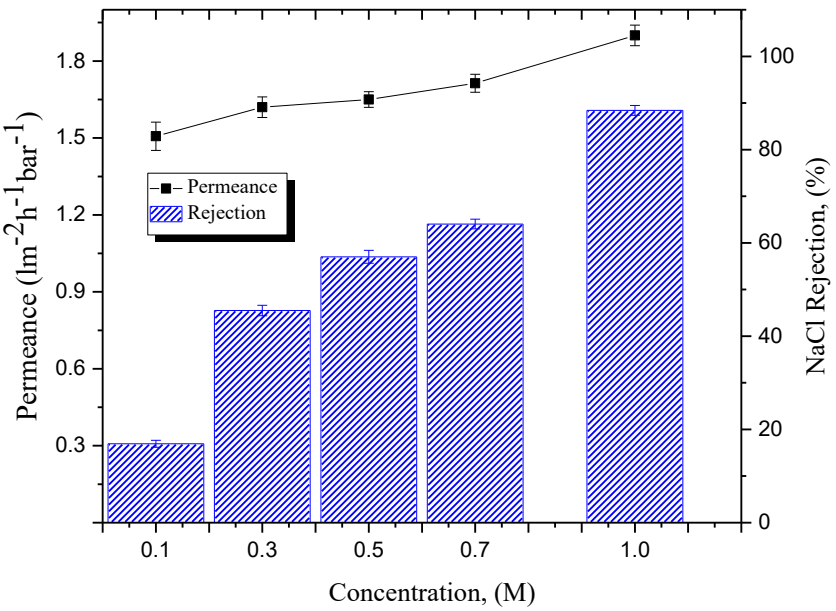

Figure 5.4: Separation performance of the GO membrane after cross-linking at different Al^{3+} concentration values for NaCl rejection

In general, it is believed that the spacing between the GO flakes and the charge on the GO flakes constitute the two dominant factors that would determine the overall rejection rate of the GO membrane. Based on these results, it is quite obvious that increasing the amount of cross-linked cations would result in an increased rejection of the ions. This finding possibly suggests that the rejection of the ions is significantly influenced by the charge of the cross-linked GO membrane. From the cross-section elemental analysis of the cross-linked membrane using the EDX analysis, (see Figure 5. 5 and Table 5. 2) it may be observed that the amount of Al^{3+} increases as the concentration of $AlNO_3$ increases.

Table 5. 2: Al analysis in GO layer

Concentration (M)	**Al composition (wt%)**
0.1	0.51
0.3	1.73
0.5	2.09
0.7	2.62
1.0	3.66,

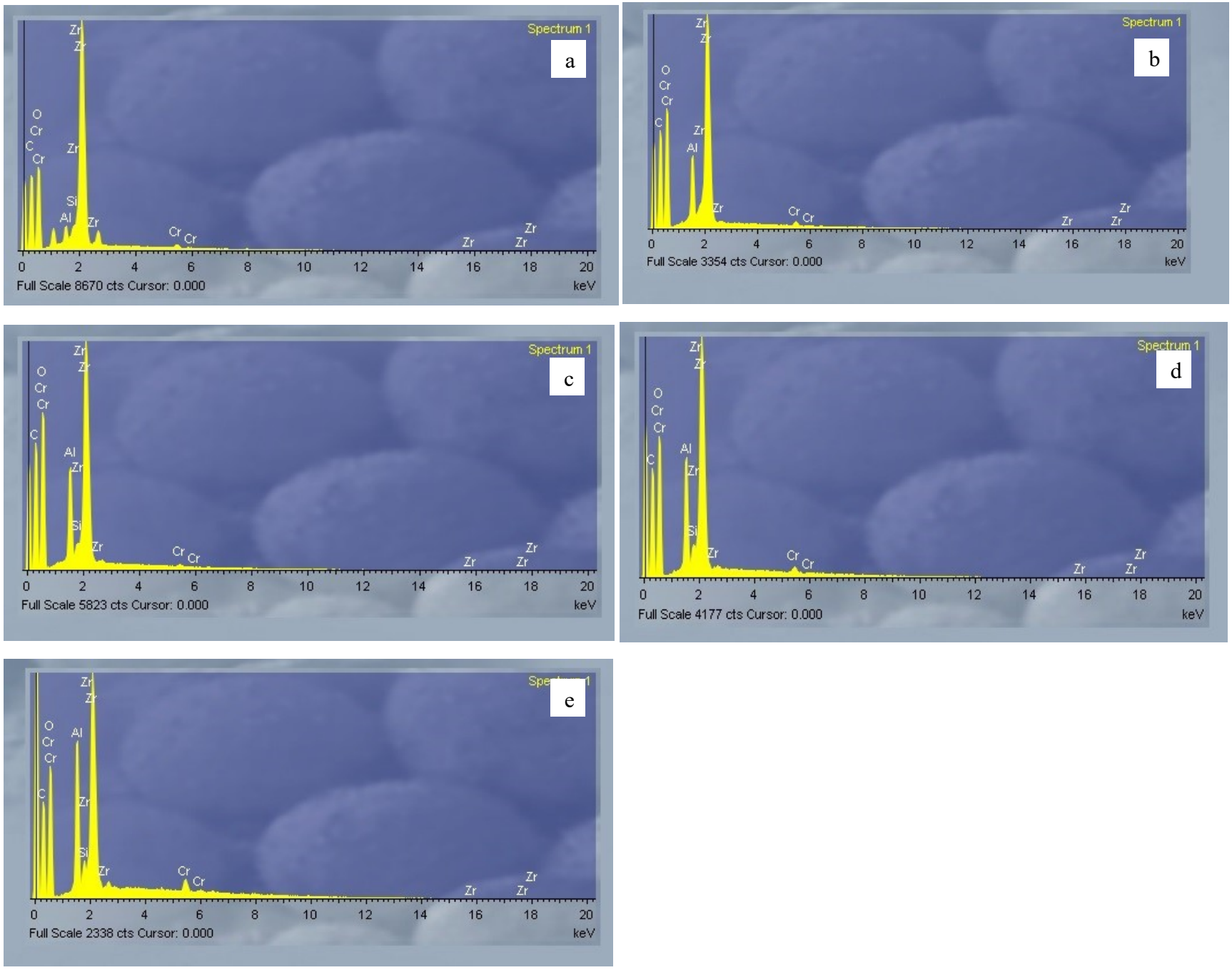

Figure 5. 5: EDX analysis of the cross-linked GO membrane: (a) 0.1M; (b) 0.3M; (c) 0.5M; (d) 0.7M; (e) 1.0M

The increase of the cation numbers in the GO sheets may be able to increase the surface charge density, and therefore the rejection of the membrane towards salt ions become more efficient. Table 5.3 lists the zeta potential value of the pristine GO solution and the GO solution with a different concentration of $Al(NO_3)_3$. As can be seen from the table, the zeta potential value of the GO membrane increases as the concentration of cross-linker increases which means that cross-linking has successfully turned the GO membrane from a negatively charged to a positively charged membrane. For pristine GO membrane which is widely known to be negatively charged due to the deprotonation of the carboxylic groups, its absolute zeta potential is higher than the cross-linked GO membranes, however giving the lowest salt rejection rate. It may be expected that, with the attachment of Al^{3+}, the effective interlayer space between GO flakes narrowed, which would be more effective to increase salt rejection even when the surface charge density is considerably low [108].

Table 5.3: Zeta potential value of the GO and the mixture of GO with Al(NO3)3

Solution	**Zeta potential (mV)**
GO	-41.62
GO+0.1M $Al(NO_3)_3$	15.52
GO+0.3M $Al(NO_3)_3$	18.82
GO+0.5M $Al(NO_3)_3$	20.61
GO+0.7M $Al(NO_3)_3$	24.41
GO+1.0M $Al(NO_3)_3$	38.28

In order to further understand the importance of the charge effect in determining the GO membrane separation performance, the rejection of the NaCl and $MgCl_2$ solutions was studied at different concentrations using the 1.0M cross-linked GO membrane, ranging from 0.2 wt% to 4 wt%. As shown in Figure 5.6, the rejection rate and permeance decreased significantly as the solution concentration increased for $MgCl_2$ and NaCl in each case. Decrease in the rejection can be explained by the fact that the electrostatic repulsion between the ions and the charged membrane decreases because of the thinning of the electrostatic double layers as the Debye length decreases, which in turn reduces the rejection rate. In this case, debye length at 0.1 wt% is This observation echoes the findings of Hu and Mi [70] who observed an identical behaviour. This result is an obvious indication that the charge effect is a significant factor that contributes towards the separation performance of the GO membrane in salt rejection.

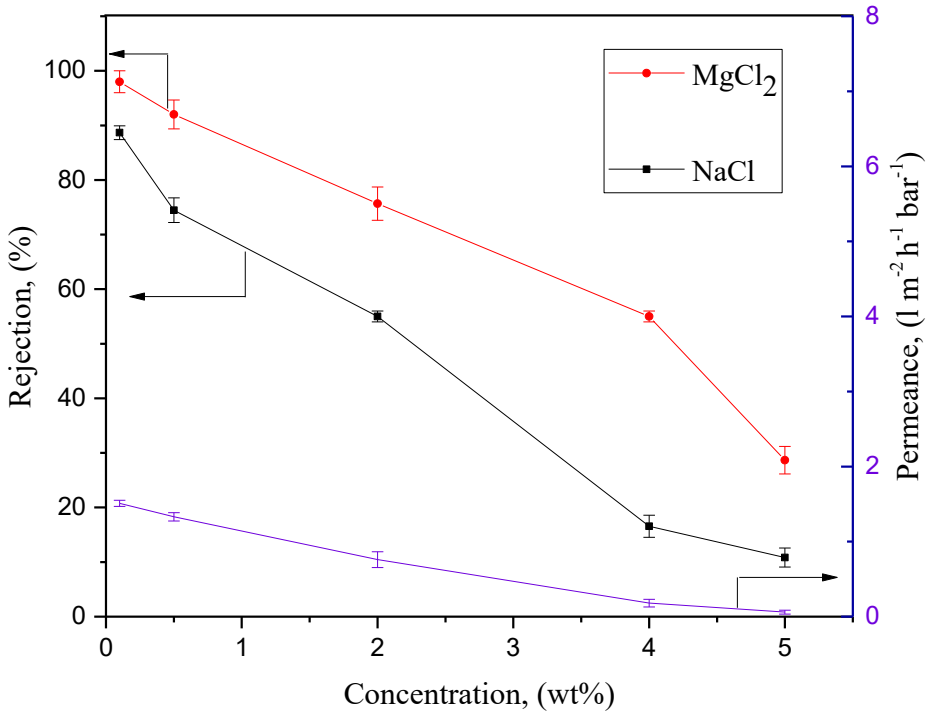

Figure 5.6: Effect of salt concentration on the cross-linked GO membrane.

It is of interest to understand whether the cation cross-linked on the GO is fully responsible for the enhanced rejection to the salts, and whether the other factors also play a role therein. In general, the membrane microstructure should have also played a role in determining the overall performance of the GO membrane. It can be seen that there was difference in water permeance when the concentration of $Al(NO_3)_3$ was increased, indicating that there might be some changes at the level of the membrane structure. In Figure 5.7, which shows the results of the XRD analysis on the cross-linked membrane, an apparent difference in peak intensity may be observed. It clearly shows that the increase in the $Al(NO_3)_3$ concentration has changed the microstructure of the GO membrane from a good laminar ordered one (0.1M) to a disordered one (1.0M), which is reflected by the loss of intensity at the peak of around 10°. This could be due to the fact that when the cross-linking between $Al(NO_3)_3$ and the GO sheets occurred, the GO sheets had the tendency to form crumbles and wrinkles, resulting in the loss of the laminar structure of the membrane, which explained the slightly increased permeance of the GO membrane after cross-linking.

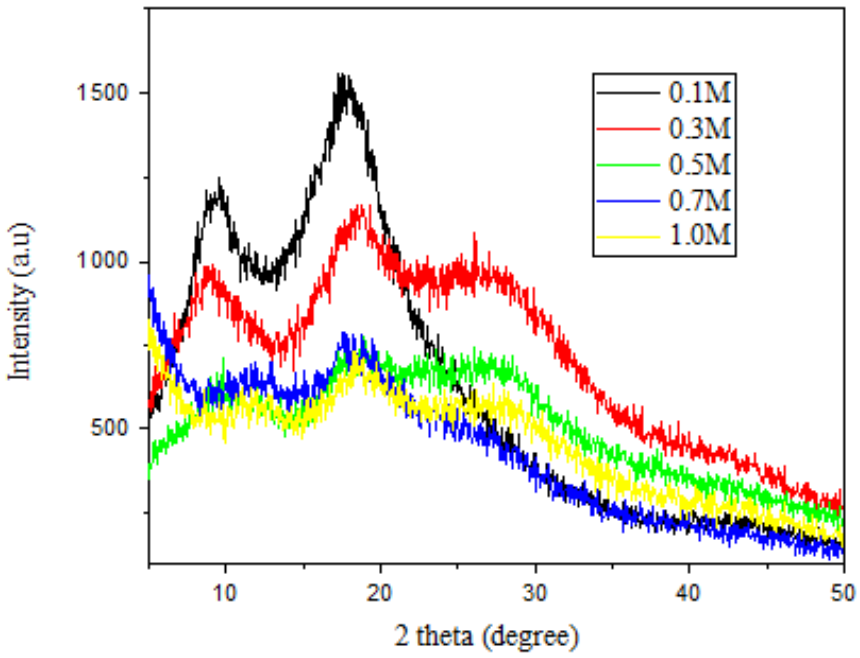

Figure 5.7: XRD analysis of the GO membrane cross-linked at different concentration values

From the cross-sectional SEM images (Figure 5. 8), one can clearly see the difference in the membrane microstructure between the 0.1M and 1.0M cross-linked samples. It is quite apparent that the 1.0M cross-linked membrane has a more buckling (disordered) structure as opposed to the 0.1M cross-linked membrane, which shows a more ordered laminar structure. This further confirms the result of the XRD analysis (Figure 5.7) where the peaks disappear entirely after cross-linking with 1.0M $Al(NO_3)_3$.

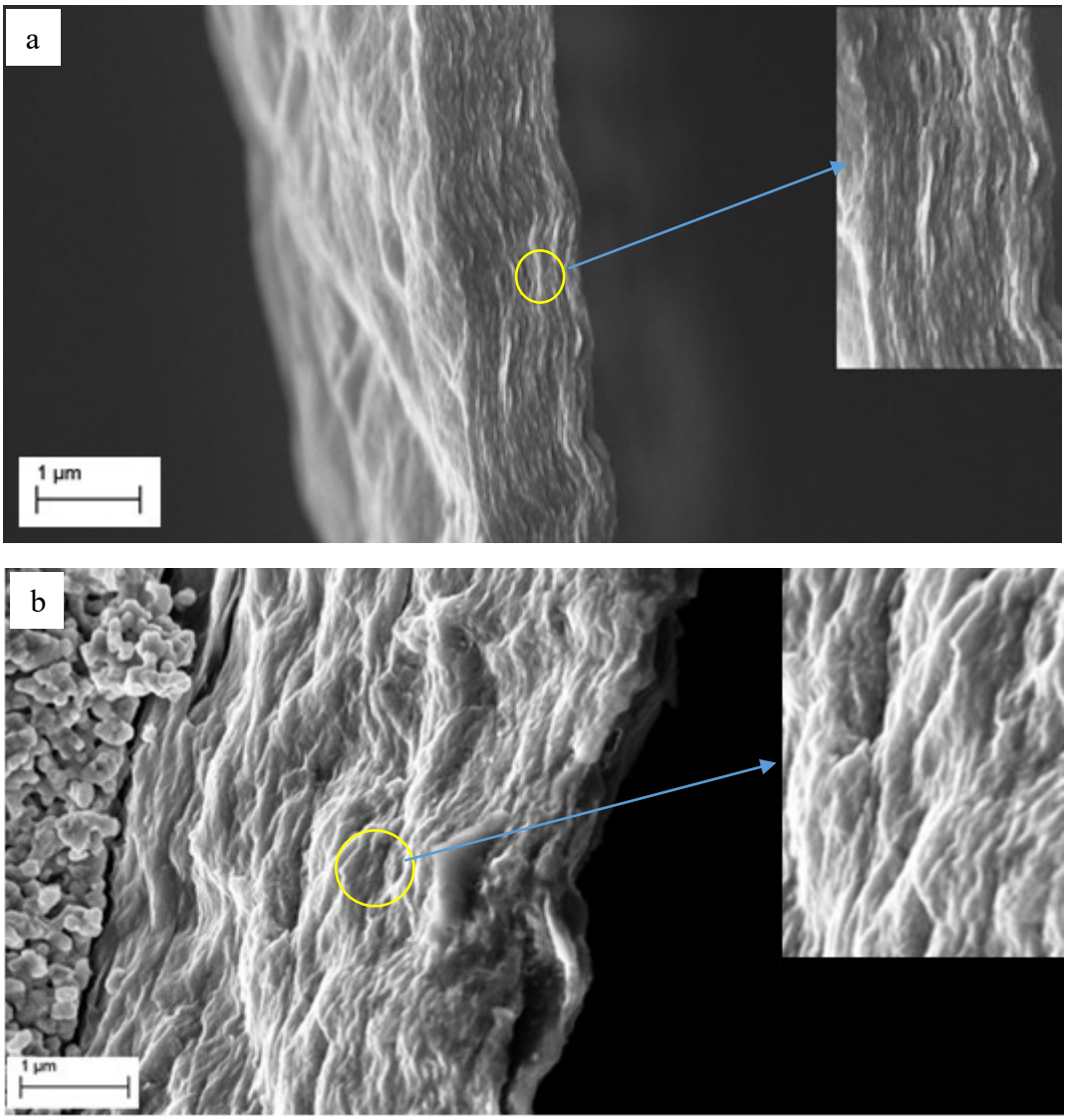

Figure 5. 8:SEM images of cross-section GO membrane; (a) 0.1M cross-linked;(b) 1.0M cross-linked

It was found that the GO membranes obtained using pressure assisted self-assembly method exhibit a compaction behaviour [74]. The compaction in the GO membrane occurs when a pressure is introduced during the filtration process, which renders the microstructure of the GO membrane more compact. In this study, the compaction problem is not very severe for the membrane cross-linked with a low concentration of $Al(NO_3)_3$, but it then becomes more

serious when the concentration increases, especially in the case of 1.0M $Al(NO_3)_3$. As shown in

Figure 5.9, within the first few minutes after the membrane was pressurised, the permeance was very high and reached around 5 $lm^{-2}h^{-1}bar^{-1}$. After the first hour, the permeance continued to decrease but at a slower pace than in the initial stage. Only after 3 hours of permeation, the permeance stabilised, but as it may be observed, the stable permeance decreased significantly from the initial permeance of 5 $lm^{-2}h^{-1}bar^{-1}$ recorded in the first 5 minutes to only around 1.85 $m^{-2}h^{-1}bar^{-1}$ at the end of the test. In contrast, in the case of the 0.1M cross-linked membrane, a less severe compaction occurred, where the permeance did not significantly decrease after the pressure was applied.

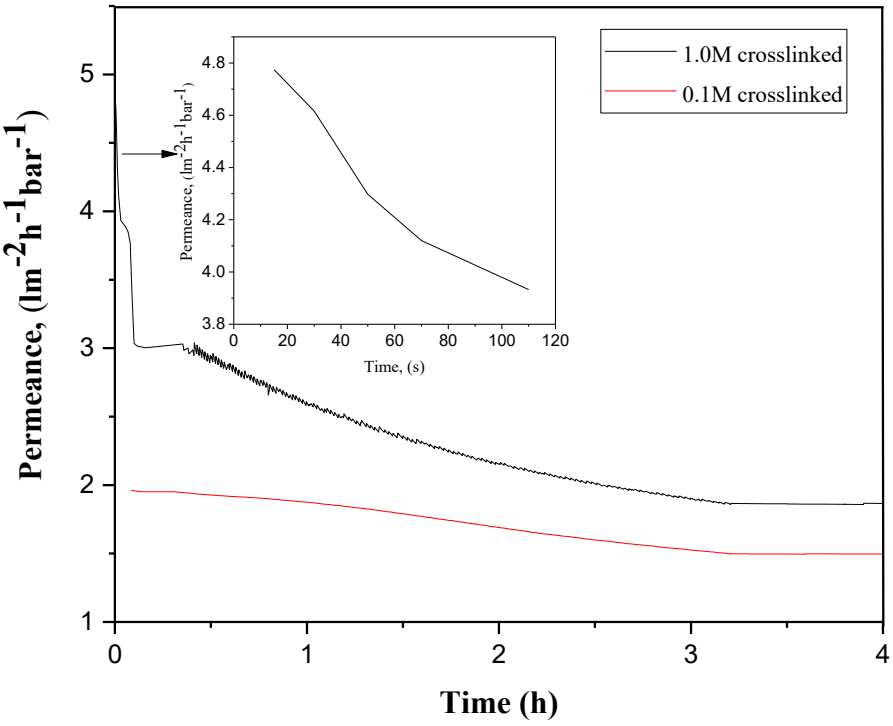

Figure 5.9: Compaction analysis of the GO membrane cross-linked at 0.1M and 1.0M. Inset is the compaction analysis for 1.0M crosslinked GO membrane at the first 100 seconds to clearly show when the permeation starts.

It can be hypothesised that the serious compaction that occurred in the 1.0M cross-linked membrane might be attributed to the re-arrangement of the initial highly disordered GO sheets (refer to XRD, Figure 5.7). When pressure was introduced, the disordered sheets were forced to re-arrange their stacking into more ordered structures. The high permeance recorded during the first 30 minutes was caused by the disorder of the membrane, in which the transport path for the solutes to pass through was short as a result of the wrinkles and crumples that introduced shortcuts in the GO membrane microstructure. On the other hand, the decrease in permeance was attributed to the fact that the GO membrane became more ordered and the shortcuts were compressed and partially sealed, which resulted in a longer transport path for the solvents to permeate through. Figure 5. 10 represents the XRD pattern of the 1.0M cross-linked membrane following the filtration of the NaCl solution. As can be seen, the order of the membrane has been recovered upon filtration, which is in agreement with the permeation results. Hu and Mi also found that the performance of the GO membrane in which the nanosize channels were introduced using nanostrands was highly dependent on pressure [70]. It should be noted that, the above hypothesis is on the basis of XRD analysis and it is quite difficult to precisely determine the order of the membranes before and after the compaction analysis. However, the above hypothesis might give some new insight on how important the order of the GO membranes in determining the overall performance of the membranes.

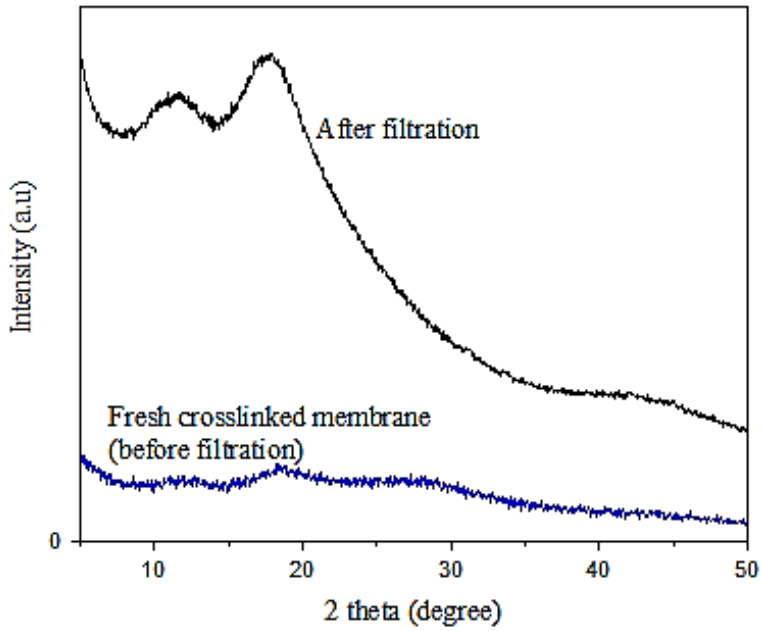

Figure 5. 10:XRD analysis of the 1.0M cross-linked GO membrane before and after filtration with NaCl

The recovery of the orderliness of the membrane has reduced the water permeance and at the same time increased salt rejection (Figure 5.11). Based on Figure 5.11 provided, it may be clearly noted that within the first hour of filtration, the permeance was high, whereas the salt rejection rate was as low as 16%. The permeance of the membrane decreased gradually over the filtration time, and the rejection rate started to show an increase in value and reached 89% after four hours of filtration. This result can thus be attributed to the elimination of the uncontrolled transport shortcuts which may reduce the selectivity of the membrane. It should be noted that concentration polarisation might occur as the time goes longer than 250 minutes. However, this will not be the main concern in this study, but in the future this must be taken into consideration in designing the crosslinked GO membranes and appropriate action should be taken to overcome this problem.

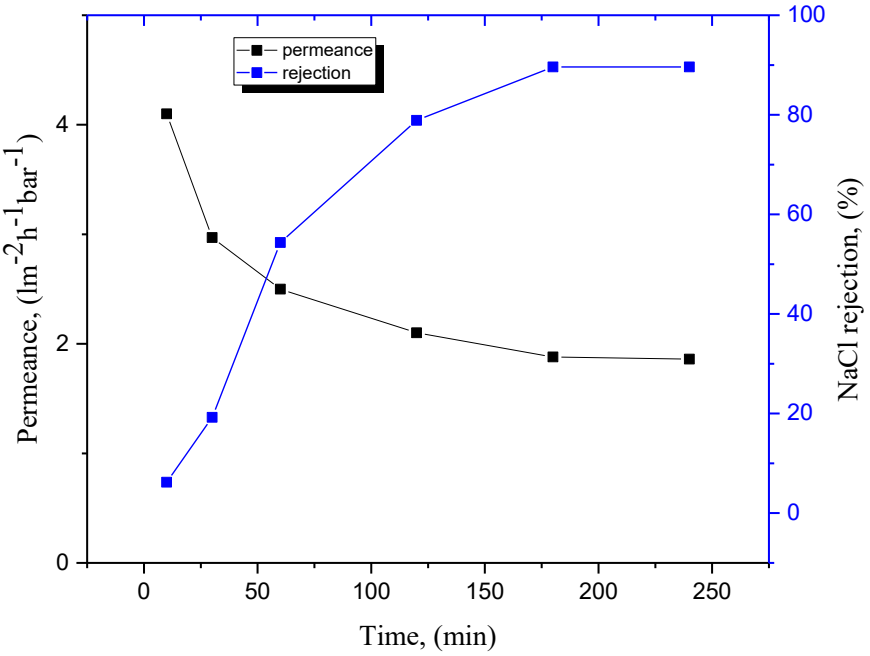

Figure 5.11: Permeance and rejection of 1.0M cross-linked membrane at different time of filtration for NaCl rejection

5.4 Conclusions

In conclusion, cations cross-linked have been successfully carried out in order to introduce excess cations into the GO membranes, which subsequently improved the rejection of divalent and monovalent ions significantly. In addition, it may be inferred that the rejection mechanism in these cross-linked GO membranes was governed by the charge effects, and that the change in the membrane microstructure considerably affects the permeation flux and the rejection rate.

CHAPTER 6

Ultrafast Water Removal from Ethanol by Pervaporation Using Surface-Modified Graphene Oxide Hollow Fibre Membranes

Abstract

Graphene oxide membranes have shown a great potential in pressure driven separation applications, such as nanofiltration and desalination. Furthermore, graphene oxide membranes also showed considerable potential in non-pressure driven separation applications, such as pervaporation. Pervaporation offered many advantages over traditional distillation in terms of energy and environmental conservation. Although the feasibility of graphene oxide membranes in the pervaporation for dehydration of ethanol has been studied, the performance thereof is still considered to be moderate especially in terms of flux. Considering that the hydrophilicity of the membrane is one of the factors determining the flux of the membrane during pervaporation, the GO membrane has been modified herein with hydrophilic silane with the objective to adsorb more water from the bulk liquid towards the surface of the GO membrane for a pervaporation dehydration of 95/5 wt % (ethanol/water). The enrichment of water at the surface of the GO membrane has improved the permeation flux, as well as the separation factors, to the exceptional permeation flux value of 18.3 $kgm^{-2}h^{-1}$ with a moderate separation factor. In addition, the techno-economic analysis shows that in the case

of this modified GO membrane, the smallest membrane area is acquired compared to other state-of-the-art pervaporation membranes.

6.1 Introduction

In common pervaporation (PV) practice, one component of the mixture is usually present in low concentrations. For example, in the PV dehydration of ethanol, the common concentration of water in the feed is only 4.37%. When the feed concentration of solute is high, concentration polarisation could be another factor that affects the overall performance of the pervaporation system [118-120]. Using a surface modification technique, water can be enriched on the membrane surface, which simultaneously increases the water content in the modification layer. A recent study showed that by simply covering the GO membrane with hydrophilic chitosan, it is possible to successfully increase the water concentration on the surface by adsorbing more water molecules from the bulk towards the membrane surface resulting in an increase of the separation factor in the dehydration of butanol by PV [72].

3-glycidoxypropyltrimethoxysilane (GPTS) is a compound frequently used to enhance the adhesion between inorganic and organic components in composites [121, 122]. It contains an epoxide ring and three methoxy groups. The methoxy groups may undergo hydrolysis and react with the surface hydroxyl groups of the inorganic material in order to form a covalent bond, whereas the epoxide ring may react with a nucleophile such as hydrophilic or hydrophobic moieties in order to link the inorganic material with another material. GPTS has been used to improve the adhesion between the GO membrane and the ceramic support and it showed a good capability of binding ceramic materials with the GO [123]. Furthermore, GPTS can be cross-linked by the silanol and methoxy groups to form an oligomerised network

(condensation) on the material surface, subsequently building a multilayer structure that can potentially adsorb and contain water [124].

Herein, taking into account that the feed water concentration is important in determining the overall performance of the membrane, it was reported that the grafting hydrophilic silane agent can successfully increase the permeation flux, with considerable separation factor. Furthermore, the transport mechanism of this modified GO membranes is discussed. In addition, the energy and membrane area required for the pervaporation dehydration of ethanol were also calculated using the GO hollow fibre membrane and subsequent comparisons were made with other high performance membranes.

6.2 Experimental

6.2.1 Surface modification procedure

In the case of the surface modification of the GO membrane, the sintered YSZ hollow fibre support was modified with grafting 3-glycidoxypropyltrimethoxysilane (GPTS) as a modified silanisation agent. In the surface modification step, the sintered YSZ hollow fibre support with an approximate length of 10 cm was immersed in a GPTS/ethanol mixture for 1 hour at 40 °C in order to allow for the grafting of the polymer on the surface of the substrate. The modified YSZ hollow fibre support was then rinsed with ethanol in order to remove any unreacted chemicals and was subsequently dried in the oven at 110 °C for 8 hours prior to the deposition of the GO layers. The next step in the modification process was the grafting of GPTS on the GO hollow fibre membrane.

6.2.2 Pervaporation experiment

The pervaporation of the ethanol/water mixture was tested on a homemade setup and the scheme of the setup can be seen in Figure 5. 1. Briefly, the GO hollow fibre membrane was connected to the system and submerged in a flask containing 1 L of the ethanol/water mixture. Magnetic stirring was used in order to ensure a uniform mixture concentration over the course of the pervaporation test. The test was conducted at 70 °C. The flask containing the water/ethanol mixture was placed in a pre-heated water bath at a specific temperature to control the temperature required. The permeate side pressure was maintained at 3 mbar. Ethanol concentrations were determined by gas chromatography (GC) (Varian 3900).

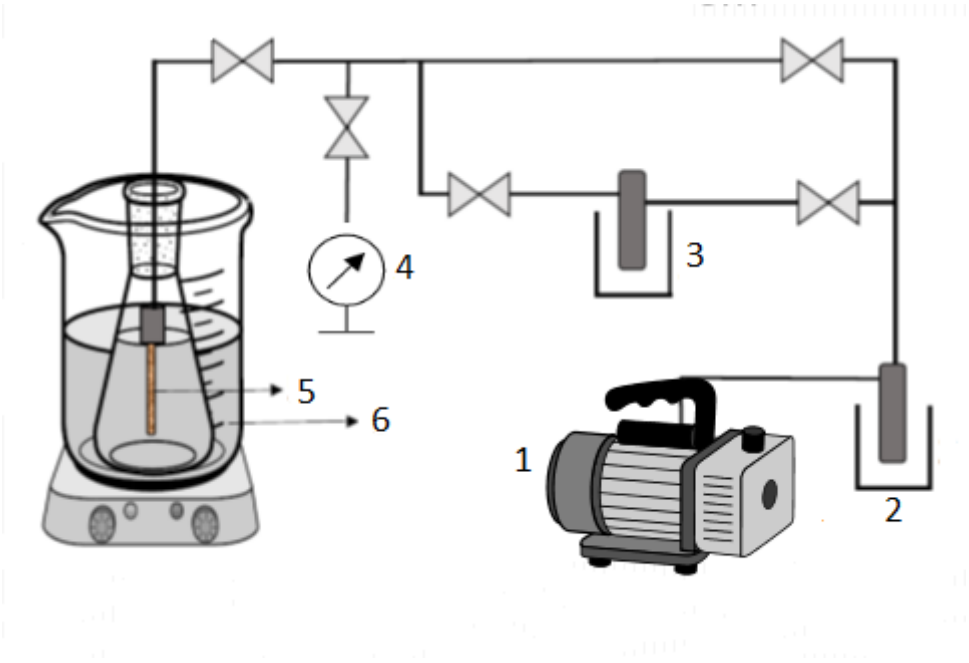

Figure 6. 1: Pervaporation scheme of the ethanol/water mixture: 1. Vacuum pump; 2. Cold trap (liquid nitrogen); 3. Collecting trap (liquid nitrogen); 4. Vacuum gauge; 5.GO hollow fibre membrane; 6.Water bath

The performance of the GO membrane was evaluated on the basis of the permeation flux (J) and the separation factors:

$$J = \frac{Q}{A\ x\ t}$$

$$\alpha = \frac{y/(1-y)}{x/(1-x)}$$

Where Q is the mass of the collected permeate, A is the membrane area and t is the time required for the sample collection. Whereas y and x are the mass fractions of the permeate and feed components, respectively.

6.3 Results and Discussion

6.3.1 Membrane characterisations

Figure 6.2 shows the scanning electron micrograph image of the YSZ hollow fibre substrate and the GO layer that adhere on the support. As shown by Figure 6.2(a), the cross-section of the YSZ hollow fibre shows a sandwich-like structure. The surface of the YSZ substrate is composed of fine YSZ particles and inter-granule pores, the size of which varies between 80 nm and 170 nm, respectively (Figure 6.2(b)). In addition, as depicted in Figure 6.2(c), it may be clearly observed that the GO layer adhere on the YSZ hollow fibre substrate. The laminar structure of the GO layers with a thickness of approximately 1μm can also be identified.

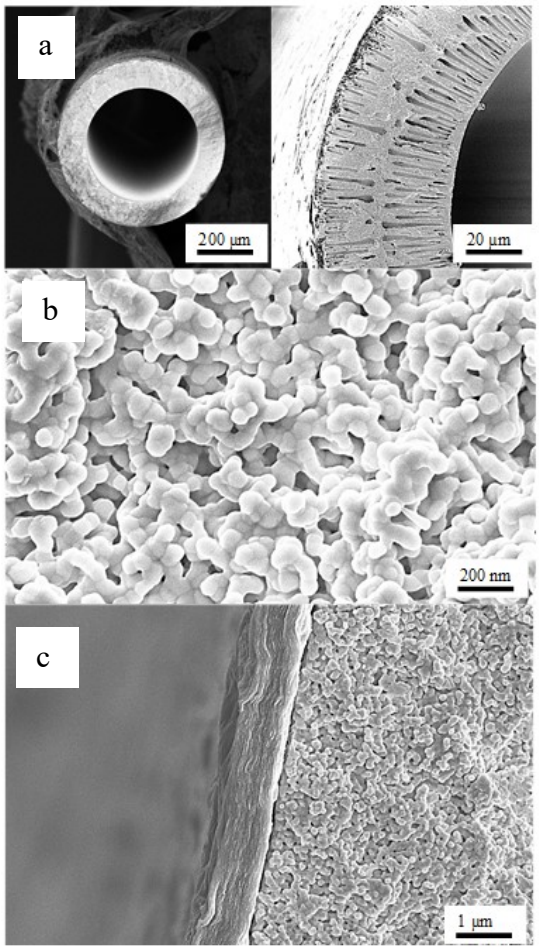

Figure 6.2: SEM images of (a) a cross-section of the YSZ hollow fibre substrate; (b) the outer surface of the YSZ hollow fibre; (c) the GO layer on the YSZ hollow fibre substrate

The XRD analysis has confirmed the laminar structure of the GO layer. Figure 6.3 shows the XRD patterns of the membrane in a dried state prepared via vacuum-facilitated methods on the flat sheet PES membrane. It is to be noted that the sharp peak at $2\theta=11°$ corresponds to an interlayer space of 0.8 nm between the GO flakes. The same figure also indicates that the interlayer space between the GO flakes did not change after surface modification.

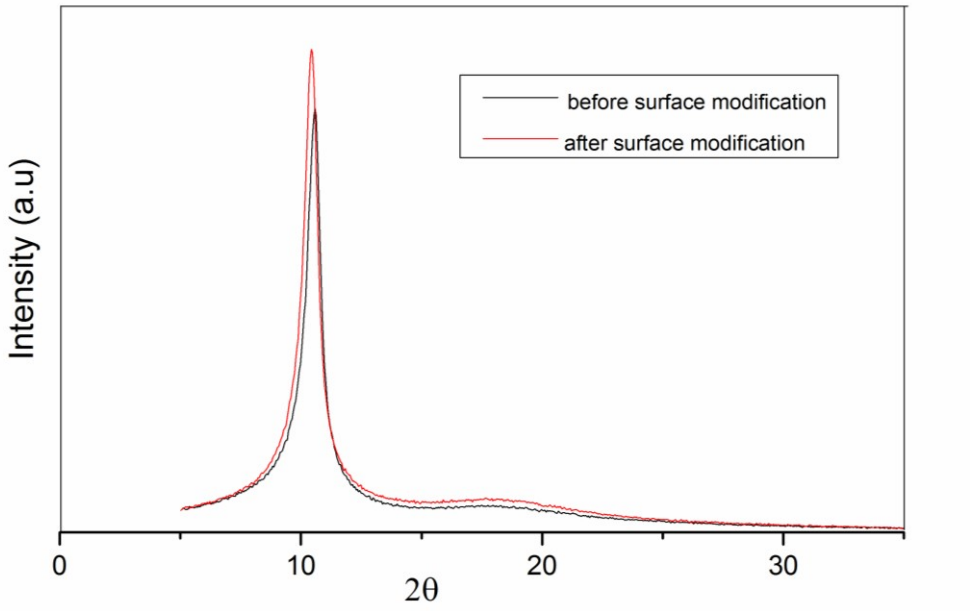

Figure 6.3: XRD pattern of the GO membrane before and after surface modification

6.3.2 Surface modification of the GO hollow fibre membrane

In this study, 3-glycidoxypropyltrimethoxysilane (GPTS) is used as a modification agent. GPTS is commonly used in order to enhance the adhesion between organic and inorganic compounds. The study has shown that by modifying the surface of the ceramic support, the adhesion strength between the graphene oxide layer and ceramic support can be successfully increased [58, 123]. Figure 6.4 summarise the overall modification steps used in this study.

.

Briefly, the first step is the modification on the surface of the YSZ ceramic hollow fibre support in order to improve the adhesion between the support and the GO layer. On the other hand, the second step is applied on the surface of the GO membrane where the main aim is to further increase the hydrophilicity of the GO membrane. The modification of the YSZ hollow

fibre support is carried out by means of hydrolysis and condensation reactions. Firstly, the GPTS will undergo a hydrolysis process, in which the hydrolysed molecules were produced. The hydrolysed molecules were bonded with the OH^- groups on the YSZ ceramic support either by means of condensation in order to form a siloxane bond or by means of hydrogen bonding to the surface hydroxyls [125]. The hydrophilic YSZ hollow fibre support is now ready for the deposition of the GO suspension. The pH of the GO suspension is controlled under acidic conditions of around 4-5 in order to ensure that the GO reacts with the epoxy group of the GPTS. Once the modified YSZ hollow fibre support came into contact with the GO suspension, the polymerisation occurred between the epoxy group of the GPTS and the epoxy group of the GO suspension. The polymerisation reaction will further produce C-O-C bonds [58, 126].

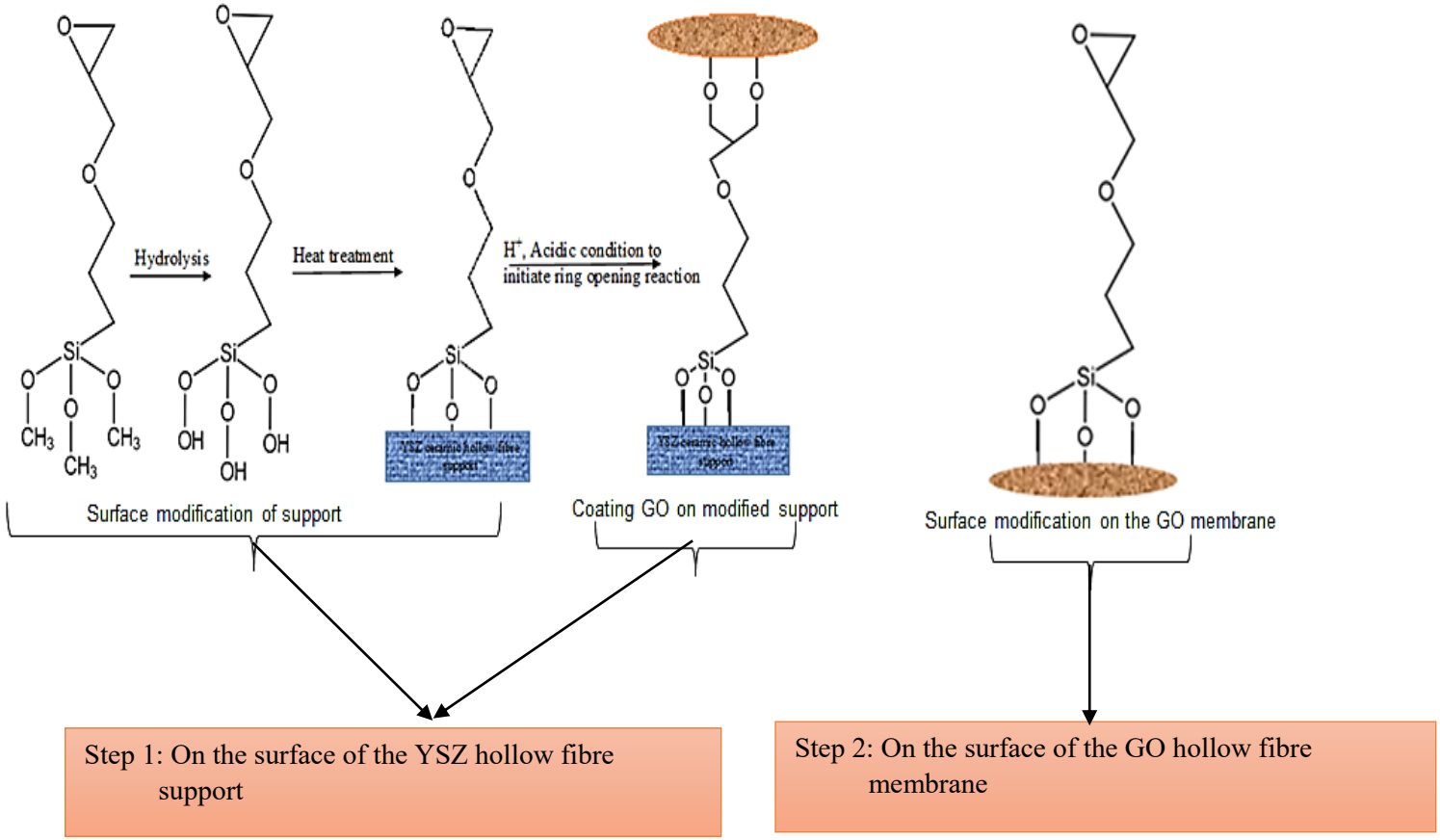

Figure 6.4: Summary of the surface modification steps used in this study

As stated above, the aim of the modification on the ceramic support is to provide an improved adhesion between the support and the GO layer. Therefore, it is important to ensure that the grafting process will chemically bind the ceramic support and the GO layer. The thermal gravimetric analysis (TGA) has confirmed that the GPTS is chemically bonded to the surface of the ceramic support. As depicted in Figure 6.5(a), the YSZ support without modification shows no significant loss and remains stable up to 800 °C. On the other hand, the YSZ support after surface modification shows a significant weight loss at 270 °C, which can be attributed to the weight loss of the GPTS. In order to further confirm this, the TGA analysis was conducted on the GPTS (Figure 6.5(b)), and from the graph it may be clearly inferred that the GPTS degraded at around 200 °C. As the GPTS grafted on the YSZ support, it degraded at about 270 °C. The considerable increase in the degradation temperatures indicates strong chemical bonding between the GPTS and the YSZ support.

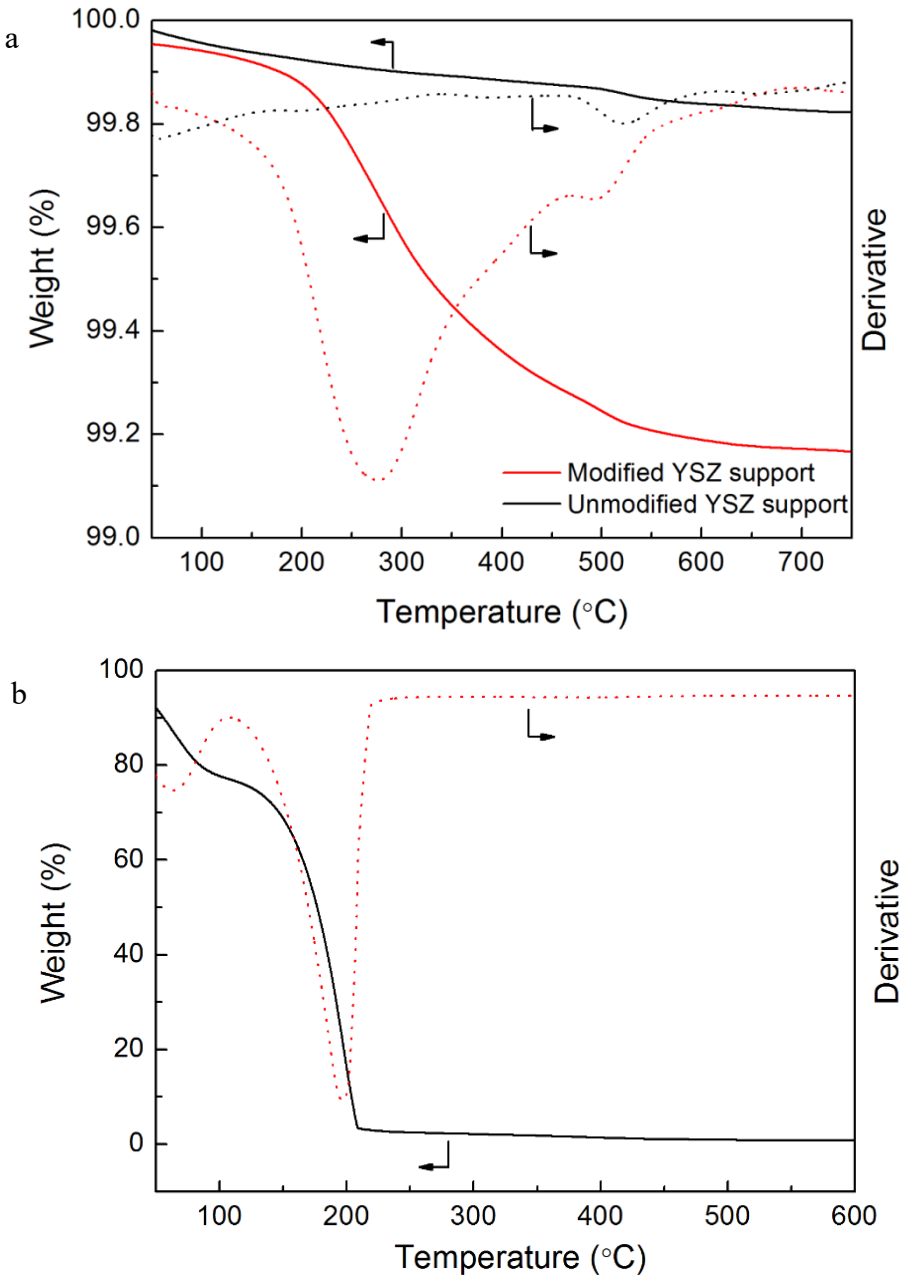

Figure 6.5: TGA analysis of: (a) the YSZ ceramic support before and after surface modification; (b) the GPTS.

Furthermore, the FTIR analysis has further proved that the GPTS is chemically grafted on the surface of the GO membrane. The FTIR spectra include the original GPTS, the original YSZ support and the GPTS modified YSZ support. Figure 6.6(a) represents the FTIR spectra for the GPTS which consist of peaks of 3000 cm^{-1} and 2869 cm^{-1} corresponding to CH_2, and 1089 cm^{-1} and 1194 cm^{-1} for the ether group (including the epoxy group). In addition, an absorption peak may be observed at about 910 cm^{-1}, which corresponds to the Si-O-C bond. The FTIR spectra of the unmodified ceramic support (Figure 6.6(b)) and the GPTS modified ceramic support (Figure 6.6(c)) are then compared, which indicates that the absorption peaks belonging to the GPTS such as CH_2, along with the epoxy and ether groups appeared in the case of the modified support. In addition, the absorption peaks representing Si-O-C were missing, which in turn demonstrated that the methoxy groups in the GPTS have been converted.

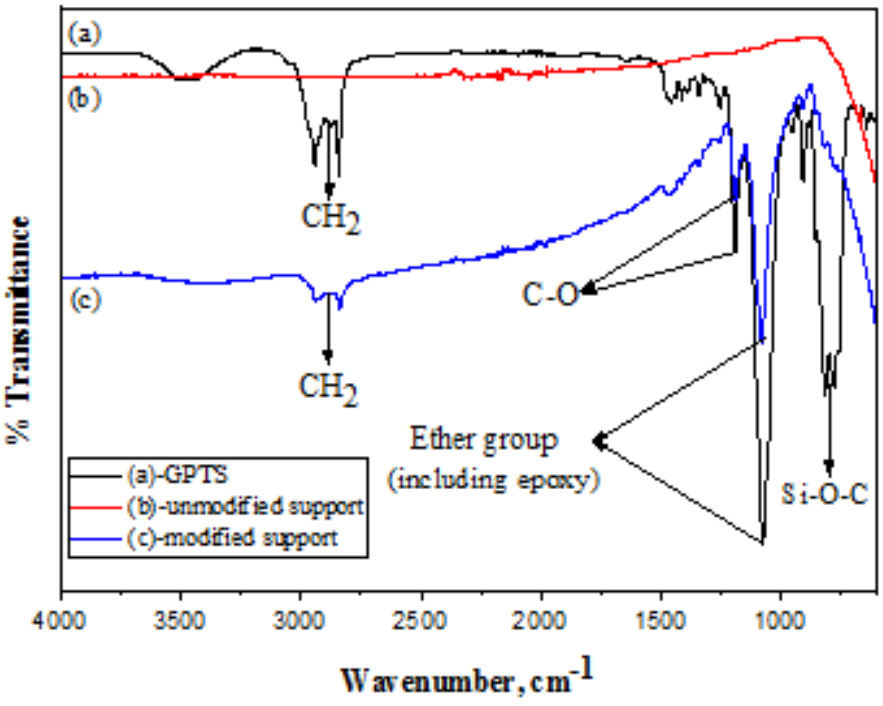

Figure 6.6: FTIR spectra of the GPTS, unmodified support and modified support

After grafting the GPTS on top of the selective layer of the GO membrane, the surface of the membrane exhibited an apparently smoother surface than the pristine GO membrane under the scanning electron microscope (Figure 6.7). As can be seen from Figure 6.7(a) and (b), the GO hollow fibre surface before modification shows a typical morphology of the graphene oxide film, in which the boundary of the GO flakes can be clearly seen. On the other hand, the GO hollow fibre membrane after surface modification (Figure 6.7(c) and (d)) shows a smooth surface without visible boundaries of the graphene oxide flakes.

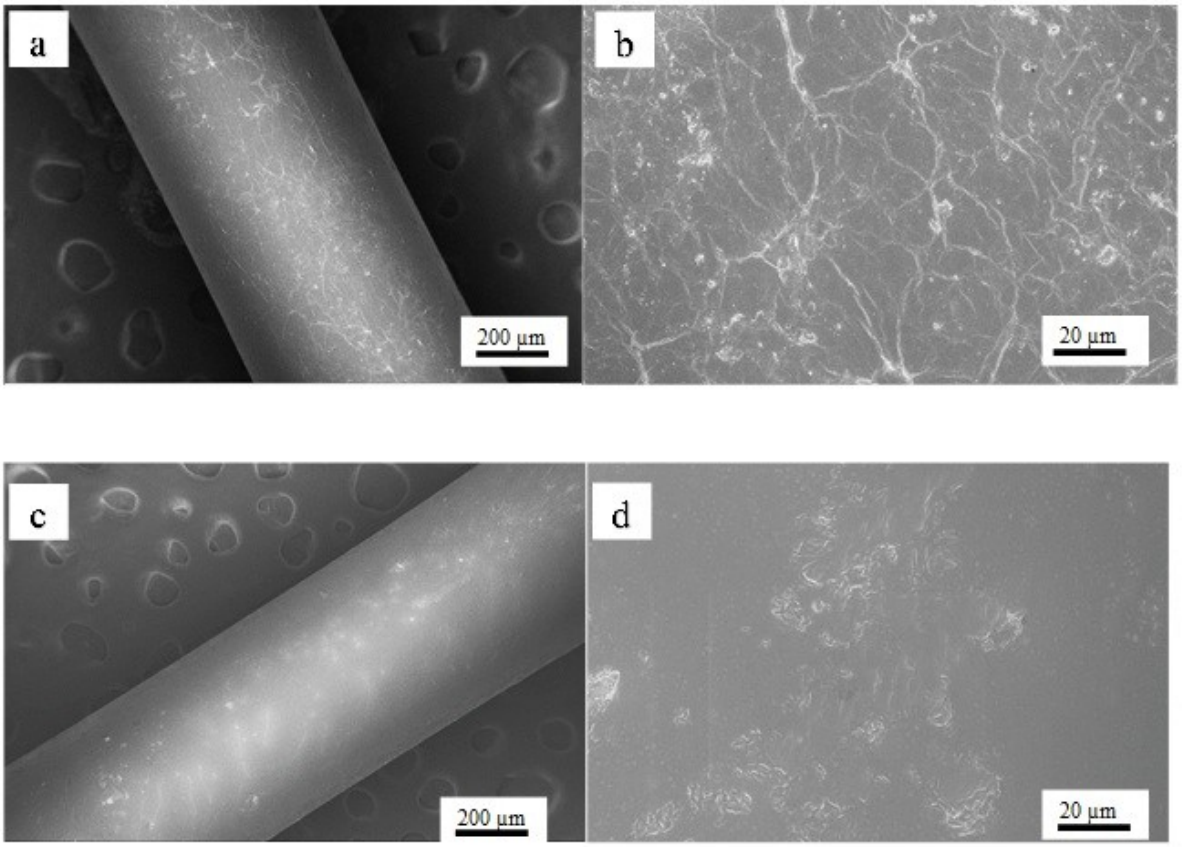

Figure 6.7: SEM images of (a) the GO hollow fibre membrane before surface modification, (b) the typical morphology of the graphene oxide film (c) the GO hollow fibre membrane after surface modification, (d) the smooth surface without visible boundaries between the GO flakes.

The improvement of surface smoothness was further confirmed by the atomic force microscope (AFM) (Figure 6.8(a-b)), which showed that the root mean square (RMS) roughness of the modified GO membrane decreased from 67 nm to 39 nm. This finding is in agreement with other research studies which indicated that surface modification can effectively reduce surface roughness [127-129]. Furthermore, the AFM phase analysis (Figure 6.8 (c-d)) showed that the texture was different from other parts of the membrane surface. The same topology was also observed on the GPTS grafted silica and glass by Wong et al., [124]. The change in the surface morphology and the texture found are believed to be due to the formation of the multilayer GPTS network, which has also been reported in previous studies [124, 125].

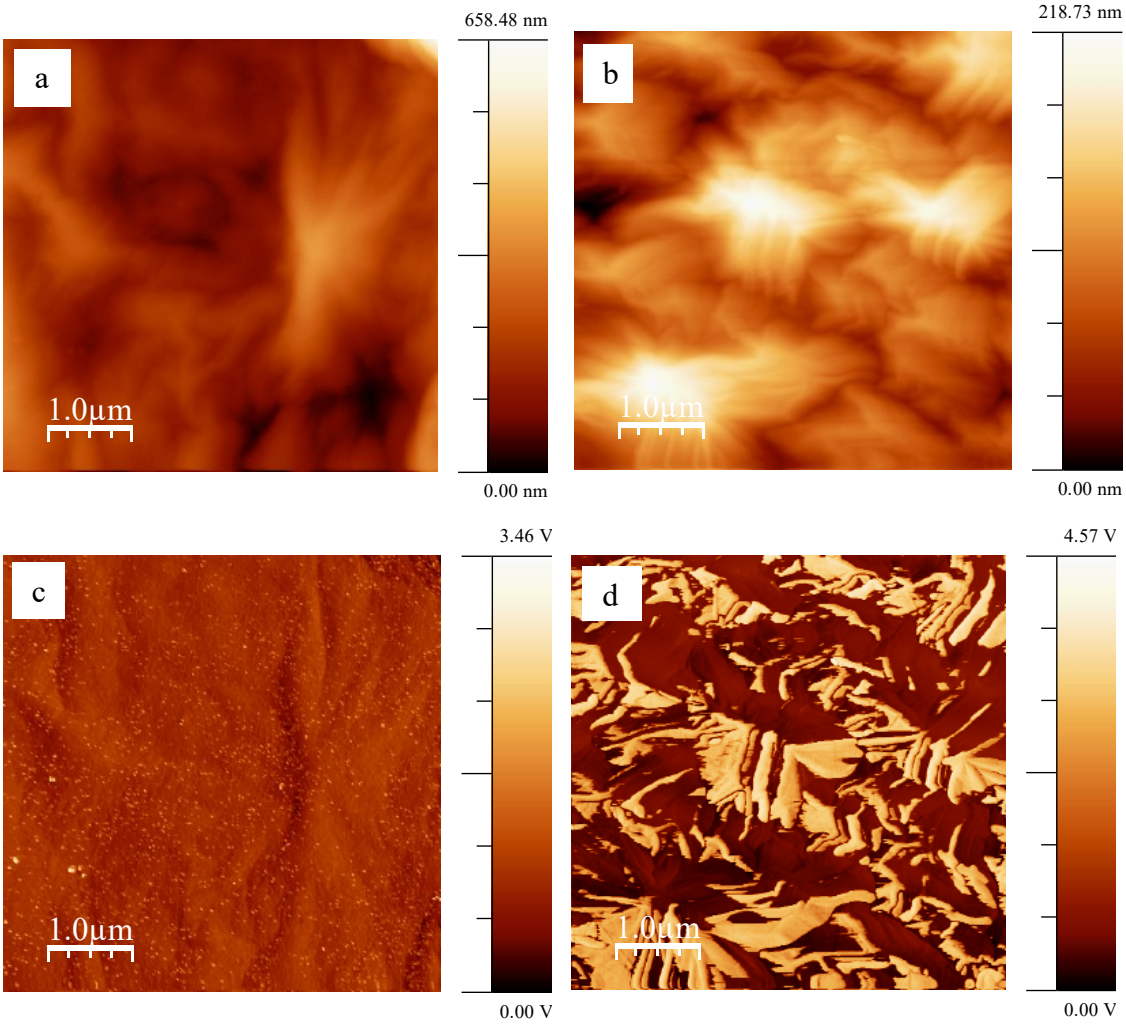

Figure 6.8: (a)AFM analysis of the GO hollow fibre membrane before and (b) after surface modification; (c) Phase analysis of GO membrane before surface modification (d) after surface modification.

6.3.3 Pervaporation performance of the surface-modified GO membrane

6.3.3.1 Effects of the surface modification

Figure 6.9 depicts the performance of the GO hollow fibre membrane in the PV dehydration of the 95/5 wt% ethanol/water mixture at 70 °C. The pristine GO membrane showed a total permeation flux of 4.07 kg m^{-2} h^{-1} with a separation factor of 59. In contrast, the modified GO membrane showed a total flux of 18.30 kg m^{-2} h^{-1} with a separation factor of 133. The XRD analysis initially showed (Figure 6.3) that the interlayer space of the GO membrane did not change after surface modification with GPTS. Therefore, the increase in the separation factor implies that the increase of the total permeation flux was not due to the development of microstructural defects or to the change in the interlayer space.

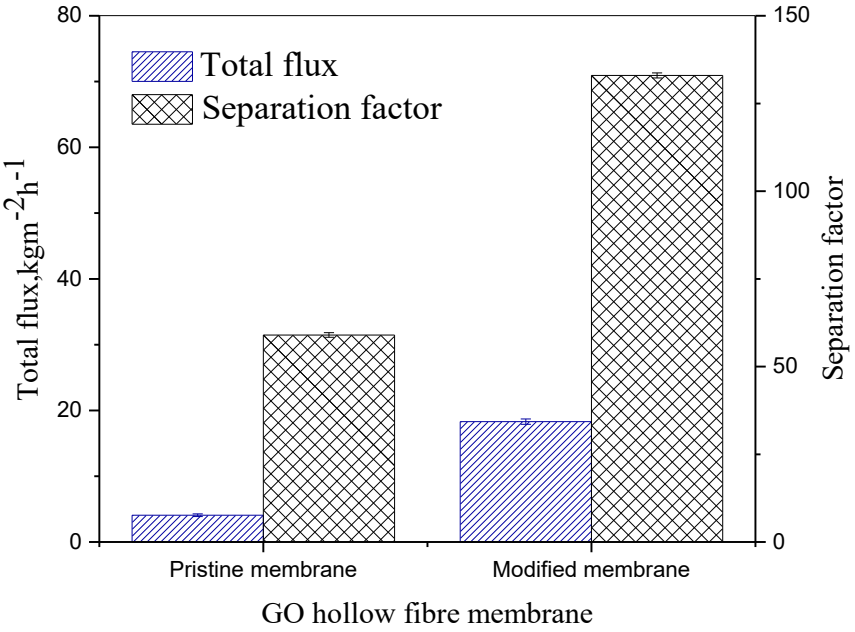

Figure 6.9: PV ethanol dehydration performance of pristine and modified GO membranes

Thus, the improvement of the permeation flux should be attributed to the change of the membrane surface as a result of the GPTS grafting. Figure 6.10 shows the water contact angle tests of the GO membrane before and after surface modification. It shows that the GO surface has a significantly improved affinity to water after grafting, with a contact angle of 7° compared to 46° in the case of the pristine GO membrane.

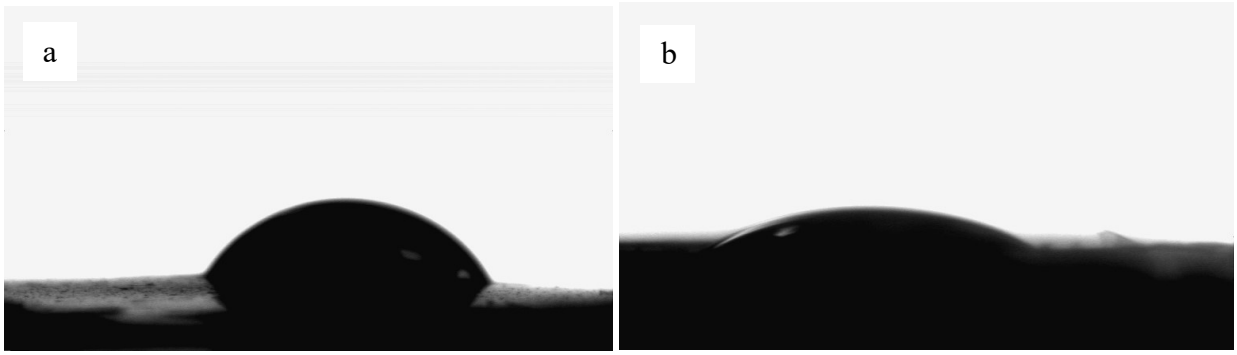

Figure 6.10: Water contact angles of the GO membrane (a) before and (b) after surface modification with GPTS

However, the reduced water contact angle after GPTS grafting should not have led to such an increase in the permeation flux. This is due to the fact that the ethanol/water feed solution used in this case wets the surface of both the pristine GO membrane and the grafted membrane perfectly (contact angle = 0°). In addition, it could be estimated on the basis of the permeation flux in the pristine GO membrane that the water concentration at the membrane surface was very close to the bulk solution. Hence, even if the concentration polarisation was completely eliminated, it would not improve the permeation flux significantly.

6.3.3.2 Discussion on the transport mechanism

In order to understand the improvement by the GPTS layer, it is essential to initially understand the transport mechanism under the PV conditions. It is known that water in the liquid state can pass through the GO membrane under pressure-driven conditions with pure water, with both surfaces wetted by liquid water. Nevertheless, it is unclear how water enters and leaves the pores (interlayer space) on the feed side and permeate side surfaces. It could be by means of viscous flow or adsorption-diffusion mechanisms, but in either of the two cases, the long transport path in the GO membrane would lead to very low permeation fluxes. In Chapter 4 of this thesis, it has been discussed that a GO membrane with a fine laminar structure produced by drying with a low-surface tension solvent would allow water to permeate with an extremely low flux. Conversely, a GO membrane with a loose structure, similar to the membranes used in this study, allowed pure water to pass through the membrane with a flux of 1.04 L $m^{-2}h^{-1}$ bar^{-1}, considerably lower than the fluxes under the PV conditions.

With respect to the PV conditions used in this study, it is unlikely that the mixture of ethanol and water would enter into the interlayer space via viscous flow, or the selectivity of water over ethanol would be very low as a result thereof. In fact, when trying to test the permeability of the 95/5 wt% ethanol/water mixture through the GO membrane under the pressure-driven mode, it was found that the mixture could not pass through the membrane at all under a 7 bar transmembrane pressure. This constitutes an interesting result, as previous studies have indicated that pure solvents, such as ethanol and acetone, can permeate through the GO membrane under the pressure-driven mode [130]. Nevertheless, in this study it was found that the mixture is incapable of achieving the same result. More interestingly, it was also found that when pure solvents, such as acetone and ethanol, are used under the pressure-driven permeation mode, permeation does not occur at the beginning, but rather after a period of time

that is much longer than the time needed to fill the pores. The solvent could then permeate through the membrane continuously. These phenomena could be attributed to the effective tension of the interface (Korteweg stress) between two miscible liquids when there is a steep concentration gradient across the interface [131, 132].

It has been widely acknowledged by physical scientists that even in the case of miscible liquids, a transient interfacial tension exists at the level of the temporary interface before the interface disappears as a result of inter-diffusion [131, 133-135]. The value of the transient interfacial tension is related to the concentration gradient across the interface, and the reported tension values can vary from 0.001 to 0.6 mN m^{-1}, depending on the miscible liquids and the concentration gradient [134, 135]. In the case of the GO membrane, due to the high content of the OH^- group on the GO flakes, water would be preferentially adsorbed into the interlayer space between the GO flakes, and then condensed in the interlayer space due to the extremely small size of the interlayer space.

Assuming that the interlayer space is 0.9 – 1.0 nm, which is a recommended value in the case of hydrated GO membranes [2], and that the temperature is 25 °C, the following estimation may be made based on the Kelvin equation:

$$\ln \frac{P}{P_0} = \frac{2\gamma V_m}{rRT}$$

Where P is the actual vapour pressure, P_0 is the saturated vapour pressure, γ is the surface tension of water, V_m is the molar volume of the liquid, r is the radius, R is the gas constant and T is the temperature expressed in Kelvin.

From the calculation, it was found that water would condense at a partial vapour pressure of water as low as 2.2 – 3.0 mbar (10-12% relative humidity), equivalent to 9.44 x 10^{-8} – 1.23 ×10^{-7} mol mL^{-1}, and a water concentration of 1.7 – 2.2 ppm in an ethanol solution.

Therefore, it can be concluded that under the pressure-driven test conditions implemented herein (relative humidity higher than 60% and water concentration of 5 wt%), water will be condensed in the interlayer space. Once water is preferentially condensed in the interlayer space, the liquids found inside and outside the interlayer space form an interface at the entrance of the interlayer space and a steep concentration gradient across the interface: water constitutes the dominant component inside the interlayer space, whereas ethanol is the major component outside the interlayer space. Since water is preferentially adsorbed on the wall of the interlayer space, the meniscus of the interface would be towards the water side and the interfacial tension would be against the pressure from the outside of the membrane. The effective interfacial tension is related to the concentration gradient. Using the Young–Laplace equation, it would be possible to determine the capillary pressure:

$$p_c = \frac{2\gamma \cos\theta}{r}$$

Where p_c is capillary pressure, γ is the interfacial tension, θ is the wetting angle (in this case the value thereof is 0), and r is the radius of the interface (in this case the interlayer space of the GO). Assuming that the interfacial tension is 0.2 mN m^{-1}, which is a moderate value within the reported range, a capillary pressure of 8.0 - 8.9 bar can be generated, which is high enough to resist the external pressure applied during the pressure-driven measurement. (Please refer to appendix F for other assuming interfacial tension and the capillary pressure obtained[12]). When the feed contains a small quantity of water, it can be expected that the interfacial tension at the interlayer space entrance will be maintained over time, since the GO will preferentially keep adsorbing water from the feed. Furthermore, since the steep concentration gradient across the interface always exists, and therefore in this case, the mixture feed will not be able to pass through the GO membrane. When the feed is pure ethanol, the initial steep concentration gradient will decrease over time due to the inter-diffusion of the

condensed water and ethanol. As a result, the interfacial tension will decrease to a value that cannot sustain the external pressure, and as a result ethanol starts to permeate. Because of the extremely narrow interlayer space, the inter-diffusion is very slow, and it will take a considerable amount of time to reduce the interfacial tension to the critical level. Thus, ethanol would start to permeate only after a long duration. It has also been observed that even pure solvents, such as ethanol and hexane, could not pass through the GO membrane when the pressure difference across the membrane is too small, that is to say with a pressure difference of 0.1 bar [2]. This could also be attributed to the interfacial tension that can be maintained to be enough to resist the small external pressure.

Under the PV operation mode, the transport mechanism does not rely on external pressure. Instead, it relies on the capillary pressure of the condensed water in the interlayer space at the vacuum side. Since the GO will selectively adsorb water from the feed, as aforementioned, the interface at the feed side would not change or move, whereas the supply of water from the feed can only do so by means of adsorption, which would be highly selective. It is widely accepted that the PV through the polymeric and zeolite membranes is achieved by means of the solution-diffusion or adsorption-diffusion process. Nevertheless, it is very unlikely that molecular diffusion would play a dominant role in the GO PV case. Firstly, extensive studies by molecular simulation have indicated that water would be in the condensed state in the GO membrane under ambient conditions and that water molecules bind to each other by hydrogen bonding. Therefore, the diffusion of the individual water molecules in the interlayer space is unlikely unless high vacuum is applied. Secondly, diffusion is normally a slower process as opposed to the bulk flow in confined nano-sized pores, but in this study, the water permeation flux through the GO membrane under the PV mode is considerably higher than in the pressure-driven mode. Nair et al., used pristine GO membranes in order to test the permeability of water, where one side of the GO membrane is exposed to liquid water, and the

other side is applied with low water partial pressure. The researchers found that water can be transported through evaporation at a very fast rate, which is essentially the rate of unimpeded evaporation, and they attributed it to a high capillary pressure (~ 1000 bar) generated in the interlayer space, which drives the condensed water to pass through the membrane with an extraordinary speed [2]. The scenario in Nair's study is analogous to the PV study, except for the fact that in the PV case, water is dissolved in a concentrated solvent, whereas in both cases water is believed to enter the interlayer space of the GO membrane by preferential adsorption. If we adopt Nair's interpretation stating that the capillary pressure is the main factor to enabling water to pass through the GO membrane under the PV mode, we can then analyse the transport steps and influencing factors on the whole.

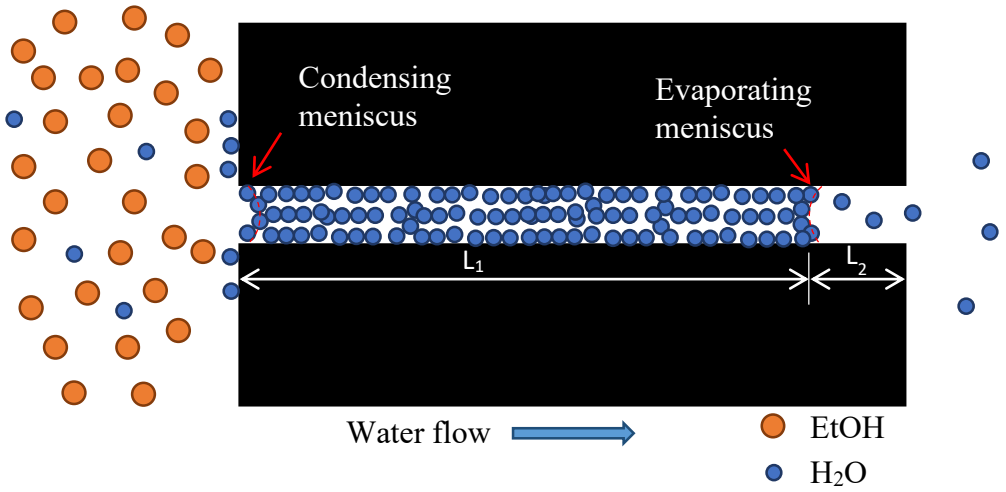

Figure 6.11: Scheme of the proposed water transport mechanism under the PV operation mode

From Figure 6.11 it may be observed that at the condensing meniscus (the feed side interface) water is selectively condensed into the interlayer space, and its rate is related to the concentration of water in the ethanol-water mixture, $Q_1 \propto c_w$. Then, the condensed water flow through the interlayer space driven by the capillary pressure is generated by the evaporating

meniscus at the other side, $Q_2 \propto p_c/L_1$, (where p_c is the capillary pressure, and L_1 is the passage length of the condensed water). At the evaporating interface, the evaporation of water occurs, and the vapour pressure at the interface can be considered to be the saturated pressure, which is determined by the temperature and pore size. The evaporated water vapour then diffuses out of the interlayer space, $Q_3 \propto D \times (p_I - p_V)/L_2$ (where D is the diffusivity of water in the interlayer space, p_I is the vapour pressure at the meniscus, p_V is the vacuum pressure, and L_2 is the passage length of the water vapour). In a steady state, $Q_1=Q_2=Q_3$, and the position of the evaporating meniscus, which determines L_1 and L_2, is movable to suit the permeation rate. Since under such a high capillary pressure the transport of condensed water through L_1 is much faster than the diffusion, it is reasonable to believe that the evaporating meniscus would be close to the permeate side outlet, so that the diffusion distance for the water vapour is short, and the mass transfer rate is decided by the evaporation, as demonstrated by Nair et al. [2], provided that the condensing rate at the feed side is also high enough. In Nair's work, pure water was used for the feed side, therefore the supply of water was fast enough to compensate for the loss of water from the other side. However, in the current study, water is present in the feed mixture only in a proportion of 5%, which is indicative of the fact that the adsorption and condensation rate of water into the interlayer space may be insufficient. Therefore, increasing the water concentration will be an effective measure to enhance the water permeation rate.

Therefore, the improvement of the permeation flux and the separation factor could be attributed to the enrichment of the water molecules on the modified membrane surface. As previously mentioned, grafting GPTS on the membrane surface would form a 3-D structure on the membrane surface. This GPTS layer can then act as a water retention layer that would capture more water molecules from the bulk solution, thus increasing the concentration of water near the membrane surface. Assuming that each GPTS monomer in the 3-D network has two hydroxyl groups that absorb a trimer water cluster in each case, and that the density of the

GPTS network is similar to its free form (1.07 g cm^{-3}), it can be estimated that the water concentration near the membrane surface can be as high as 0.54 g cm^{-3}, significantly higher than in the 5 wt% bulk solution (0.04 g cm^{-3}). It is fair to say that with such high levels of water concentration, the water permeation flux could be improved significantly.

6.3.4 Techno-economic analysis

The separation performance of the superhydrophilic GO hollow fibre membrane used in this experiment was compared with other polymeric membranes, ceramic membranes, as well as the GO membrane. As depicted in Figure 6.12, the performance of the GO hollow fibre lies at the upper bound of the highest flux among other pervaporation membranes. Although the separation factor of the modified GO hollow fibre membrane exhibits a moderate perfomance it is sufficient to met the requirements of normal dehydration.

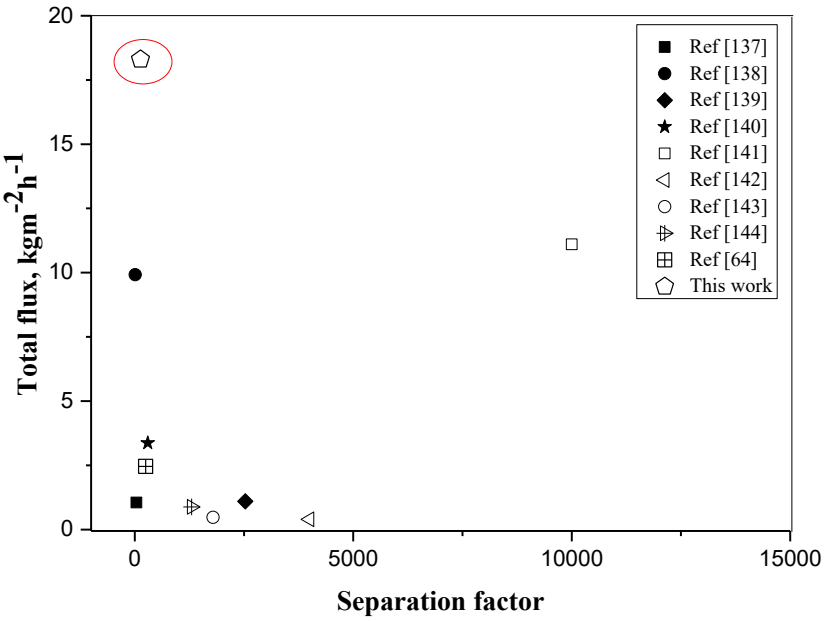

Figure 6.12: Total flux comparison of the modified GO membrane used in this study with other polymeric, ceramic and GO membranes

It is a well known fact that pervaporation would make it possible to save energy, thus reducing the cost of operations. Energy savings of almost 50% as opposed to traditional distillation techniques are easy to achieve when the membrane is implemented. The energy normalised per unit of water required in order to evaporate the permeate in the pervaporation process is calculated as follows [136]:

$$Q_{norm}^{evap} = \frac{\sum_i H_i^{evap} F_i}{F_{water}}$$

Where H_i^{evap} is the heat of vaporisation of the species *i* , and F_i is the flux of the species *i*. When water and ethanol dominate the feed and the permeate, rewriting the equation above in terms of the concentration of water in the feed, and the water-ethanol separation factor α would have the following structure:

$$Q_{norm}^{evap} = H_{water}^{evap} + H_{ethanol}^{evap} \frac{1 - C_{ethanol}^{feed}}{\alpha C_{water}^{feed}}$$

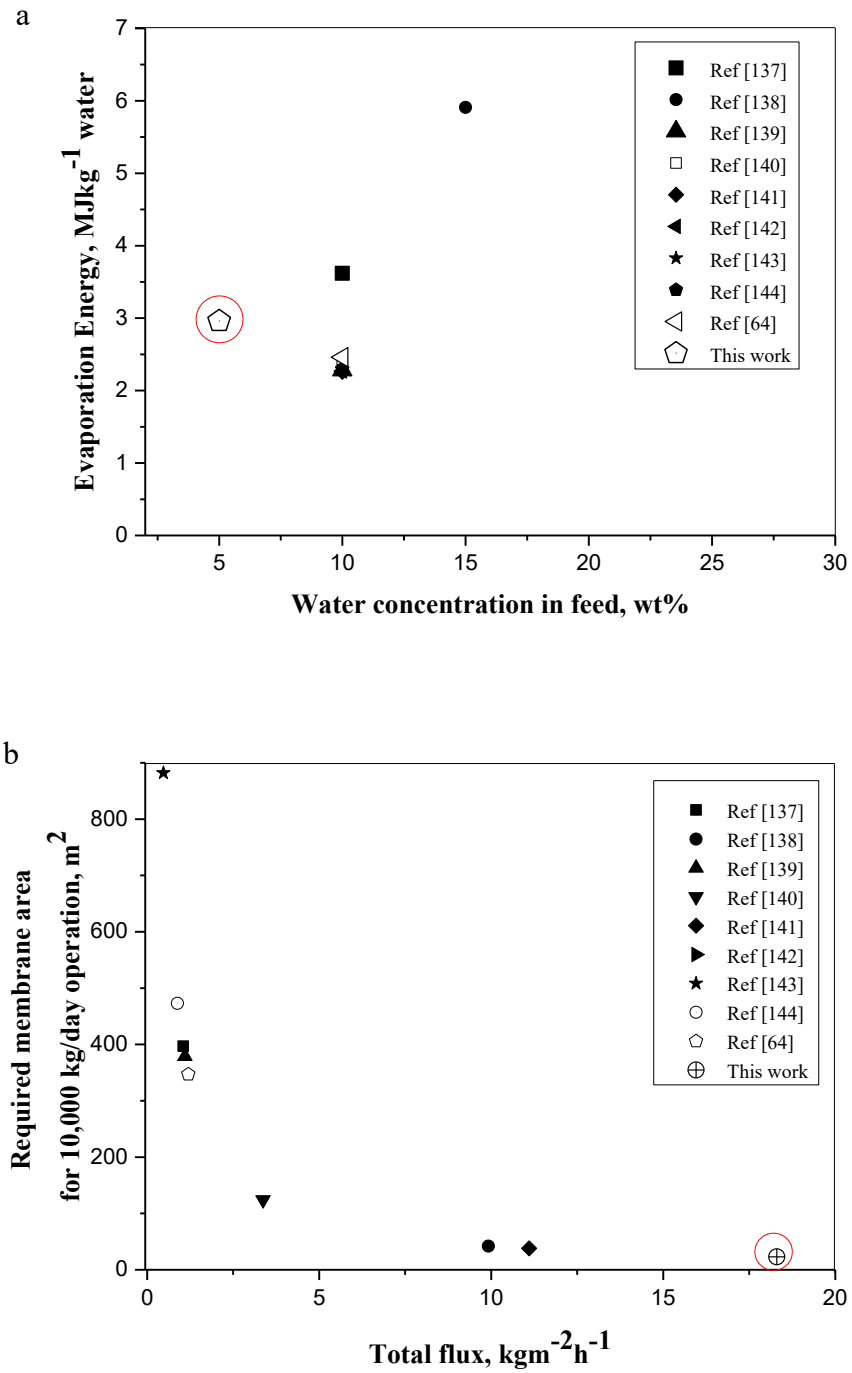

Figure 6.13: Performance comparison between the modified GO membrane used in this study with other polymeric, ceramic and GO membranes: (a) the evaporation energy required; (b) the membrane area required

As depicted in Figure 6.13(a), the energy required for the pervaporation per unit of water for the modified GO hollow fibre membrane is 2.96MJ/kg, which is not significantly

different from GO/Al_2O_3 with separation factors of 250 and a required evaporation energy value of 2.46 MJ/kg [65].

In real industrial applications, the required membrane area for certain process flow rates is also one of the most important factors to be considered. Since the modified GO hollow fibre membrane yields the highest flux, the required membrane area for an estimated 10,000kg/day rate of operations is only 23m^2 (Figure 6.13(b)). None of the other membranes compared in this study would be able to operate at a rate of 10,000 kg/day with a required membrane area of less than 30m^2. The overall comparison is also tabulated in Table 6. 1.

Table 6. 1:Comparison of the PV dehydration of ethanol and performance between the surface-modified GO membrane and other membranes

Membrane/Reference	**Ethanol/water mixture (wt%)**	**Feed temperature (°C)**	**Separation factor**	**Total flux ($kgm^{-2}h^{-1}$)**	**Evaporation energy required (MJ/kg water)**	**Required membrane area (m^2)**
PVA/A_2O_3**[137]**	90/10	70	38	1.05	3.62	397
PBI/ZIF8**[138]**	85/15	60	10	9.92	5.91	42
COBALT DOPED SILICA**[139]**	90/10	75	2530	1.1	2.28	379
ZEOLITE X**[140]**	90/10	65	296	3.37	2.43	124
ZEOLITE NAA**[141]**	90/10	75	10000	11.1	2.26	38
PAN-VP & PAN-AA**[142]**	90/10	50	4000	0.4	2.27	1042
CHITOSAN**[143]**	90/10	60	1791	0.472	2.29	882
SODIUM SULFONATE POLYSULFONE**[144]**	90/10	45	1300	0.88	2.3	473
GO/AL_2O_3**[65]**	90/10	70	250	1.2	2.46	347
GO/YSZ (this work)	95/5	70	133	18.3	2.96	23

6.4 Conclusions

In conclusion, the GO hollow fibre membrane was prepared with an exceptionally high flux and moderate separation factors after the surface modification with hydrophilic silane modified agents. In addition, undertaking the preferential water behaviour of the GO membrane combined with the fast water transport throughout the GO channels was beneficial in terms of providing a good selectivity in the pervaporation dehydration of ethanol. Taking into consideration the importance of water in the feed solution, it was possible to produce the GO hollow fibre membrane with a high permeation flux and to improve the separation factor. Moreover, the energy effectiveness of the GO hollow fibre membrane was successfully demonstrated, indicating that the latter requires the smallest membrane area when compared to other membranes used for industrial application purposes.

CHAPTER 7

Conclusions and Future Works

7.1 General Conclusions

This thesis focused on the fabrication and development of graphene oxide (GO) membranes supported on ceramic hollow fibres for various solution-based applications, such as nanofiltration, desalination and pervaporation. The studies proved that GO is a versatile membrane material for use in different solution-based applications involving varied solutes and operating conditions. In addition, the study also examined the separation performance of GO membranes in terms of permeation and rejection/separation factors, as well as the stability of the membranes in an aqueous environment. The GO membranes were further enhanced by modification and cross-linking in order to suit the requirements in different applications. Finally, the separation mechanisms of GO membranes were subsequently discussed.

7.2 Major Findings

7.2.1 Microstructural stability of the GO membrane and its nanofiltration performance

In Chapter 4, the GO membrane was shown to be unstable under dry conditions. This observation was verified by the performance degradation during gas permeation tests. The performance of the GO membrane degraded over time, which indicated that defects developed during either the test or the storage. This behaviour was attributed to drying-related shrinkage, which contributes to defect formation. Experimental results showed that free-standing GO membranes had a linear shrinkage of 1% after drying overnight, when a tensile stress up to 320 MPa was imposed, which is far beyond the maximum fracture stress (120 MPa) of typical GO membranes [145]. In order to overcome this, GO membranes need to be stored in water to keep them wet at all times. The structural and performance stabilities of GO membranes in nanofiltation applications have been tested, with results further proving that GO membranes are not stable in dry conditions. The rejection of the membranes towards dyes degraded after three weeks when they were exposed to air, while GO membranes kept in water remained unchanged after three weeks. Finally, the transport path of GO membranes in nanofiltration was discussed. The defects in GO membranes provide shortcuts for permeation and lead to a considerable permeation flow rate.

7.2.2 Improved performance of GO membranes in desalination

In Chapter 5, pristine GO membranes were successfully cross-linked with Al^{3+}, while the surface was turned from negatively to positively charged. Al^{3+} cations played roles in the rejection of salts by increasing the surface charge density, and at the same time narrowing the effective channel size for the ion transport, which prevented the solute from passing through

the membrane. The rejection of $MgCl_2$ and NaCl was successfully increased to 95% and 90% after cross-linking with Al^{3+}, respectively. In addition, the microstructure of GO membranes was significantly changed after cross-linking with Al^{3+}, which also affected the flux and the rejection of the GO membranes. For the cross-linked GO membranes, we discussed that the transport mechanism was not only attributed to the microstructure of the membrane, but was also governed by the charge effects.

7.2.3 Enhanced water permeation for pervaporation dehydration of ethanol

In Chapter 6, the feasibility of GO membranes in pervaporation dehydration of ethanol was investigated. It showed that pristine GO membranes have relatively low permeation fluxes and moderate separation factors. The modification of the GO membrane surface was carried out in order to increase the hydrophilicity of the GO membrane, with both water permeation flux and separation factor significantly increased. The improvement was interpreted by the preferential adsorption of water on the feed side, where the adsorption rate is strongly affected by the local water concentration. The modified hydrophilic membrane surfaces should be able to adsorb more water from the bulk liquid, leading to increased concentration next to the surface of a GO membrane. It is discussed that the capillary pressure of condensed water in the interlayer space on the vacuum side contributes to the high water permeation flux, while the mass transfer rate is decided by the evaporation, as demonstrated by Nair et al. [2].

7.3 Recommendations for Future Work

GO membranes have shown promising permeation properties for different applications, such as pressure-driven separation applications, non-pressure-driven applications and gas separation. Despite the claims of the ultra-fast transport of water, gases and some small molecules and ions, more experiments and simulations are needed to further clarify inconsistency between different research findings. On the other hand, although GO membranes represent a new generation of membrane material, which offers many exciting characteristics, their use in industrial applications remains far off. Therefore, here are some recommendations for future research:

7.3.1 Fabrication methods of the GO membrane

Although several methods have been established concerning the fabrication of GO membranes, the membranes obtained have a structure, which is far from the ideal laminar structure, where imperfect assembly of GO flakes exists, meaning that the selectivity of the membrane is compromised. There is still significant scope to improve membrane fabrication techniques in order to precisely control the microstructure of the membrane.

7.3.2 Separation mechanism

Within scientific communities, there is a great deal of interest to establish an appropriate separation mechanism related to GO membranes. The theory of a fast water transport mechanism through GO membranes is yet to be fully understood. Thus, more specific and accurate transport models should be proposed for GO membranes in near future. To this extent, a proper experimental protocol, as well as advanced characterization, could be beneficial in

determining the overall separation or transport mechanism. Moreover, accurate simulation and modelling could also be beneficial in further supporting the results.

7.3.3 Long-term stability

The long-term stability of GO membranes in an aqueous environment with regards to their structure and physiochemical properties remains unclear. Although GO membranes have been proven to be stable in water by proper drying or cross-linking, the main concern concerning the long-term stability of GO membranes during operations should be taken seriously. In response, GO membranes should be subjected to cross-flow filtration in order to investigate the long-term stability, as well as simulate the industrial environment.

7.3.4 Broadened applications

Besides the utilization of GO membranes in pressure-driven separation applications, the exciting characteristics offered by GO could be further exploited with regard to different applications, such as energy-related processes and as membrane materials for dialysis. By fine-tuning the microstructure as well as the charge of the membrane, this new generation membrane material could go further alongside various applications.

References

1. Alzahrani, A.Z., *Structural and Electronic Properties of Graphene upon Molecular Adsorption: DFT Comparative Analysis*. Graphene Simulation. 2011.
2. Nair, R.R., et al., *Unimpeded Permeation of Water Through Helium-Leak–Tight Graphene-Based Membranes.* Science, 2012. **335**(6067): p. 442-444.
3. Tsou, C.-H., et al., *Effect of microstructure of graphene oxide fabricated through different self-assembly techniques on 1-butanol dehydration.* Journal of Membrane Science, 2015. **477**(0): p. 93-100.
4. Mkhoyan, K.A., et al., *Atomic and Electronic Structure of Graphene-Oxide.* Nano Letters, 2009. **9**(3): p. 1058-1063.
5. Kim, H.W., et al., *Selective Gas Transport Through Few-Layered Graphene and Graphene Oxide Membranes.* Science, 2013. **342**(6154): p. 91-95.
6. Sidney, L., S. Sriniva, and D.E. Weaver, *High flow porous membranes for separating water from saline solutions*. 1964, Google Patents.
7. Brodie, B.C., *On the Atomic Weight of Graphite.* Philosophical Transactions of the Royal Society of London, 1859. **149**: p. 249-259.
8. He, H., et al., *A new structural model for graphite oxide.* Chemical Physics Letters, 1998. **287**(1–2): p. 53-56.
9. Li, H., et al., *Ultrathin, Molecular-Sieving Graphene Oxide Membranes for Selective Hydrogen Separation.* Science, 2013. **342**(6154): p. 95-98.
10. Han, Y., Z. Xu, and C. Gao, *Ultrathin Graphene Nanofiltration Membrane for Water Purification.* Advanced Functional Materials, 2013. **23**(29): p. 3693-3700.

11. Sun, P., et al., *Selective Ion Penetration of Graphene Oxide Membranes.* ACS Nano, 2013. **7**(1): p. 428-437.

12. Vandevivere, P.C., R. Bianchi, and W. Verstraete, *Review: Treatment and reuse of wastewater from the textile wet-processing industry: Review of emerging technologies.* Journal of Chemical Technology & Biotechnology, 1998. **72**(4): p. 289-302.

13. Shao, L., et al., *Polymeric membranes for the hydrogen economy: Contemporary approaches and prospects for the future.* Journal of Membrane Science, 2009. **327**(1–2): p. 18-31.

14. Shao, P. and R.Y.M. Huang, *Polymeric membrane pervaporation.* Journal of Membrane Science, 2007. **287**(2): p. 162-179.

15. Kang, G.-d. and Y.-m. Cao, *Application and modification of poly(vinylidene fluoride) (PVDF) membranes – A review.* Journal of Membrane Science, 2014. **463**: p. 145-165.

16. Ji, J., et al., *Poly(vinylidene fluoride) (PVDF) membranes for fluid separation.* REACTIVE & FUNCTIONAL POLYMERS, 2015. **86**: p. 134-153.

17. Hashim, N.A., F. Liu, and K. Li, *A simplified method for preparation of hydrophilic PVDF membranes from an amphiphilic graft copolymer.* JOURNAL OF MEMBRANE SCIENCE, 2009. **345**: p. 134-141.

18. Martínez Galeano, Y., L. Cornaglia, and A.M. Tarditi, *NaA zeolite membranes synthesized on top of APTES-modified porous stainless steel substrates.* Journal of Membrane Science, 2016. **512**: p. 93-103.

19. Okubo, T., et al., *Formation mechanism of crack-free porous YSZ membrane.* Journal of Membrane Science, 1997. **125**(2): p. 311-317.

20. Tan, X., Z. Pang, and K. Li, *Oxygen production using La0.6Sr0.4Co0.2Fe0.8O3-alpha (LSCF) perovskite hollow fibre membrane modules.* JOURNAL OF MEMBRANE SCIENCE, 2008. **310**: p. 550-556.

21. Othman, N.H., Z. Wu, and K. Li, *An oxygen permeable membrane microreactor with an in-situ deposited Bi1.5Y0.3Sm0.2O3-delta catalyst for oxidative coupling of methane.* JOURNAL OF MEMBRANE SCIENCE, 2015. **488**: p. 182-193.

22. Yu, X., et al., *CO2 capture using a superhydrophobic ceramic membrane contactor.* Journal of Membrane Science, 2015. **496**: p. 1-12.

23. Tan, X., S. Liu, and K. Li, *Preparation and characterization of inorganic hollow fiber membranes.* Journal of Membrane Science, 2001. **188**(1): p. 87-95.

24. Das, R., et al., *Carbon nanotube membranes for water purification: A bright future in water desalination.* Desalination, 2014. **336**: p. 97-109.

25. Hinds, B.J., et al., *Aligned Multiwalled Carbon Nanotube Membranes.* Science, 2004. **303**(5654): p. 62-65.

26. Majumder, M., et al., *Nanoscale hydrodynamics: Enhanced flow in carbon nanotubes.* Nature, 2005. **438**(7064): p. 44-44.

27. Kalra, A., S. Garde, and G. Hummer, *Osmotic water transport through carbon nanotube membranes.* Proceedings of the National Academy of Sciences, 2003. **100**(18): p. 10175-10180.

28. Corry, B., *Designing carbon nanotube membranes for efficient water desalination.* The Journal of Physical Chemistry B, 2008. **112**(5): p. 1427-1434.

29. Verweij, H., M.C. Schillo, and J. Li, *Fast Mass Transport Through Carbon Nanotube Membranes.* Small, 2007. **3**(12): p. 1996-2004.

30. Novoselov, K.S., et al., *Electric Field Effect in Atomically Thin Carbon Films.* Science, 2004. **306**(5696): p. 666-669.

31. Geim, A.K. and K.S. Novoselov, *The rise of graphene.* Nat Mater, 2007. **6**(3): p. 183-191.

32. Liu, G., W. Jin, and N. Xu, *Graphene-based membranes.* Chemical Society Reviews, 2015. **44**(15): p. 5016-5030.

33. Castro Neto, A.H., et al., *The electronic properties of graphene.* Reviews of Modern Physics, 2009. **81**(1): p. 109-162.

34. Gao, W., *Graphene oxide : Reduction recipes, spectroscopy, and applications.* 2015: C Cham: Springer.

35. Staudenmaier, L., *Verfahren zur Darstellung der Graphitsäure.* Berichte der deutschen chemischen Gesellschaft, 1898. **31**(2): p. 1481-1487.

36. Hummers, W.S. and R.E. Offeman, *Preparation of Graphitic Oxide.* Journal of the American Chemical Society, 1958. **80**(6): p. 1339-1339.

37. Kovtyukhova, N.I., et al., *Layer-by-Layer Assembly of Ultrathin Composite Films from Micron-Sized Graphite Oxide Sheets and Polycations.* Chemistry of Materials, 1999. **11**(3): p. 771-778.

38. Hirata, M., et al., *Thin-film particles of graphite oxide 1:: High-yield synthesis and flexibility of the particles.* Carbon, 2004. **42**(14): p. 2929-2937.

39. Marcano, D.C., et al., *Improved Synthesis of Graphene Oxide.* ACS Nano, 2010. **4**(8): p. 4806-4814.

40. Li, J., et al., *The Preparation of Graphene Oxide and Its Derivatives and Their Application in Bio-Tribological Systems.* Lubricants, 2014. **2**(3): p. 137.

41. He, H., et al., *Solid-State NMR Studies of the Structure of Graphite Oxide.* The Journal of Physical Chemistry, 1996. **100**(51): p. 19954-19958.

42. Lerf, A., et al., *International Symposium on the Reactivity of Solids13C and 1H MAS NMR studies of graphite oxide and its chemically modified derivatives.* Solid State Ionics, 1997. **101**: p. 857-862.

43. Bagri, A., et al., *Structural evolution during the reduction of chemically derived graphene oxide.* Nat Chem, 2010. **2**(7): p. 581-587.

44. Paredes, J.I., et al., *Graphene Oxide Dispersions in Organic Solvents.* Langmuir, 2008. **24**(19): p. 10560-10564.

45. Gómez-Navarro, C., et al., *Atomic Structure of Reduced Graphene Oxide.* Nano Letters, 2010. **10**(4): p. 1144-1148.

46. Ishigami, M., et al., *Atomic Structure of Graphene on SiO2.* Nano Letters, 2007. **7**(6): p. 1643-1648.

47. Kudin, K.N., et al., *Raman Spectra of Graphite Oxide and Functionalized Graphene Sheets.* Nano Letters, 2008. **8**(1): p. 36-41.

48. Mattevi, C., et al., *Evolution of Electrical, Chemical, and Structural Properties of Transparent and Conducting Chemically Derived Graphene Thin Films.* Advanced Functional Materials, 2009. **19**(16): p. 2577-2583.

49. Paredes, J.I., et al., *Atomic Force and Scanning Tunneling Microscopy Imaging of Graphene Nanosheets Derived from Graphite Oxide.* Langmuir, 2009. **25**(10): p. 5957-5968.

50. Lou, Y., et al., *A facile way to prepare ceramic-supported graphene oxide composite membrane via silane-graft modification.* Applied Surface Science, 2014. **307**(0): p. 631-637.

51. Huang, H., *Ultrafast viscous water flow through nanostrand-channelled graphene oxide membranes.* Nat. Commun., 2013. **4**: p. 2979.

52. Huang, H., et al., *Salt concentration, pH and pressure controlled separation of small molecules through lamellar graphene oxide membranes.* Chemical Communications, 2013. **49**(53): p. 5963-5965.

53. Li, H., *Tuning the underwater oleophobicity of graphene oxide coatings via UV irradiation.* Chem. Commun., 2014. **50**: p. 9849-9851.

54. Andrikopoulos, K.S., et al., *The Effect of Thermal Reduction on the Water Vapor Permeation in Graphene Oxide Membranes.* Advanced Materials Interfaces, 2014. **1**(8): p. n/a-n/a.

55. Sun, P., et al., *Selective Trans-Membrane Transport of Alkali and Alkaline Earth Cations through Graphene Oxide Membranes Based on Cation−π Interactions.* ACS Nano, 2014. **8**(1): p. 850-859.

56. Talyzin, A.V., et al., *The structure of graphene oxide membranes in liquid water, ethanol and water-ethanol mixtures.* Nanoscale, 2014. **6**(1): p. 272-281.

57. Yang, H., et al., *Covalent functionalization of chemically converted graphene sheets via silane and its reinforcement.* Journal of Materials Chemistry, 2009. **19**(26): p. 4632-4638.

58. Bhowmik, K., et al., *Covalently functionalized reduced graphene oxide by organically modified silica: a facile synthesis of electrically conducting black coatings on glass.* Journal of Materials Chemistry, 2012. **22**(47): p. 24690-24697.

59. Park, S., et al., *Graphene Oxide Papers Modified by Divalent Ions—Enhancing Mechanical Properties via Chemical Cross-Linking.* ACS Nano, 2008. **2**(3): p. 572-578.

60. Song, S., C. Wan, and Y. Zhang, *Non-covalent functionalization of graphene oxide by pyrene-block copolymers for enhancing physical properties of poly(methyl methacrylate).* RSC Advances, 2015. **5**(97): p. 79947-79955.

61. Park, S., et al., *Graphene Oxide Sheets Chemically Cross-Linked by Polyallylamine.* The Journal of Physical Chemistry C, 2009. **113**(36): p. 15801-15804.

62. Tsou, C.-H., et al., *Effect of microstructure of graphene oxide fabricated through different self-assembly techniques on 1-butanol dehydration.* Journal of Membrane Science, 2015. **477**: p. 93-100.

63. Tang, Y.P., D.R. Paul, and T.S. Chung, *Free-standing graphene oxide thin films assembled by a pressurized ultrafiltration method for dehydration of ethanol.* Journal of Membrane Science, 2014. **458**(0): p. 199-208.

64. Chong, J.Y., et al., *UV-Enhanced Sacrificial Layer Stabilised Graphene Oxide Hollow Fibre Membranes for Nanofiltration.* Scientific Reports, 2015. **5**: p. 15799.

65. Li, G., et al., *Efficient dehydration of the organic solvents through graphene oxide (GO)/ceramic composite membranes.* RSC Advances, 2014. **4**(94): p. 52012-52015.

66. Li, K., *Preparation of Ceramic Membranes*, in *Ceramic Membranes for Separation and Reaction*. 2007, John Wiley & Sons, Ltd. p. 21-57.

67. Zhang, Y., et al., *Layer-by-layer construction of graphene oxide (GO) framework composite membranes for highly efficient heavy metal removal.* Journal of Membrane Science, 2016. **515**: p. 230-237.

68. Hung, W.-S., et al., *Cross-Linking with Diamine Monomers To Prepare Composite Graphene Oxide-Framework Membranes with Varying d-Spacing.* Chemistry of Materials, 2014. **26**(9): p. 2983-2990.

69. Joshi, R.K., et al., *Precise and Ultrafast Molecular Sieving Through Graphene Oxide Membranes.* Science, 2014. **343**(6172): p. 752-754.

70. Hu, M. and B. Mi, *Enabling Graphene Oxide Nanosheets as Water Separation Membranes.* Environmental Science & Technology, 2013. **47**(8): p. 3715-3723.

71. Huang, K., et al., *A Graphene Oxide Membrane with Highly Selective Molecular Separation of Aqueous Organic Solution.* Angewandte Chemie International Edition, 2014. **53**(27): p. 6929-6932.

72. Huang, K., et al., *High-Efficiency Water-Transport Channels using the Synergistic Effect of a Hydrophilic Polymer and Graphene Oxide Laminates.* Advanced Functional Materials, 2015. **25**(36): p. 5809-5815.

73. Holt, J.K., et al., *Fast Mass Transport Through Sub-2-Nanometer Carbon Nanotubes.* Science, 2006. **312**(5776): p. 1034-1037.

74. Wei, Y., et al., *Declining flux and narrowing nanochannels under wrinkles of compacted graphene oxide nanofiltration membranes.* Carbon, 2016. **108**: p. 568-575.

75. Sun, P., et al., *Ultrafast liquid water transport through graphene-based nanochannels measured by isotope labelling.* Chemical Communications, 2015. **51**(15): p. 3251-3254.

76. Wissler, M., *Graphite and carbon powders for electrochemical applications.* Journal of Power Sources, 2006. **156**(2): p. 142-150.

77. Nakajima, T., A. Mabuchi, and R. Hagiwara, *A new structure model of graphite oxide.* Carbon, 1988. **26**(3): p. 357-361.

78. Mermoux, M., Y. Chabre, and A. Rousseau, *FTIR and 13C NMR study of graphite oxide.* Carbon, 1991. **29**(3): p. 469-474.

79. Lerf, A., et al., *Structure of Graphite Oxide Revisited.* The Journal of Physical Chemistry B, 1998. **102**(23): p. 4477-4482.

80. Koch, K.R., *Oxidation by Mn207: An impressive demonstration of the powerful oxidizing property of dimanganeseheptoxide.* Journal of Chemical Education, 1982. **59**(11): p. 973.

81. Zhou, K., et al., *Preparation of graphene-TiO2 composites with enhanced photocatalytic activity.* New Journal of Chemistry, 2011. **35**(2): p. 353-359.

82. Zhang, Y. and C. Pan, *TiO2/graphene composite from thermal reaction of graphene oxide and its photocatalytic activity in visible light.* Journal of Materials Science, 2011. **46**(8): p. 2622-2626.

83. Song, J., X. Wang, and C.-T. Chang, *Preparation and Characterization of Graphene Oxide.* Journal of Nanomaterials, 2014. **2014**: p. 6.

84. Choi, E.-Y., et al., *Noncovalent functionalization of graphene with end-functional polymers.* Journal of Materials Chemistry, 2010. **20**(10): p. 1907-1912.

85. Yang, S., et al., *A facile green strategy for rapid reduction of graphene oxide by metallic zinc.* RSC Advances, 2012. **2**(23): p. 8827-8832.

86. Zhang, J., et al., *Reduction of graphene oxide vial-ascorbic acid.* Chemical Communications, 2010. **46**(7): p. 1112-1114.

87. Luo, Z., et al., *High Yield Preparation of Macroscopic Graphene Oxide Membranes.* Journal of the American Chemical Society, 2009. **131**(3): p. 898-899.

88. Zhou, Y., et al., *Hydrothermal Dehydration for the "Green" Reduction of Exfoliated Graphene Oxide to Graphene and Demonstration of Tunable Optical Limiting Properties.* Chemistry of Materials, 2009. **21**(13): p. 2950-2956.

89. Becerril, H.A., et al., *Evaluation of Solution-Processed Reduced Graphene Oxide Films as Transparent Conductors.* ACS Nano, 2008. **2**(3): p. 463-470.

90. Li, K., *Ceramic Membranes for Separation and Reaction*. 2007, Chichester: John Wiley & Sons Ltd.

91. Goh, K., et al., *Graphene oxide as effective selective barriers on a hollow fiber membrane for water treatment process.* Journal of Membrane Science, 2015. **474**: p. 244-253.

92. Huang, K., et al., *A Graphene Oxide Membrane with Highly Selective Molecular Separation of Aqueous Organic Solution.* Angewandte Chemie International Edition, 2014.

93. Kingsbury, B.F.K. and K. Li, *A morphological study of ceramic hollow fibre membranes.* Journal of Membrane Science, 2009. **328**(1–2): p. 134-140.

94. Wang, B. and Z. Lai, *Finger-like voids induced by viscous fingering during phase inversion of alumina/PES/NMP suspensions.* Journal of Membrane Science, 2012. **405–406**: p. 275-283.

95. Nair, R.R., et al., *Unimpeded Permeation of Water Through Helium-Leak-Tight Graphene-Based Membranes.* Science, 2012. **335**(6067): p. 442-444.

96. Li, H., et al., *Ultrathin, molecular-sieving graphene oxide membranes for selective hydrogen separation.* Science, 2013. **342**(6154): p. 95-8.

97. Townsend, P.H., D.M. Barnett, and T.A. Brunner, *Elastic relationships in layered composite media with approximation for the case of thin films on a thick substrate.* Journal of Applied Physics, 1987. **62**(11): p. 4438-4444.

98. Dikin, D.A., et al., *Preparation and characterization of graphene oxide paper.* Nature, 2007. **448**(7152): p. 457-60.

99. Bagri, A., et al., *Structural evolution during the reduction of chemically derived graphene oxide.* Nature Chemistry, 2010. **2**(7): p. 581-587.

100. Sun, P.Z., et al., *Selective Ion Penetration of Graphene Oxide Membranes.* Acs Nano, 2013. **7**(1): p. 428-437.

101. Van der Bruggen, B., M. Mänttäri, and M. Nyström, *Drawbacks of applying nanofiltration and how to avoid them: A review.* Separation and Purification Technology, 2008. **63**(2): p. 251-263.

102. Marchetti, P., et al., *Molecular Separation with Organic Solvent Nanofiltration: A Critical Review.* Chemical Reviews, 2014.

103. Bhanushali, D., et al., *Performance of solvent-resistant membranes for non-aqueous systems: solvent permeation results and modeling.* Journal of Membrane Science, 2001. **189**(1): p. 1-21.

104. Machado, D.R., D. Hasson, and R. Semiat, *Effect of solvent properties on permeate flow through nanofiltration membranes. Part I: investigation of parameters affecting solvent flux.* Journal of Membrane Science, 1999. **163**(1): p. 93-102.

105. Machado, D.R., D. Hasson, and R. Semiat, *Effect of solvent properties on permeate flow through nanofiltration membranes - Part II. Transport model.* Journal of Membrane Science, 2000. **166**(1): p. 63-69.

106. Geens, J., et al., *Modelling of solute transport in non-aqueous nanofiltration.* Journal of Membrane Science, 2006. **281**(1-2): p. 139-148.

107. Wei, N., X. Peng, and Z. Xu, *Understanding water permeation in graphene oxide membranes.* ACS Applied Materials Interfaces, 2014. **6**(8): p. 5877-83.

108. Wang, X.-L., et al., *Electrolyte transport through nanofiltration membranes by the space-charge model and the comparison with Teorell-Meyer-Sievers model.* Journal of Membrane Science, 1995. **103**(1): p. 117-133.

109. Cohen-Tanugi, D. and J.C. Grossman, *Nanoporous graphene as a reverse osmosis membrane: Recent insights from theory and simulation.* Desalination, 2015. **366**: p. 59-70.

110. Han, Y., Z. Xu, and C. Gao, *Ultrathin Graphene Nanofiltration Membrane for Water Purification.* Adv. Funct. Mater., 2013. **23**: p. 3693-3700.

111. Konatham, D., et al., *Simulation Insights for Graphene-Based Water Desalination Membranes.* Langmuir, 2013. **29**(38): p. 11884-11897.

112. Joshi, R.K., *Precise and Ultrafast Molecular Sieving Through Graphene Oxide Membranes.* Science, 2014. **343**: p. 752-754.

113. Mi, B., *Graphene Oxide Membranes for Ionic and Molecular Sieving.* Science, 2014. **343**(6172): p. 740-742.

114. Nair, R.R., et al., *Unimpeded Permeation of Water Through Helium-Leak-Tight Graphene-Based Membranes.* Science, 2012. **335**: p. 442-444.

115. Yeh, C.N., et al., *On the origin of the stability of graphene oxide membranes in water.* Nat Chem., 2015. **7**: p. 166-170.

116. Yang, D., et al., *Chemical analysis of graphene oxide films after heat and chemical treatments by X-ray photoelectron and Micro-Raman spectroscopy.* Carbon, 2009. **47**(1): p. 145-152.

117. Stankovich, S., et al., *Synthesis of graphene-based nanosheets via chemical reduction of exfoliated graphite oxide.* Carbon, 2007. **45**(7): p. 1558-1565.

118. Baker, R.W., et al., *The effect of concentration polarization on the separation of volatile organic compounds from water by pervaporation.* Journal of Membrane Science, 1997. **137**(1–2): p. 159-172.

119. Psaume, R., et al., *Pervaporation: importance of concentration polarization in the extraction of trace organics from water.* Journal of Membrane Science, 1988. **36**: p. 373-384.

120. Raghunath, B. and S.T. Hwang, *Effect of boundary layer mass transfer resistance in the pervaporation of dilute organics.* Journal of Membrane Science, 1992. **65**(1–2): p. 147-161.

121. He, W., et al., *Influence of Reaction Conditions on the Grafting Pattern of 3-Glycidoxypropyl trimethoxysilane on Montmorillonite.* Bulletin of the Korean Chemical Society, 2013. **34**(1): p. 112-116.

122. Park, Y.-i. and M. Nagai, *Proton-Conducting Properties of Inorganic-Organic Nanocomposites Proton-Exchange Nanocomposite Membranes Based on 3-Glycidoxypropyltrimethoxysilane and Tetraethylorthosilicate.* Journal of The Electrochemical Society, 2001. **148**(6): p. A616.

123. Lou, Y., et al., *A facile way to prepare ceramic-supported graphene oxide composite membrane via silane-graft modification.* Applied Surface Science, 2014. **307**: p. 631.

124. Wong, A.Y. and U. Krull, *Surface characterization of 3-glycidoxypropyltrimethoxysilane films on silicon-based substrates.* Analytical and Bioanalytical Chemistry, 2005. **383**(2): p. 187-200.

125. Daniels, M.W. and L.F. Francis, *Silane Adsorption Behavior, Microstructure, and Properties of Glycidoxypropyltrimethoxysilane-Modified Colloidal Silica Coatings.* Journal of Colloid and Interface Science, 1998. **205**(1): p. 191-200.

126. Medda, S.K. and G. De, *Inorganic−Organic Nanocomposite Based Hard Coatings on Plastics Using In Situ Generated Nano-SiO2 Bonded with ≡Si—O—Si—PEO Hybrid Network.* Industrial & Engineering Chemistry Research, 2009. **48**(9): p. 4326-4333.

127. Yoshida, W. and Y. Cohen, *Topological AFM characterization of graft polymerized silica membranes.* Journal of Membrane Science, 2003. **215**(1–2): p. 249-264.

128. Wei, C.C. and K. Li, *Preparation and Characterization of a Robust and Hydrophobic Ceramic Membrane via an Improved Surface Grafting Technique.* Industrial & Engineering Chemistry Research, 2009. **48**(7): p. 3446-3452.

129. Xu, X. and M.R. Coleman, *Atomic force microscopy images of ion-implanted 6FDA-pMDA polyimide films.* Journal of Applied Polymer Science, 1997. **66**(3): p. 459-469.

130. Huang, L., et al., *Graphene Oxide Membranes with Tunable Semipermeability in Organic Solvents.* Advanced Materials, 2015. **27**(25): p. 3797-3802.

131. Lacaze, L., et al., *Transient surface tension in miscible liquids.* Physical Review E, 2010. **82**(4): p. 041606.

132. Chen, C.-Y., L. Wang, and E. Meiburg, *Miscible droplets in a porous medium and the effects of Korteweg stresses.* Physics of Fluids, 2001. **13**(9): p. 2447-2456.

133. Sugii, Y., et al., *Effect of korteweg stress in miscible liquid two-layer flow in a microfluidic device.* Journal of Visualization, 2005. **8**(2): p. 117-124.

134. Pojman, J.A., et al., *Evidence for the Existence of an Effective Interfacial Tension between Miscible Fluids: Isobutyric Acid−Water and 1-Butanol−Water in a Spinning-Drop Tensiometer.* Langmuir, 2006. **22**(6): p. 2569-2577.

135. Zoltowski, B., et al., *Evidence for the Existence of an Effective Interfacial Tension between Miscible Fluids. 2. Dodecyl Acrylate−Poly(dodecyl acrylate) in a Spinning Drop Tensiometer.* Langmuir, 2007. **23**(10): p. 5522-5531.

136. Vane, L.M., *A review of pervaporation for product recovery from biomass fermentation processes.* Journal of Chemical Technology & Biotechnology, 2005. **80**(6): p. 603-629.

137. Peters, T.A., et al., *Ceramic-supported thin PVA pervaporation membranes combining high flux and high selectivity; contradicting the flux-selectivity paradigm.* Journal of Membrane Science, 2006. **276**(1–2): p. 42-50.

138. Wang, X.-S., et al., *Novel polyelectrolyte complex membranes containing free sulfate groups with improved pervaporation dehydration of ethanol.* Journal of Membrane Science, 2014. **452**(0): p. 73-81.

139. Wang, J. and T. Tsuru, *Cobalt-doped silica membranes for pervaporation dehydration of ethanol/water solutions.* Journal of Membrane Science, 2011. **369**(1–2): p. 13-19.

140. Zhou, H., et al., *Ultrathin zeolite X membranes for pervaporation dehydration of ethanol.* Journal of Membrane Science, 2012. **399–400**(0): p. 106-111.

141. Shao, J., et al., *Zeolite NaA membranes supported on alumina hollow fibers: Effect of support resistances on pervaporation performance.* Journal of Membrane Science, 2014. **451**: p. 10-17.

142. Won, H.J., S.K. Yong, and J.K. Hyo, *Association behavior in copolymer blend membranes and the pervaporation of water/ethanol mixtures.* Journal of Membrane Science, 1993. **85**(1): p. 81-88.

143. Ge, J., et al., *The effect of structure on pervaporation of chitosan membrane.* Journal of Membrane Science, 2000. **165**(1): p. 75-81.

144. Hung, M.-Y., et al., *Pervaporation separation of a water/ethanol mixture by a sodium sulfonate polysulfone membrane.* Journal of Applied Polymer Science, 2003. **90**(12): p. 3374-3383.

145. Dikin, D.A., et al., *Preparation and characterization of graphene oxide paper.* Nature, 2007. **448**(7152): p. 457-460.

Appendix A: List of Abbreviations

AFM	Atomic force microscopy
FEGSEM	Field emission gun scanning electron microscopy
GO	Graphene oxide
UV-vis	Ultraviolet-visible spectroscopy
XPS	X-ray photoelectron spectroscopy
XRD	X-ray diffraction
FTIR	Fourier transform infrared spectroscopy
TGA	Thermal gravimetric analysis
PES	Polyethersulfone
GPTS	3-glycidoxypropyltrimethoxysilane
YSZ	Yttria stabilized zirconia
$Al(NO_3)_3$	Aluminium nitrate

Appendix B: Permissions for third party copyright works

Page No.	Type of work:	License content publication	License content publisher	I have permission yes /no	Requested license No.
23	figure	Chemical Physics Letters	Elsevier	yes	3980480352472
39	figure	Science	The American Association for the Advancement of Science	yes	3973560195076
43	figure	Science	The American Association for the Advancement of Science	yes	3980471048371
53	figure	Science	The American Association for the Advancement of Science	yes	3980471278396
91-117	Re-use in a thesis(full article)	Journal of Membrane Science	Elsevier	yes	3980480053080

Appendix C: Image J measurements of GO flakes size used in this study

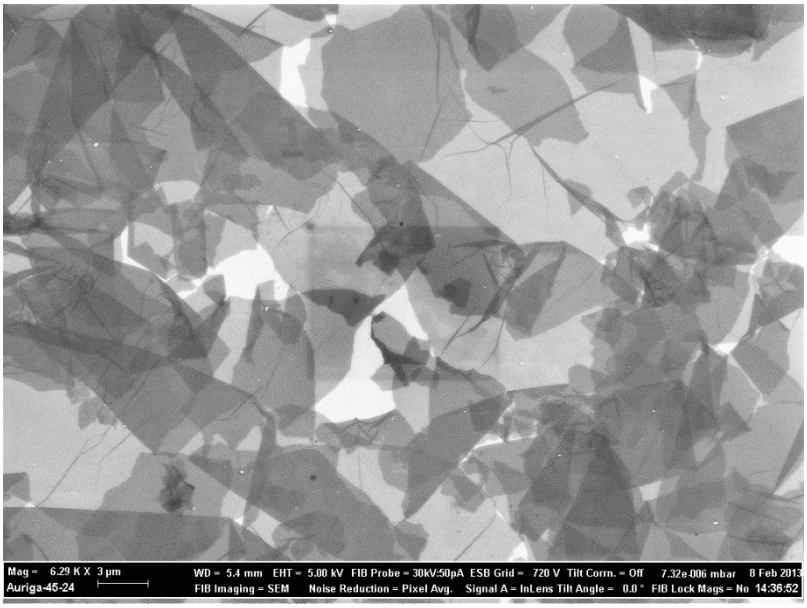

Tabulated Image J analysis results:

	Label	Mean	StdDev	Min	Max	Angle	Length (µm)
1		162.491	4.551	139.344	172.067	0.335	7.758
2		170.596	27.124	130.1	247	0	5.333
3		144.101	23.558	86.94	169.778	0.387	6.728
4		149.024	40.298	74.333	203.327	0.562	9.273
5		167.821	15.633	138.886	214.168	0.289	9.031
6		181.71	24.959	124.014	206.208	0.244	10.667
Summary of analysis							
7	Mean	162.624	22.687	115.603	202.091	0.206	8.131
8	SD	14.021	11.953	27.969	28.729	0.305	1.922
9	Min	144.101	4.551	74.333	169.778	0.289	5.333
10	Max	181.71	40.298	139.344	247	0.562	10.667

Appendix D: Shrinkage analysis of GO membranes

Experimental steps:

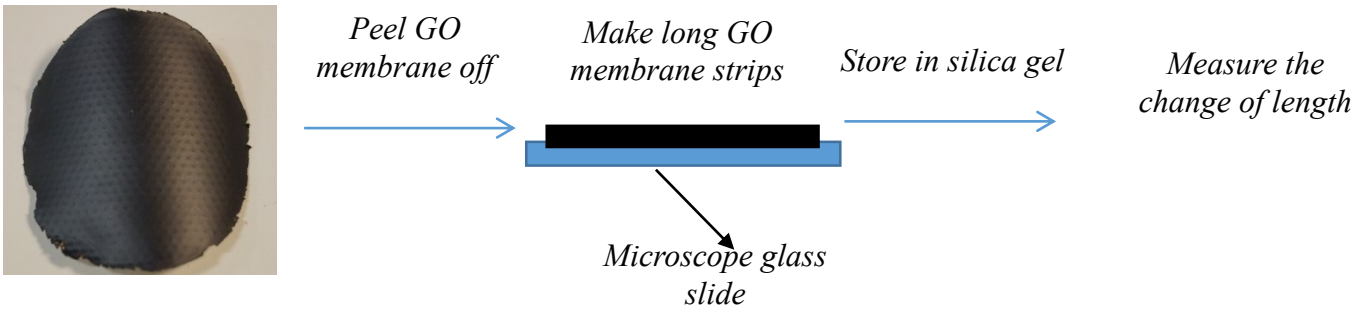

Raw Data:

Two lines were measured.

	Fresh membrane	After 3 days	After one week	After three months	After annealing
Line 1	48.08 mm	47.70 mm	47.67 mm	47.67 mm	46.40 mm
Line 2	35.41 mm	35.00 mm	35.00 mm	35.01 mm	34.32 mm

Mechanism of shrinkage in lateral dimension : (X-Y) direction

The measurement of the shrinkage due to the stress of the GO membrane strips is along the lateral dimension of the GO membrane strip (X-Y) direction and not on the thickness direction (Z direction).

Visually, no delamination occurred along the thickness (Z) direction, hence the shrinkage was mainly occurred in X-Y direction. In principle, the shrinkage in the thickness direction (Z direction) can be assumed to occur freely without introducing stress, because the position of the outer surface is not fixed and it is freely move.

For more detail explanation about the shrinkage analysis, please refer to Chapter 4 of this thesis.

Appendix E: Simple mass balance on UV analysis for adsorption study

GO has been known to effectively adsorb dyes, thus in order to exclude this effect, throughout the experimental process, the filtration process was tested for at least 3 hours and 1 hour was allowed for the membrane to stable.

The following shows a simple mass balance analysis of GO membranes, taking methyl orange as an example of dye. *Note that all the UV-Vis analysis of the rejection was carried out as soon as after the rejection test was done to ensure the accuracy of the reading.*

In order to determine that the membranes are not adsorbing or adsorption is not the main contribution to the rejection of this GO membranes, total feed (in) must be equal to (out) permeate and retentate.

Volume of feed x Absorption of feed = Volume of permeate x Absorption of permeate

+ Volume of Retentate x Absorption of retentate

350 mL x 1.282 = (4 ml x 0.007) + (346 mL x 1.277)

448.70 = 441.87

* About 1.5 % of dye is adsorb on the membrane which can be considered as minor in determining overall rejection performance of GO membranes.

Appendix F: Capillary pressure calculation for different interfacial tension value

The reported value for transient interfacial tension varies from 0.001 to 0.6 mN m^{-1} [134, 135].

Using Young Laplace Equation, capillary pressure can be calculated:

$$p_c = \frac{2\gamma \cos\theta}{r}$$

Where p_c is capillary pressure, γ is the interfacial tension, θ is the wetting angle (in this case the value thereof is 0), and r is the radius of the interface (in this case the interlayer space of the GO).

Consider the lowest interfacial tension as 0.001 mN m^{-1}, the capillary pressure was determined to be 0.044 bar and at the highest interfacial tension of 0.6 mN m^{-1}, the capillary pressure would be 26.6 bar. It should be noted that with the concentration of 95/5 wt% of ethanol/water mixture, it can be expected that that the interfacial tension is high, which should be greater than 0.001 mN m^{-1}, due to high concentration gradient. Thus, it is reasonable in this study to assume that the interfacial tension is 0.2 mN m^{-1} as a moderate value to use for the capillary pressure calculation.